2-P (mix)

X-553-72-290

PREPRINT

NASA TM X- 66018

TRACKING OF THE ATS-3 SYNCHRONOUS SATELLITE BY THE VERY LONG BASELINE INTERFEROMETER (VLBI) TECHNIQUE

J. RAMASASTRY

B. ROSENBAUM

R. D. MICHELINI

D. FROST

S. ROSS

A. BOORNAZIAN

JULY 1972

Details of illustrations in this document may be better studied on microfiche

GSFC

GODDARD SPACE FLIGHT CENTER

GREENBELT, MARYLAND

X-553-72-290

TRACKING OF THE ATS-3 SYNCHRONOUS SATELLITE BY THE VERY LONG BASELINE INTERFEROMETER (VLBI) TECHNIQUE

J. Ramasastry
B. Rosenbaum
Geodynamics Branch
Trajectory Analysis and Geodynamics Division
Goddard Space Flight Center

R. D. Michelini
D. Frost
Smithsonian Astrophysical Observatory
Cambridge, Mass.

S. Ross
A. Boornazian
S. Ross and Company,
Boston, Mass.

July 1972

GODDARD SPACE FLIGHT CENTER
Greenbelt, Maryland

CONTENTS

CONTENTS (Continued)

ILLUSTRATIONS

ILLUSTRATIONS (Continued)

ILLUSTRATIONS (Continued)

ILLUSTRATIONS (Continued)

TABLES

TRACKING OF THE ATS-3 SYNCHRONOUS SATELLITE BY THE VERY LONG BASELINE INTERFEROMETER (VLBI) TECHNIQUE

J. Ramasastry, B. Rosenbaum
Geodynamics Branch
Trajector Analysis and Geodynamics Division
Goddard Space Flight Center

R. D. Michelini, D. Frost
Smithsonian Astrophysical Observatory
Cambridge, Massachusetts

S. Ross, A. Boornazian
S. Ross and Company
Boston, Massachusetts

SUMMARY

During 1971, a series of very long baseline interferometer (VLBI) observations were made of the C-band (6 cm) radio signals from the ATS-3 communications satellite which is in a synchronous, near-equatorial orbit. The first series of observations were conducted during May-June 1971 from Rosman, North Carolina (NASA/ATS Station 85' dish) and Mojave, California (NASA/ATS Station, 40' dish). The second series of observations were conducted during August-September, 1971 from Rosman, North Carolina (NASA/ATS Station, 85' dish), Owens Valley, California (Cal Tech, 130' dish) and Agassiz, Massachusetts (SAO Agassiz Radio Observatory, 84' dish). The ATS-3 Spacecraft position has been determined with a precision of 70-100 meters and its velocity with a precision of less than a mm/sec. The ATS-3 orbital elements have been computed using the GEODYN program and the derived values are consistent with those derived from conventional tracking data.

1. INTRODUCTION

During 1971, a series of very long baseline interferometer (VLBI) observations were made of the C-band (6 cm) radio signals from the ATS-3 communications satellite which is in a synchronous, near-equatorial orbit. The first series of observations were conducted during May-June 1971 from Rosman, North Carolina (NASA/ATS Station, 85' dish) and Mojave, California (NASA/ATS Station, 40' dish). The second series of observations were conducted during August - September, 1971 from Rosman, North Carolina (NASA/ATS Station, 85' dish), Owens Valley, California (Cal Tech, 130' dish) and Agassiz, Massachusetts (SAO Agassiz Radio Observatory, 84' dish). The ATS-3 Spacecraft position has been determined with a precision of 70-100 meters and its velocity with a precision of less than a mm/sec. The ATS-3 orbital elements have been computed using the GEODYN program and the derived values are consistent with those derived from conventional tracking data.

2. EXPERIMENT DESCRIPTION

2.1 EXPERIMENT #1

During May - June, 1971, the first series of interferometric observations were made of the C-band (6 cm) radio signals from the ATS-3 communications satellite which is in a synchronous, near equatorial orbit. Figure 1 shows the schematic set-up of the experiment in which Rosman and Mojave ATS stations were used as an interferometer pair. Some of the experimental parameters are given in Table 1.

TABLE 1

ATSR Antenna Parameters - Experiment #1

System Parameter		Rosman	Mojave
Diameter		85'	40'
Type of Mount		X-Y	X-Y
System Noise Temperature (Cooled Parametric Amplifiers)		65° K	65° K
Receiver Gain		58 db	51 db
Receiver Beam Width		0.2°	0.47°
Signal Frequency		4178.59072 MHz	4178.59072 MHz
Geodetic Coordinates	Latitude	35° 11' 56" .07 N	35° 19' 53" .78 N
	Longitude	277° 7' 27" .19 E	243° 6' 43" .86 E
	Altitude	828 meters	887 meters

Scheduling at the tracking stations permitted normal observational runs of up to four hours per day. On several occasions, extended observations were made for over 12 hours. Most of the observations were with the ATS-3 satellite even though a few observations were made with the ATS-1 satellite.

There are two C-band transponders on the ATS-1 and ATS-3 satellites. Transponder #1 receives at 6212.094 MHz and transmits at 4178.59072 MHz. Transponder #2 receives at 6301.050 MHz and transmits at 4119.5990 MHz. It is transponder #1 that was used in most of our observations. The orbital parameters of the ATS-1 and 3 satellites are given in Table 2.

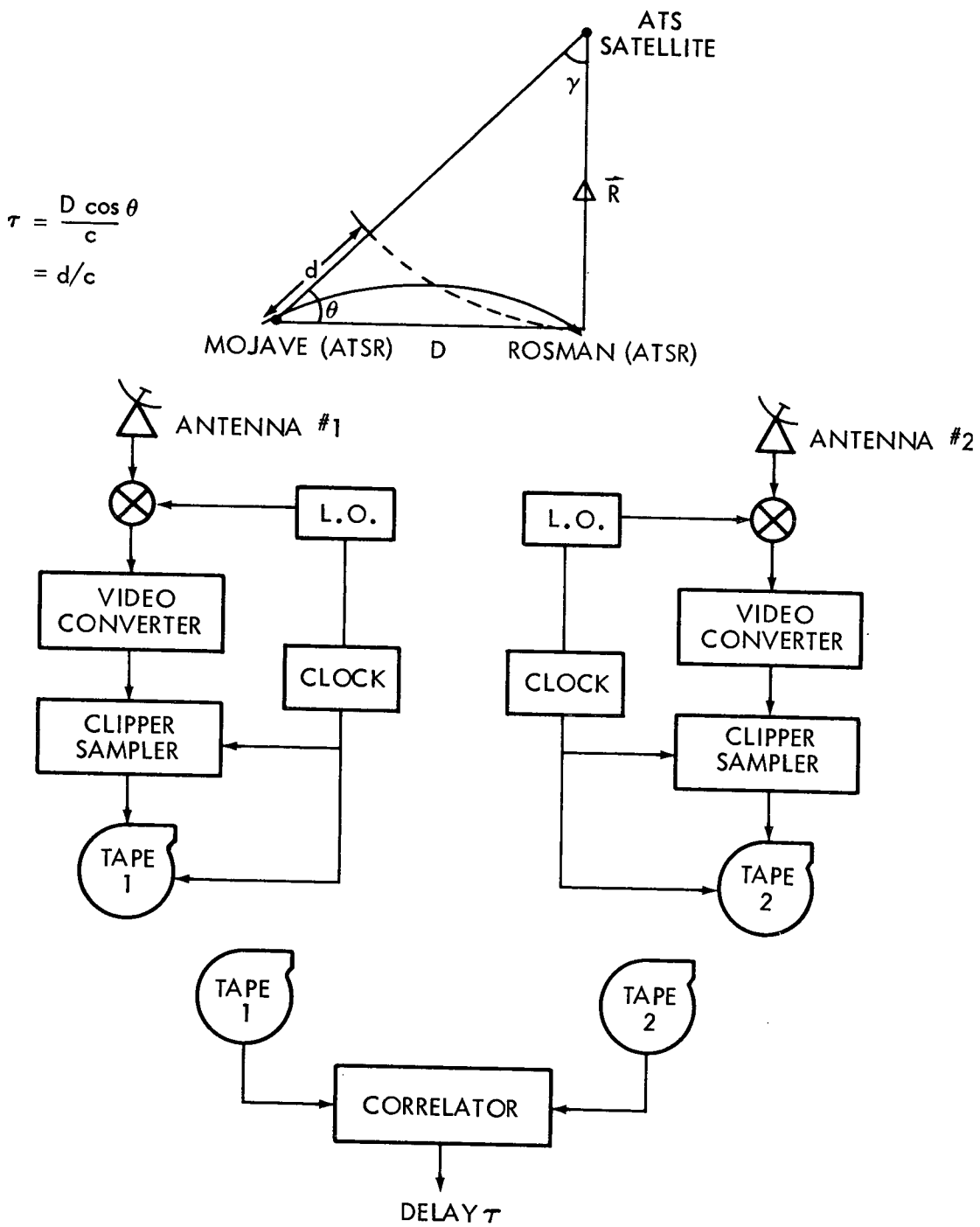

Figure 1. Schematic Set-up of VLBI Experiment

TABLE 2

ATS-1 & ATS-3 Orbital Elements

(Furnished by the GSFC ATS Projects Office)

Orbital Element	ATS-1	ATS-3
Apogee (km)	35813.15	35910.12
Perigee (km)	35760.045	35664.40
Longitude (degrees)	149° .152	78°.850
Latitude (degrees)	0°.021	1°.103
Period (minutes)	1436.101	1436.018
Drift Rate (deg/day)	0°.008 E/day	0°.013E/day
Inclination (deg)	3°.349	1°.706
Eccentricity	0.00625	0.00291
Semi-major Axis (Km)	42164.96	42165.43
Spacecraft Attitude { Right Ascension	161°.5	165°.5
Spacecraft Attitude { Declination	85°.6	88°.3

The satellite transponder radiated signals with an EIRP (effective isotropic radiated power) of 446 watts centered at 4178.59072 MHz and extending over a 20 MHz bandwidth. The signal is so strong - nearly six orders of magnitude larger than those from natural celestial sources, one could have used very small (~3') microwave horns in the place of the large parabolic antennas that are available at the sites. The quality of the satellite fringes is, as expected, superior to those from the quasars due to the enhanced signal-to-noise ratio.

2.2 EXPERIMENT #2

The second experiment was performed during August - September 1971. In this experiment, simultaneous observations were made from three stations: Rosman, North Carolina (ATS-85' dish); Owens Valley, California (Cal Tech-130' dish); Agassiz, Massachusetts (SAO-84' dish). The quasar observations were made at 4995 MHz and the ATS-3 satellite observations were made at 4178 MHz. Results of the second experiment are reported separately.

2.3 THE INTERFEROMETER SYSTEM:

A VLBI interferometer system consists of a pair of terminals (Rosman and Mojave in this case) with the following elements (Figure 2).

- Antenna and feed
- Radiometer/receiver
- IF interface and calibrating equipment
- VLBI Backend (data conditioning and recording equipment)
- Timing and Frequency control system
- Correlator/Computer

2.3.1 Antenna/Receiver System:

Antenna and receiver specifications at Mojave and Rosman have been discussed earlier.

2.3.2 IF Interface and Calibrating Equipment

The receiver IF frequency at the Rosman and Mojave stations is 70 MHz. However, the video converter of the VLBI backend is designed to accept either a 30 MHz signal or a 150 MHz signal as an input. In order to derive the required 30 MHz signal, suitable "IF Interface" equipment is used. This interface equipment is merely a synthesizer/mixer combination which uses a 40 MHz signal to mix with the station IF of 70 MHz and thereby generates a new 30 MHz IF (Figure 3).

2.3.3 VLBI Backend and Recording System

The principal components of the instrumentation system are the video converter, the sampler formatter and the video recorder. Figure 4 is a diagram of the instrumentation system. One rack contains the time-keeping equipment and the frequency source and the other contains the video converter and the data-formatting circuitry. The latter is modularly assembled from DTL-logic integrated-circuit cards.

The backend system accepts either a 30- or 150-MHz IF signal from the receiver. After two or three stages of phase-coherent conversion, the filtered video signal is amplified, limited, and clipped to provide only zero crossing information within the selected video passband.

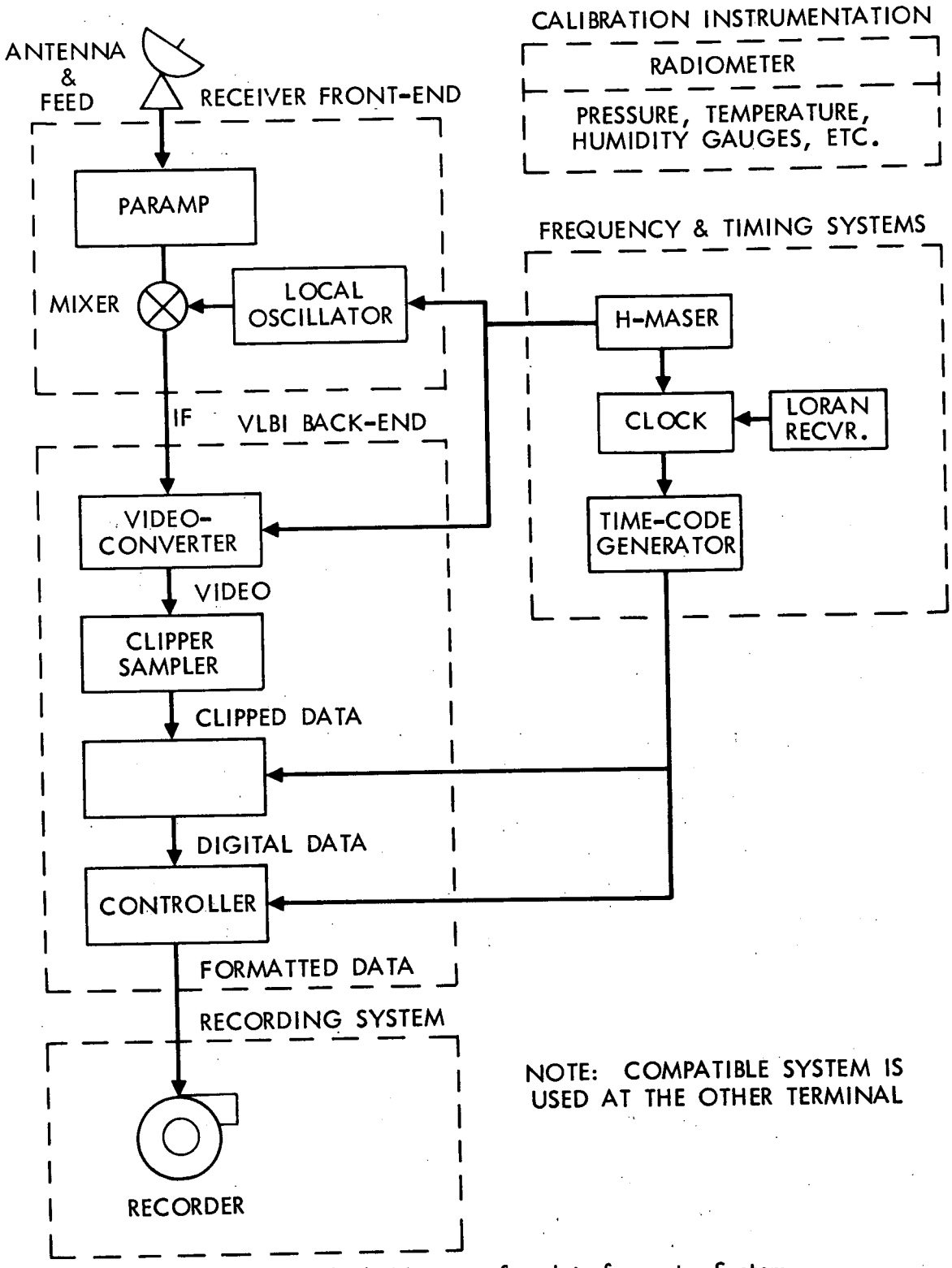

Figure 2. Block Diagram of an Interferometer System

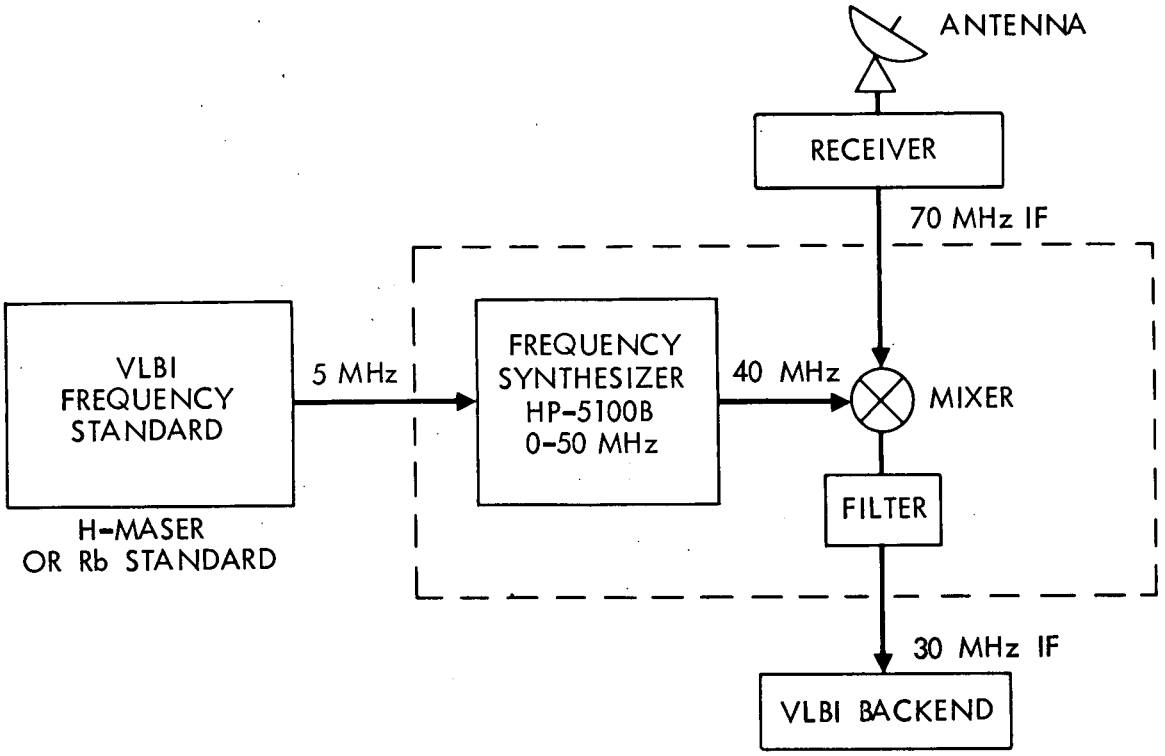

Figure 3. IF Interface Equipment

The nonreturn-to-zero (NRZ) sampler samples 40-nsec windows of the clipped video at a rate controlled by the frequency standard which also provides the basic frequency for phase coherent conversion of the IF to video frequency. After being sampled, the 1-bit data (zero if sampled below the baseline, one if sampled above) are serially applied to a multiplex circuit that arranges the format of the data frame. At the start of each video frame, the multiplex unit inserts a recorder head-switching period (all ones), a 60 bit synchronization word (all zeroes), and a BCD time-code word. These nondata bits are generated at the same sampling rate as are the data bits, and their position within the frame is fixed by the clock counter and the event decoder. The time-code word is transferred once each frame from the digital clock into a register and is then transferred to the multiplexer. A recording "start time" is preset by thumbwheel switches. Recording is automatically initiated upon receipt of the first frame time occurring after the selected "second" of time.

The data frame is encoded in the modulator into a self-clocking recording format. Either bi-phase return to zero (RZ) or Manchester Coding

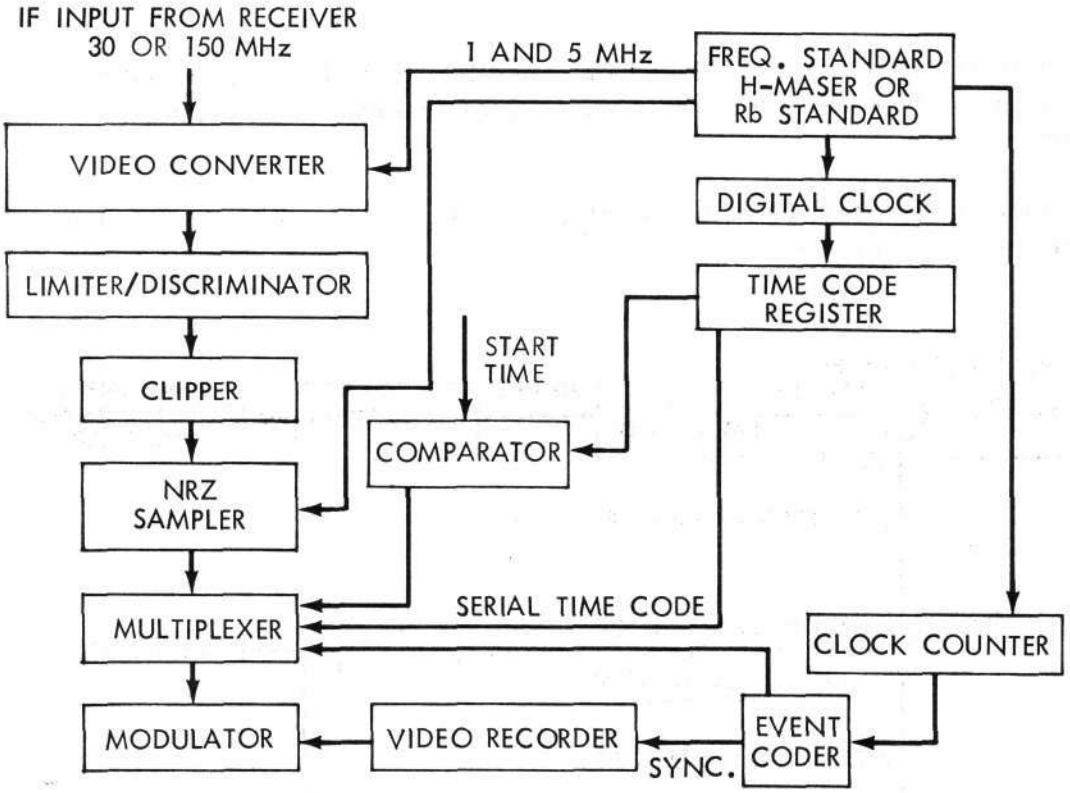

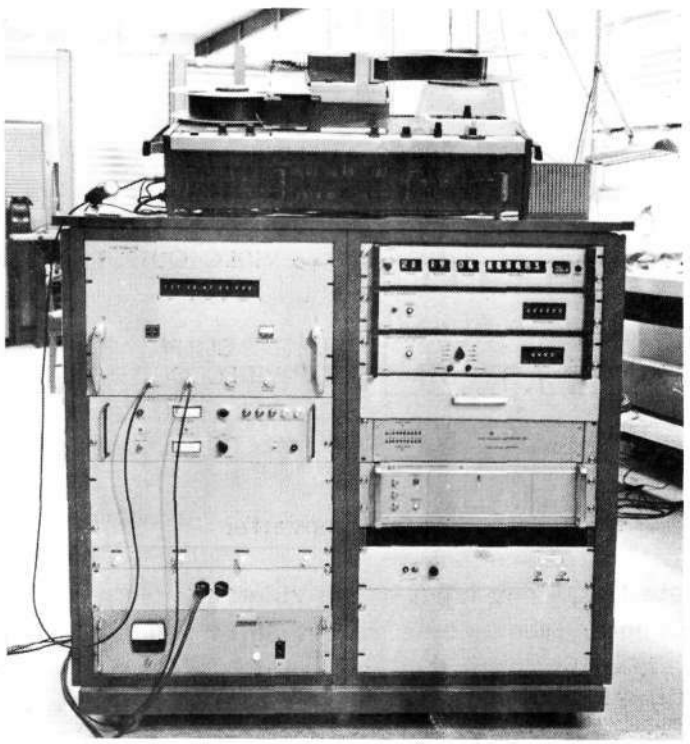

Figure 4. The Instrumentation System

may be selected. The videotape recorder used is a modified Ampex 660-C helical scan TV-type recorder with provision for external head-drum synchronization.

2.3.3.1 Video Converter, Clipper/Sampler. The basic circuitry of the video converter is shown in Figure 5.

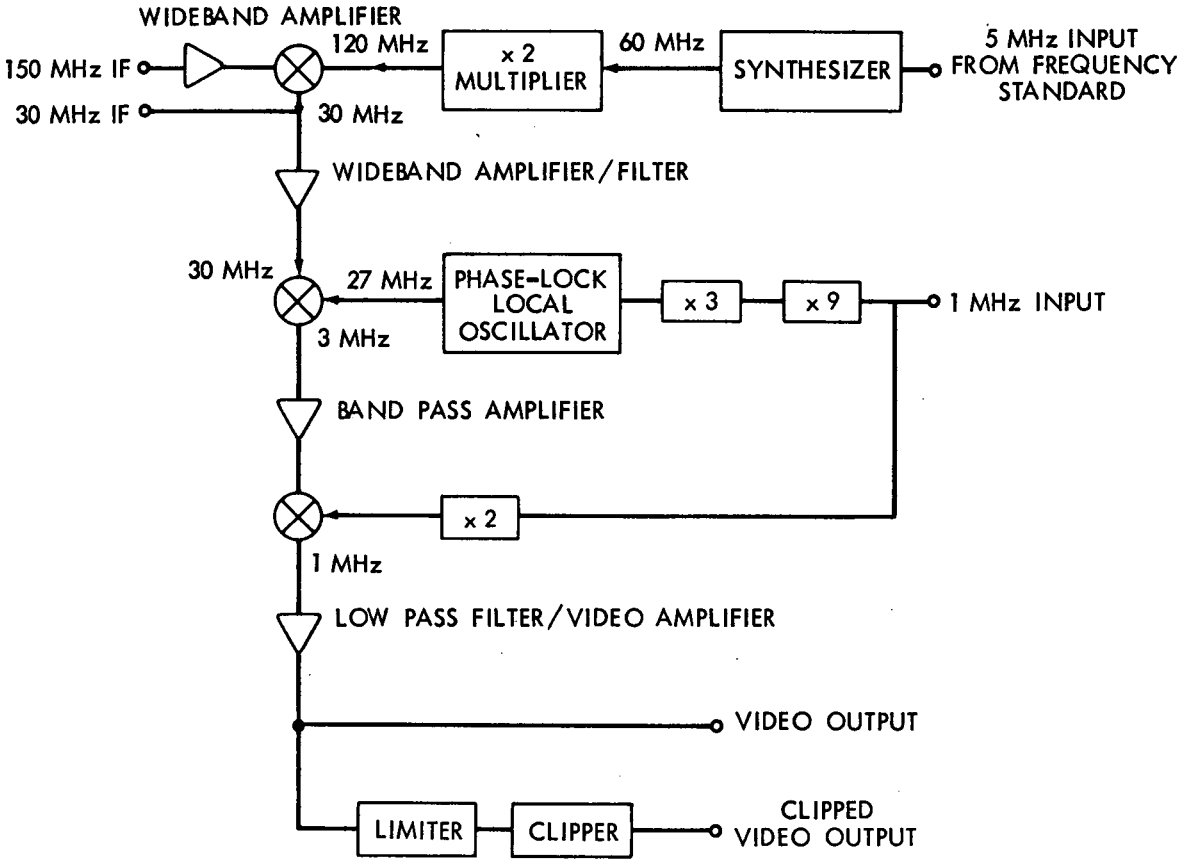

Figure 5. Video-Converter

The intermediate frequency input to the video converter is single side-band filtered around a center frequency of either 30 or 150 MHz. The video converter converts the IF from the low-noise receiver into a video signal suitable for 1-bit digital sampling and subsequent recording. The IF signal is amplified and filtered; the phase is coherently converted in frequency to establish a single side-band output signal in which the carrier frequency is zero (dc).

The output video signal band extends from a lower frequency cut off of 50 kHz to an upper frequency (3-db) cut off of one of the four selectable steps: 350 kHz, 480 kHz, 960 kHz and 2.0 MHz. Uniform response is achieved throughout the band with sharp rejection at the edges using appropriate filtering process.

The video converter contains the necessary frequency multiplier, frequency synthesizers and phase-locked oscillator circuitry to generate 120, 27 and 2 MHz phase-coherent local oscillator signals from the 1 and 5 MHz signals supplied by the precision frequency standard. The 150 MHz signal is amplified by a broad band (100-200 MHz) amplifier and fed to a 150/30 MHz mixer.

When the video converter is operated with a 30 MHz input signal, the IF signal is fed through a broad band amplifier that acts as a gain-control element in the video converter. The 30 MHz signal is fed to a 30/3 MHz mixer. The local-oscillator signal at 27 MHz is obtained from a phase-locked oscillator. The reference or phase-locking signal for this 27 MHz oscillator is obtained by two multipliers (x3 and x9) in sequence driven by a 1 MHz reference signal from the frequency standard. An unlock oscillator circuit is connected to the phase-locked oscillator to provide automatic frequency searching and visual indication of loss of phase-lock.

The output band from the 30/3 MHz mixer is fed to a series of bandpass amplifiers centered on 3.0 MHz. Each bandpass amplifier utilizes three tuned LC circuits to achieve a uniform response in the 2.0-4.0 MHz band with high rejection below 2.0 MHz and above 4.0 MHz. Tuned LC trap circuits between the first and second and the second and third bandpass amplifiers provide additional rejection in the frequency region just below 2.0 MHz.

The output of the band pass amplifier is fed to the 3/1 MHz mixer, where a 2 MHz local oscillator signal is mixed with the 2 to 4 MHz signal band. The 2.0 MHz local oscillator signal is derived from a frequency doubler driven by the 1 MHz signal from the frequency standard. A video amplifier with a lower frequency cut off of approximately 25 kHz and an upper frequency cut off of approximately 1.8 MHz is a part of the mixer-output circuitry. The output of the video amplifier/filter is a single sideband signal that has a carrier frequency of zero. An increase in frequency in the IF (30 or 150 MHz) will provide a corresponding increase in the frequency of the video band.

The diode limiter removes a major portion of the amplitude fluctuation in the video signal. The broad band noise input produces the same signal level on each of the bandwidth settings through internal adjustments of the relative gain.

The signal output from the limiter is connected to the clipper circuitry. Here the video-band signal is amplified and clipped in amplitude so that only the zero-crossing information is retained. For a noise input signal, the output from the clipper is a random square wave in which the voltage level is either zero or + 4 volts.

2.3.3.2 Data Recording System. The data format used in recording the 1-bit digital data on videotape is illustrated in Figure 6. The individual data bits consist of self-clocking bi-polar or phase-modulated pulses, depending upon the modulation mode selected.

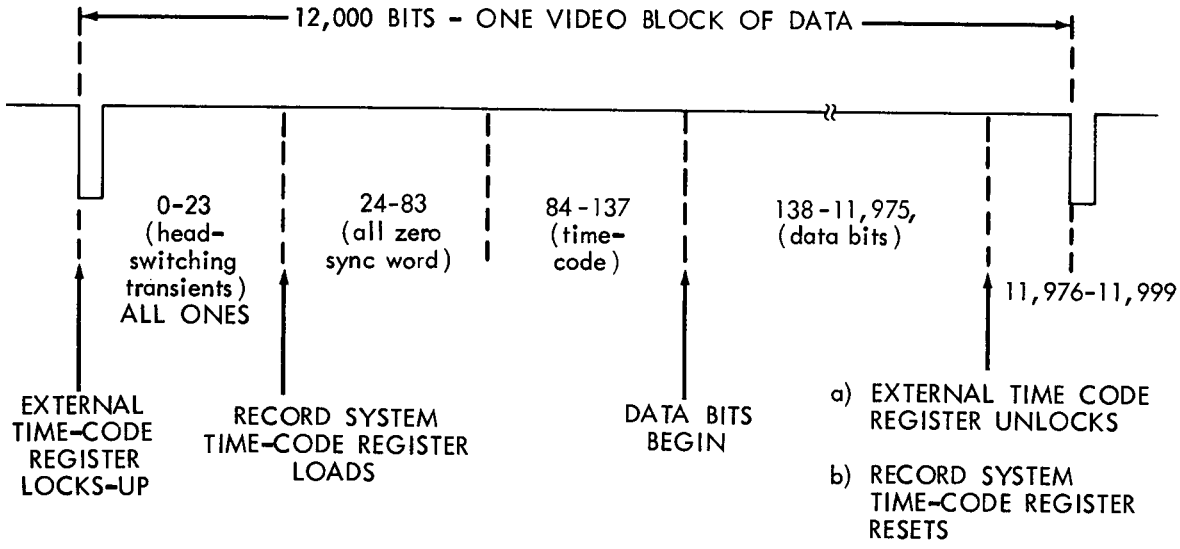

Figure 6. Video-Tape Format

A frame of data occupies the time required for one pass of the record head across the tape, or 16-2/3 msec. At a nominal sampling rate of 720 kbits/sec, a frame would accomodate 12,000 bits. Of these, 11,838 bits represent data; the remaining 162 are used for time-code and housekeeping words. At the beginning of each frame, the vertical sync signal corresponds to the beginning of a 24 bit all-one sequence designed to bracket the head-switching transient of the video play-back. Thus transients occurring during this period do not affect the data. Following the 24-bit sequence, a 60-bit all zero sequence is written. This serves as an unambiguous synchronization and frame-identifier during playback and is used to control the reformatting on the digital tape. Immediately after the 60-bit sequence, a 54-bit 8-4-2-1 BCD time-code, which registers the time of occurrence of the start of the frame (coinciding with the vertical sync pulse), is recorded. The time code extends from day of year to

units of microseconds. The data bits follow the time code. Prior to the end of the frame, 24 more ones are inserted to complete the head-switch word that brackets the start of the frame. Because each pulse is precisely related to each other pulse and because the time-code tags the start of the sync-word, recorder time-base errors in play-back (or recording) are not important. Also, signals to lock and unlock the external clock and load the recording system's time-code register are generated coinciding with the boundaries of the words in the frame.

The circuitry required to record the format described above on a video recorder is presented in Figure 7.

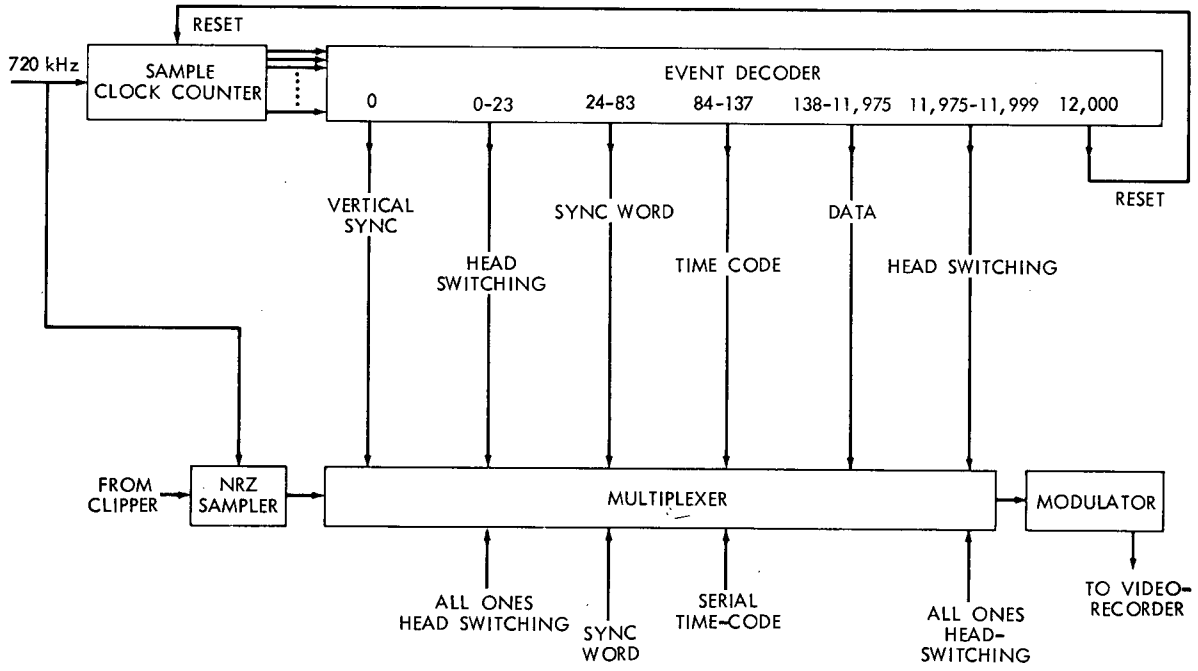

Figure 7. Data-Formatter Circuitry

The sampling frequency (720,960 kbits/sec) is generated either by direct division of the 5 MHz standard frequency or with the use of a nonintegral divider or frequency synthesizer. This sampling signal is used both to toggle the NRZ sampler flip-flop (which provides the clipped data to the multiplexer) and to drive the sample clock counter. Outputs of this counter are selected and combined to produce a number of logical commands. These commands trigger the multiplexer gates that assemble the various words that comprise the data frame. The decoding process which is all done on a bit-count basis, produces consecutively the trigger signals for the vertical sync, first head-switch,

sync-word, time-code, data-bits, and the second head-switch. At the end of the frame, a reset signal is initiated.

All bits that reach the modulator are generated in the multiplexer by gated flip-flops. When the system switch position is "Stop", the modulator receives all ones. When the switch position is "GO", the input to the modulator is all ones until the "Start time" trigger pulse generated by the coincidence of the clock reading with the preset "Start time" sets a flip-flop. At this time, the sync word is written on the tape. It is not possible to generate a "Start time" trigger pulse when the system switch is in the "Stop" position.

The modulator generates both bipolar RZ and phase-modulated (Manchester Coding) self-clocking record signals and feeds either type signal to the record heads, depending on the choice made by the operator. The present bit-rates are considerably lower than the maximum that can be handled by the recorder. Therefore, the bipolar output is generally used since it can be visually decoded. At bit rates above 1 Mbit/sec, the phase-modulated output will be advantageous. For the bipolar output, the NRZ data are clocked into two separate RZ signals: one with pulses representing data ones and the other with pulses representing data zeroes.

The video recorder is an Ampex VR-660C model, dual-head, helical scan machine with 2" tape width space designed for color television use. The recorder has large bandwidth, high recording density, and excellent servo control. These features make it possible to use the 660C to record and play back high-speed digital data economically on a machine designed for analog data. Servo control of the head drum, Capstan drive, and tape tension permits the data frames to be precisely synchronized with one head-switching rate of the recorder during recording and playback. The recorder, which has a 4.2 MHz bandwidth, can record conventional digital data at rates up to 1.5 Mbit/sec. The data rates can be as high as 5 Mbit/sec with the use of special encoding techniques (for example, sinusoidal wave-phase encoding). Recordings up to 4 hours duration can be made on a single reel of tape which is 4,800 feet long.

In the recording process, timing information derived from the system clock is used to automatically start a recoding program and also to incorporate in each data frame a 54 bit time word with a precision of 1 μsec. For the first step, thumbwheel switches are used to set the desired start time in terms of hours, minutes and seconds. Recording of data begins when the clock reading coincides with this setting. Since the clock is interrogated at the frame rate, the first frame will appear in less than 16.67 msec after the preset recording time. Starting with the first frame, the time word is inserted. The units of time,

ranging from hours to microseconds, are transferred from the clock register to the time code register and then to the tape.

2.3.3.3 Data Playback System. The playback system demodulates the data frame and places the bits in a shift register prior to shifting them out to the inputs of a nine-track digital recorder. The play-back instrumentation is shown in Figure 8.

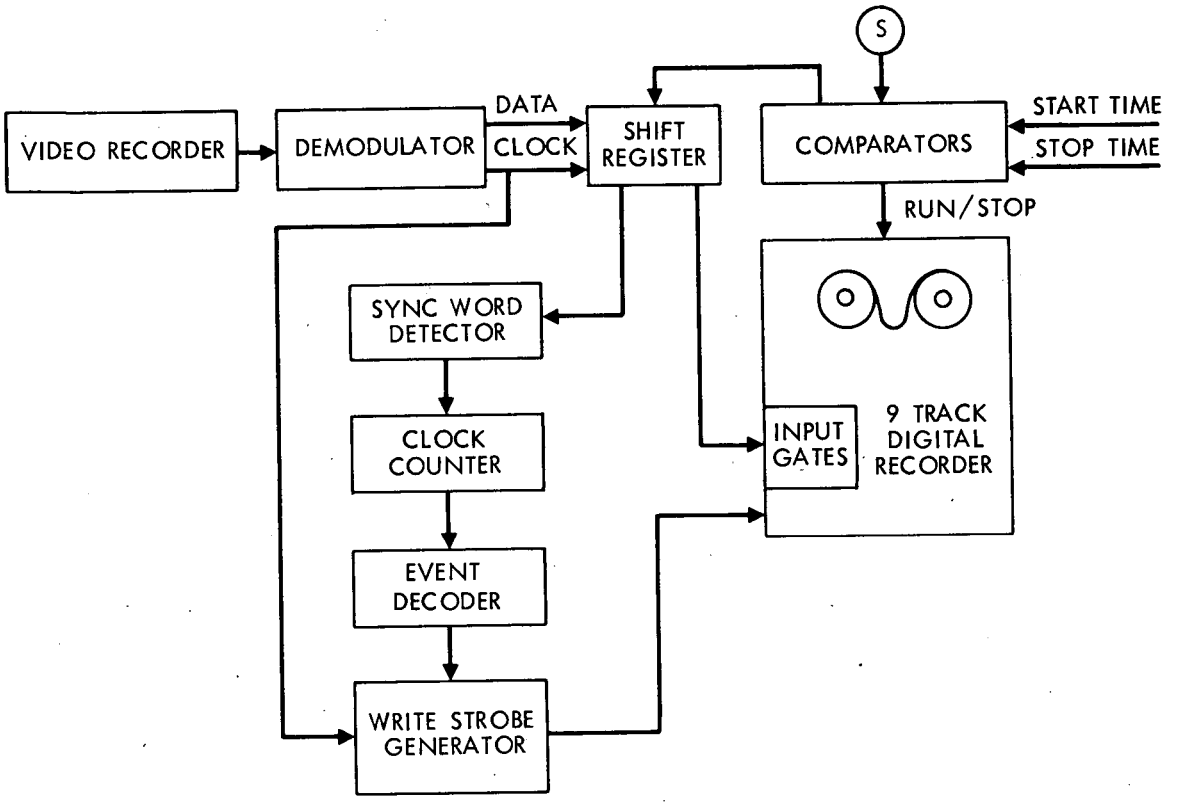

Figure 8. Playback Instrumentation

The arranging and shifting of the demodulated bits are predicted on the detection of the sync word. Similarly, the initial and terminal frames of data transcribed onto the digital tape are determined from a comparison of each time-code word with preset digital switch settings. Various formatting and housekeeping functions for the digital recording are derived from the clock counter and event decoder, which also provide the strobe signals to the recorder.

The digital data frame is transcribed from the video recorder track on to a nine-track digital tape, using a standard (ASC2) computer data format. The digital tape format is shown in Figure 9.

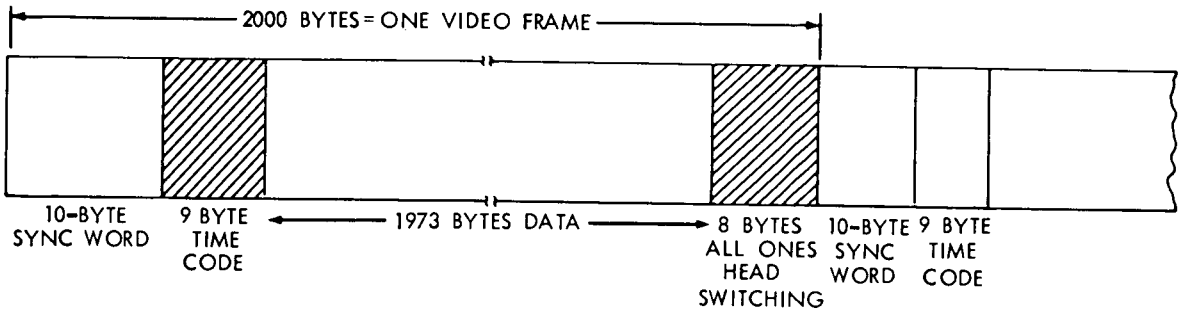

Figure 9. Digital Tape Format

Since the recorder has a maximum bit-packing density of 800 bits per inch and a tape speed of 150 inches/sec, the maximum data bit rate per track is 120 kbits/sec.

Therefore, the maximum data rate for the 9-track recorder is 960 kbit/sec; one track is used for vertical parity. The system is designed to accomodate the lower data-sampling rate of 720 kbit/sec. For data bandwidths greater than 960 kbits/sec, the bit packing density would have to be increased.

A digital-tape data frame consists of 2000 bytes (1 byte = 6 bits) recorded during 16-2/3 msec. It begins with a 10-byte sync word followed by a 9-byte time-code, 1973 bytes of data and an 8-byte word to span the period of the head-switching transients at the end of the frame. Time-base error in the video playback can be corrected by varying the length of the last word so that the digital-data rate of 120 kbyte/sec is satisfied. Each digital data frame corresponds to a video data frame. One digital record is composed of 12 data frames and is therefore 200 msec long. Part of every thirteenth video-data frame is omitted so that a 5 msec interrecord gap can be written.

The bit by bit operation of the playback system is self-clocked. The clock frequency is derived from the output of the demodulator, with the exception of the head-switch transient period, during which time a phase-locked oscillator is used to maintain the data-clocking frequency. Besides clocking the data through the 60 bit register and driving the counter, the clock output is also divided down to the 120 kbit/sec rate to drive the write strobe of the digital recorder.

Various tape interface functions such as end-of-file (EOF), vertical parity check, and check-word characters are also generated by the playback circuits. Provision is also made to reset manually the decoding sequence if the synchronization word should fail to be detected subsequent to the start of playback. The digital recorder is a 9-track Ampex TM-12 high speed recorder. In its record mode, all control functions are assumed by the playback-system electronics.

2.3.3.4 Frequency and Timing System. The sampling and recording of the data on the video recorder are controlled by a precision frequency standard which also provides the frequencies used in the coherent conversion of the radio frequency input signal to video. Either a Hydrogen maser or a rubidium vapor cell (HP-5065A) oscillator is used as the frequency standard. At C-band, the phase stability is less than one radian in 100 seconds with the rubidium standard. This is improved by almost a factor of 50 with the maser. While the maser is very essential for precision measurements of fringe frequency, the rubidium oscillator is sufficiently stable for the levels of time and phase-resolution currently required.

The frequency standard must also drive clocks and maintain a time-synchronization between stations of at least 5 μsec during the experiment. Figure 10 shows the VLBI timing system.

The frequency standard provides a 1 MHz drive to the digital clock, which accumulates and visually displays the Universal time with 1- μsec precision. Associated with the clock is a delay generator that accepts the system 1 pps signal and digitally delays it up to 999,999 μsec. The purpose of the delay generator is to set in the Loran-C propagation delay associated with various Loran stations. It can also be used to set other time signals such as the 1 pps from a portable clock in coincidence with the system 1 pps, thereby determining their relative offset.

The principal clock-setting means are comparisons with portable clocks carrying accurate UTC (USNO) time and with Loran-C transmissions. The digital clock is designed so that it can be directly reset to the 1 pps portable clock signal. Alternatively, the portable clock can be used to demand a reading of the system clock at a 1-pps rate, thereby displaying the epoch difference between the two clocks. When it is desired to set the system clock with Loran-C, a selected zero-crossing of the received radio wave form is displayed on an oscilloscope. The scope trigger is provided by the Loran Rate Generator and is the simulated Loran pulse rate delayed by the propagation time. The delayed pulse rate is produced by resetting the rate generator with a pulse generated at a time of coincidence (TOC), suitably delayed to account for propagation and

system delays. The TOC is determined from Naval Observatory tables for a particular Loran chain. On the east coast, it is Cape Fear, North Carolina. On the west coast, it is Dana Point, Indiana. After this resetting, the rate-generator output is coincidental with the time-of-arrival of the Loran-C pulses. After visual alignment is attained with the oscilloscope, the Loran 1 pps is used either to reset the clock or to determine the epoch difference.

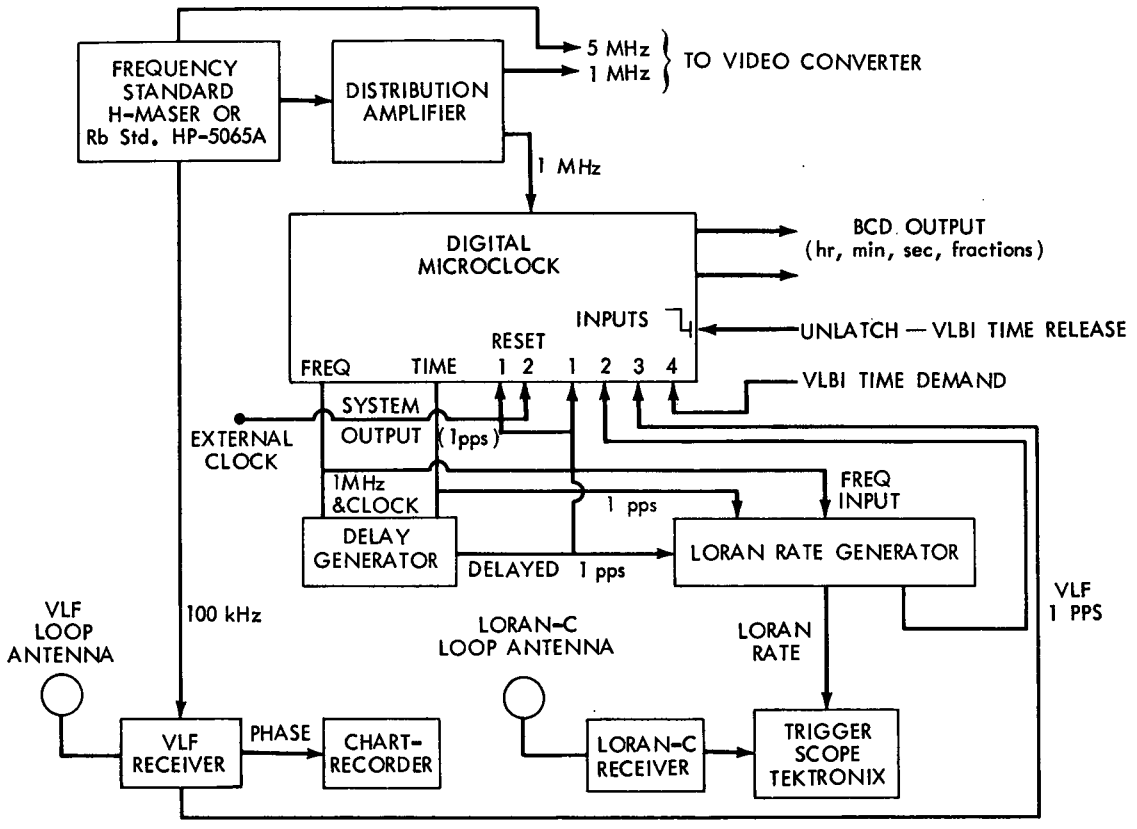

Figure 10. VLBI Timing System

The "demand" inputs of the system clock permit the clock display to be frozen at receipt of the demand input pulse. Provision is made to "demand" the clock with the Loran - generator output, the delayed clock 1 pps, a VLF 1 pps signal and the VLBI time-demand signal from the event decoder. In addition to a Loran receiver, a VLF receiver and chart recorder are included in the timing system to provide a means of monitoring long-term frequency drift of the frequency standard.

In the Rosman-Mojave experiment, the VLBI clock at Mojave was set by a portable Cesium clock and was also regularly monitored by a microwave relay signal, both derived from neighboring JPL/Goldstone Echo site. The

Rosman VLB clock was set by Loran-C transmission from Cape Fear, North Carolina.

The two VLBI clocks were also synchronized using the satellite pulse exchange technique. Pulses at C-band with very sharp rise-time and of 10 μ sec duration were exchanged by the two stations through the dual transponders of the ATS-3 geostationary satellite. At each station, a time-interval counter was started by the transmitted pulse and stopped by the pulse received via satellite from the other station. The probable error of the clock-offset as measured by the counter is 10 nanoseconds. The clock offset data was recorded regularly. Whenever the offset value exceeded 5 μ sec, the Rosman clock was adjusted using the delay-generator to keep the offset well within 5 μ sec. This technique worked out very well and added great reliability to the experiment.

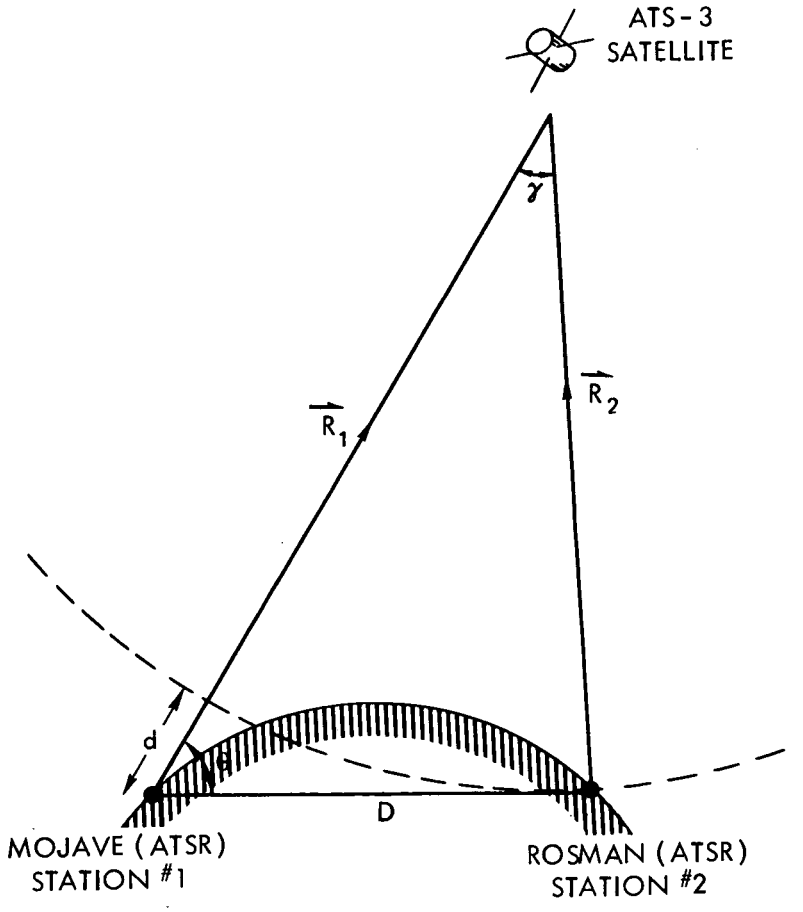

Figure 11. Geometrical Configuration of a Single Baseline Experiment

3. INTERFEROMETRIC EQUATIONS

In the simplest terms, an interferometor is an instrument for measuring the phase difference between electromagnetic waves received simultaneously at any two of its terminals. The very long baseline interferometer (VLBI) uses atomic frequency standards to preserve electrical phase coherence between its terminals, thus dispensing with the cables or microwave links customarily employed for this purpose. Closely regulated, but free-running and independent, these standards can be placed at arbitrarily chosen locations to allow the baselines to achieve a length of the order of several million wavelengths of the received signal. Given such long baselines, low-noise front-end receivers, wideband VLBI recording systems and stable local oscillators, the VLBI systems are able to resolve signal time-delays to an accuracy that is several orders of magnitude better than that is accomplished by conventional tracking techniques.

The VLBI technique has been demonstrated to have the capability to resolve radio sources with a precision of the order of a millisecond of arc. The potential for precision measurement of angular positions of radio sources is correspondingly great and is just now being exploited. The adaptation of VLBI to satellite tracking therefore appears to be a highly desirable objective.

Figure 11 shows the geometrical configuration of a single baseline VLBI experiment. From the geometry

$$d + R_2 = R_2 \cos\gamma + D \cos\theta \tag{1a}$$

$$R_2 \sin\gamma = D \cos\theta \tag{1b}$$

The difference in the time of reception of the signal at the two antennas is then given by

$$\tau_g = \frac{d}{c} = \frac{D}{c}\left[\cos\theta - \frac{(1-\cos\gamma)}{\sin\gamma}\sin\theta\right] \tag{2}$$

or

$$\tau_g = \frac{D}{c}\,\frac{\cos(\theta + \gamma/2)}{\cos\gamma/2} \tag{3}$$

since

$$\tan\frac{\gamma}{2} = \frac{1 - \cos\gamma}{\sin\gamma}$$

and c denoting the velocity of light.

If D is known and τ_g and R_2 are measured then by Eqs. 1b and 3, the angle θ is determined. When the satellite recedes to infinity, $\gamma \to 0$, the time delay expression takes the form applicable to astronomical sources, $\tau_g = \frac{D\cos\theta}{c}$.

An alternative for the satellite time delay is

$$\tau_g = \frac{R_1 - R_2}{c} \tag{4}$$

where R_1 and R_2 are station to satellite range for the respective stations.

The fringe frequency is given by

$$\nu_f = f\frac{d\tau_g}{dt} \tag{5}$$

where f is the signal frequency this can be written as a relative doppler frequency

$$\nu_f = \frac{f}{c}(\dot{R}_1 - \dot{R}_2) \tag{6}$$

Since we are interested in the nature of the correlation function, it is necessary to analyze the interferometer response to wideband noise.

The voltage induced by the source in the antenna #2 is of the form

$$V_2(t) = e^{i[\omega(t - \tau_g) + \phi_{T2}(t)]} \tag{7}$$

Where ω is the received signal frequency and ϕ_{T2} is the phase shift due to the transmission media linking station #2 and the source. τ_g is the time-delay or the differential time of arrival of the identical wavefront at station #1 relative to the arrival time at Station #2.

The voltage induced by the source at the antenna #1 is of the form

$$V_1(t) = e^{i[\omega t + \phi_{T1}(t)]} \tag{8}$$

The above expressions signify that the wavefront reaching station #1 at a time t has reached station #2 at an earlier time, $(t - \tau_g)$. $\phi_{T1}(t)$ is the phase shift due to the transmission media linking station #1 and the source.

The received signals are then mixed with corresponding local oscillator signals of the form

$$V_{10}(t) = e^{i[\omega_{10}(t) + \phi_{I1}(t)]} \tag{9}$$

For Station #1

$$V_{20}(t) = e^{i[\omega_{20}(t) + \phi_{I2}(t)]} \tag{10}$$

Where ω_{10} and ω_{20} are the local oscillator frequencies at the stations 1 and 2 respectively. $\phi_{I1}(t)$ and $\phi_{I2}(t)$ are the instrumental phases at the stations 1 and 2 respectively.

The mixed outputs at the two stations are of the form (assuming ω_{10}, $\omega_{20} < \omega$).

$$V_1'(t) = V_1(t)\, V_{10}(t) = e^{i[(\omega - \omega_{10})t + \phi_{T1}(t) + \phi_{I1}(t)]} \tag{11}$$

$$V_2'(t) = V_2(t)\, V_{20}(t) = e^{i[(\omega - \omega_{20})t - \omega\tau_g + \phi_{T2}(t) + \phi_{I2}(t)]} \tag{12}$$

In one cross-correlation process, the signal from station #1 is offset by a model time-delay τ_d and the signals are multiplied together to produce a beat signal of the form

$$\begin{aligned} V_{out} &= V_1'(t - \tau_d) V_2'(t) \\ &= e^{i[(\omega - \omega_{10})(t - \tau_d) + \phi_{T1}(t) + \phi_{I1}(t)]} \cdot \\ &\quad e^{i[(\omega - \omega_{20})t - \omega\tau_g + \phi_{T2}(t) + \phi_{I2}(t)]} \end{aligned} \tag{13}$$

$$V_{out} = e^{i\left[(\omega_{20} - \omega_{10})\, t - (\omega - \omega_{10})\, \tau_d + \omega \tau_g + \Delta\phi_T(t) + \Delta\phi_I(t)\right]} \tag{14}$$

where

$$\Delta\phi_T(t) = \phi_{T1}(t) - \phi_{T2}(t)$$

$$\Delta\phi_I(t) = \phi_{I1}(t) - \phi_{I2}(t)$$

After the heterodyne operation, one can compute the correlation function which is proportional to the real part of the beat signal.

$$R(\tau_g, \tau_d) \propto^{\ell} \text{Real}\,(V_{out}) = A \cos\left[\omega\,(\tau_g - \tau_d) + \omega_{10}\,\tau_d + \Delta\phi_T(t) + \Delta\phi_I(t)\right] \tag{15}$$

Let us assume that the two local oscillator frequencies are identical. Then

$$R(\tau_g, \tau_d) \propto^{\ell} A \cos\left[\omega\,(\tau_g - \tau_d) + \omega_o\,\tau_d + \Delta\phi_T(t) + \Delta\phi_I(t)\right] \tag{16}$$

The correlation function has a maximum when $\tau_g = \tau_d$

Then

$$R_{max}(\tau_g, \tau_d) \propto^{\ell} A \cos\left[\omega_o\,\tau_g + \Delta\phi_T(t) + \Delta\phi_I(t)\right] \tag{17}$$

If more than one local oscillator is used, ω_0 is the "effective" local oscillator frequency.

Also because of the $2\pi n$ ambiguity involved in the inversion of trigonometric functions, only the time-dependence of phase may be obtained from the correlation function. That is, the phase may be determined except for an unknown additive constant. The fourier-analysis technique is used to determine the fringe frequency.

$$\nu_f = \omega\,(\dot{\tau}_g - \dot{\tau}_d) + \omega_o\ \dot{\tau}_d + \Delta\dot{\phi}_T + \Delta\dot{\phi}_I \tag{18}$$

where the "dot" represents the time derivative of each parameter.

Position determination depends directly on the measurement of time-delay, τ_g . The accuracy of τ_g in turn depends on having a broad-bandwidth source and a capacity for recording and processing over a sufficiently wide bandwidth in the cross correlation of signals. The significance of increased

bandwidth is reflected in the nature of the correlation function. For a monochromatic signal

$$R(\tau_g) \approx A \cos[\omega_o \tau_d + \omega(\tau_g - \tau_d) + \Delta\phi_T + \Delta\phi_I] \tag{19}$$

For a wide band signal, the cross-correlation function becomes

$$R(\tau_g, \tau_d) = \Delta\omega \frac{\sin \Delta\omega (\tau_d - \tau_g)}{\Delta\omega (\tau_d - \tau_g)} \cos[\omega_o \tau_g + \Delta\phi_T + \Delta\phi_I] \tag{20}$$

Where $\Delta\omega$ is the recorder bandwidth. The uncertainty in determining τ_g decreases with increasing bandwidth as $(\Delta\omega)^{-1}$. Most recorders used in VLBI have a recording range from 360 kHz to 2.0 MHz. For bandwidths larger than 2.0 MHz, the bandwidth synthesis technique is utilized to cover a large bandwidth. In the bandwidth synthesis technique, the local oscillator and paramp, at both the terminals are switched in frequency in steps and synchronously retuned by means of programmed bias voltages. Careful phase calibration is done at the beginning of each switching.

Why is it necessary to switch the received frequency over a wideband rather than to simply record a band sufficiently broad to yield high accuracy in differential delay? The basic reason arises from the lack of real-time wideband data link between the receiver elements of a VLBI system. The necessity to record the predetected signal causes the instantaneous bandwidth of the VLBI system to be limited by that of the recorder, which in practice is a very small fraction of the received signal frequency. This constraint is overcome by varying the received frequency synchronously and coherently in cycles consisting of several steps. The bandwidth spanned is then not limited by the recording system but only by the bandwidth of the radio frequency amplifiers used.

Thus, the following steps are undertaken in the determination of the fringe phase.

1) RF signals are received, amplified and converted to video at as large a bandwidth as possible.

2) At each terminal the video signal is clipped so that all positive areas of its signal have a value of 1 and all negative areas are zero. The clipped signals are sampled at the Nyquist rate of twice the bandwidth and the bit strings are recorded on video or magnetic tape. Timing information is inserted in the data format.

3) The tapes are brought together at a correlator which may be a digital

computer (CDC-6400, IBM-360-91, 75, 95) or a computer of special design. For each record, the bit streams are shifted relative to one another by an amount that corresponds to the theoretically predicted geometrical delay plus any fixed instrumental delay. This serves to produce "white" fringes. The records are then correlated. Usually, it is advantageous to divide the correlation interval into a number of sub-intervals in each of which the earth's rotation rate can be considered a constant.

4) The correlation function for each sub-interval or "frame" is corrected for sampling and for finite record length. Then it is multiplied by the trial function $e^{j\omega_T \delta t}$ where ω_T is the sum of all frequencies that tend to rotate the fringes (eg: earth's rotation rate, fringe-rotation rate and other unknowns) and δt is the length of the sub-interval. This is repeated for a number of guesses for the unknown phase rate.

5) Each of the modified correlation functions computed above is subjected to Fourier Transform. The case for which the transform peaks is taken to be the solution. For this case, the total phase-delay that has been applied to the signal is recorded. The wider the bandwidth, the fewer are the deep fringes and therefore the more precisely the white fringe region can be identified.

For infinite record length, the correlation function has the form

$$R(\tau) = \int_{-\infty}^{\infty} x(t) \cdot x(t+\tau)\, dt \qquad (21)$$

But in practice, for finite record length

$$R_{00}(\tau) = \int_{T-\Delta t/2}^{T+\Delta t/2} x(t-\Delta t/2)\, x\,(t+\Delta t/2)\, dt \qquad (22)$$

The purpose of applying a correction is to create a modified correlation function $R_0(\tau)$ whose transform exists and is equal to the average value of the true transform. It is created by using a function known as the Hanning weighting function. It is also called the "Lag-window." The function is characterized as follows:

$\omega(0) =$ normality

$\omega(-\tau) = \omega(\tau)$ symmetry

$\omega(\tau) \geqslant T_n = 0$ where T_n is the length of the record.

Two widely used functions are

$$\omega(\tau) = \frac{1}{2}\left[1 + \cos\frac{\pi\tau}{T_m}\right] \quad ;|\tau| < T_m$$
$$= 0 \quad ;|\tau| > T_m \tag{23}$$

and

$$\omega(\tau) = 0.54 + 0.46\cos\frac{\pi\tau}{T_m} \quad ;|\tau| < T_m$$
$$= 0 \quad ;|\tau| > T_m \tag{24}$$

It is usual to guess a number of trial-delay offsets and to evaluate the Fourier Spectrum of the fringes corresponding to each offset. The offset that causes the spectral response to peak is chosen to be the correct value of delay, i.e. the value that establishes the white fringe condition.

Let us suppose that the signal received in one channel is delayed so that at that moment all frequencies within the bandwidth are in phase. If the ratio of BW to the nominal frequency is small, then all the frequencies will remain almost perfectly in phase during some subsequent time interval. Within this interval, the interferometer response will remain almost perfectly sinusoidal in shape, even though the bandwidth is of nonvanishing extent. Then the interferometer is said to be operating in the "white fringe" condition, i.e. all the frequencies are present in the deep fringes.

The power spectrum is denoted by

$$S(\omega) = \lim_{T\to\infty}\frac{1}{T}\int_{-T}^{T} R(\tau)\,e^{j\omega\tau}\,d\tau \tag{25}$$

This in general will have the complex form

$$S(\omega) = A(\omega)\,e^{j\Delta\phi}\,e^{j\omega_T t} \tag{26}$$

Where $\Delta\phi$ is the phase-delay evaluated at the beginning of the recording interval and ω_T represents the total fringe rotation rate during that interval due to all causes. The interval is chosen small enough that ω_T is taken as a constant. Some effects that contribute to the ω_T are the fringe rate offset, rotational motion of the earth, and accumulated errors due to clock instability etc. If a

modified visibility function $S'(\omega)$ is defined as

$$S'(\omega) = \frac{1}{T}\int S(\omega)\, e^{j\omega'_T t}\, dt \tag{27}$$

Where ω'_T is the trial function which includes a guess for the unknown term, then it is clear that $S'(\omega)$ is maximized when $\omega'_T = \omega_T$; because $S(\omega)$ is close to a sinusoid and the integrated product of two sinusoids is nonvanishing when and only when their frequencies are equal. In practice, the offset can be determined by this method to better than 0.001 Hz. Usually, the integrations with respect to τ and t are more conveniently reversed, for then the fourier transform need not be evaluated so frequently.

As mentioned earlier, maximum correlation is obtained if the recordings were offset by an amount equal to the time required for the wave to traverse the difference in distance between the source of the two sites. As the offset is changed from this amount, the two recordings would become more and more out of phase (up to a point) and the cross correlation would decrease.

But the cross-correlation will be a maximum for many values of τ (depending on the length of the recording) each of which differs from the other by the equivalent of 2π in the phase of the signal. Thus

$$c\tau_g = n\lambda + \delta\lambda \qquad ; \; 0 \leqslant \delta\lambda < \lambda \tag{28}$$

$$2\pi f\tau_g = 2\pi n + \phi$$

$$f\tau_g = n + \frac{\phi}{2\pi} \tag{29}$$

Where n is an integer which is not determinable from a single frequency measurement. If we record a bandwidth Δf instead, the ambiguities will now spread only over a time offset interval approximately equal to $(\Delta f)^{-1}$. Then, the cross-correlation as a function of the difference, $\Delta\tau$, between the offset and the time delay is proportional to

$$\frac{\sin\left[2\pi\Delta f\Delta\tau_g\right]}{2\pi\Delta f\Delta\tau_g}\cos\left(2\pi f\Delta\tau_g\right) \tag{30}$$

The first term provides the $\frac{\text{Sin } x}{x}$ envelope that restricts the ambiguity in the correlation maximum of $\cos 2\pi f\Delta\tau_g$ to lie within a width of $(\Delta f)^{-1}$.

There are alternate ways to minimize the error in the determination of $\Delta\tau_g$. The fringe phase is given by the expression

$$2\pi f\tau_g = 2\pi n + \phi \tag{31}$$

then

$$\frac{d\phi}{df} = 2\pi\tau_g$$

$$\tau_g = \frac{1}{2\pi}\frac{d\psi}{df} \tag{32}$$

i.e., the delay sought is simply the slope of the phase versus frequency curve: at a given instant, the cross-correlation will have a maximum at a different phase for each different frequency in the sampled band. The time offset stays constant at all frequencies. In practice, a geometrical offset is used before correlation is done. Then the error in the estimation of τ_g is

$$\Delta\tau_g = \frac{\Delta\phi}{2\pi(f_{max} - f_{min})} = \frac{\Delta\phi}{2\pi\Delta f} \tag{33}$$

Where Δf is the effective wideband (360 kHz, 2.0 MHz, 30 MHz, etc.) and $\Delta\phi$ is the net phase change in the bandwidth interval. $\tau_g + \Delta\tau_g$ is the true time-delay at any instant. One can measure the phase/frequency slope to greater accuracy than is possible in extracting the bit offset from the correlation spectrum where the region of ambiguity has a width of $(\Delta f)^{-1}$.

4. VLBI SYSTEM RESOLUTION

The sources for the interferometric measurements can be either natural or artificial radio sources. Among the natural radio sources, the most desirable are the strong, broad-band point-sources of extremely small angular dimensions (a few arc seconds) and with negligible proper motion. These are quasars.

Detectability of the noise signals from the tracked sources is a critical problem in interferometry. The total background noise coupled with the receiver noise is the dominant contributor to the system noise temperature. The effective signal noise ratio of an interferometer pair is given by:

$$\frac{S}{N} = \left[\frac{T_{a_1}}{T_{s_1}} \frac{T_{a_2}}{T_{s_2}} (BW)\,\tau \right]^{\frac{1}{2}} \tag{34}$$

Where T_{a_1} and T_{a_2} are the antenna temperatures of stations 1 and 2 respectively, T_{s_1} and T_{s_2} are their respective system temperatures, (BW) is the instantaneous recorded bandwidth and τ is the integration time.

$$T_{a_1} = \frac{S_o A_1 \eta_1}{2k}$$
$$T_{a_2} = \frac{S_o A_2 \eta_2}{2k} \tag{35}$$

Where S_0 is the observed source flux density in Watts/m^2 cps,

A_1 and A_2 are the aperture areas of antennas 1 and 2 respectively, η_1 and η_2 are their efficiencies, k is the Boltzmann Constant = 1.38×10^{-23} joules°K.

$$\frac{S}{N} = \frac{S_o}{2k} \left[\frac{(A_1\eta_1)(A_2\eta_2)(BW)(\tau)}{T_{s_1} T_{s_2}} \right]^{\frac{1}{2}} \tag{36}$$

$$\frac{S}{N} = \frac{\pi S_o}{8k} D_1 D_2 \left[\frac{\eta_1\eta_2 (BW)(\tau)}{T_{s_1} T_{s_2}} \right]^{\frac{1}{2}} \tag{37}$$

Where D_1 and D_2 are the diameters of antennas 1 and 2 respectively.

A few typical examples of signal to noise ratio is illustrated below:

Rosman-Mojave Baseline [ATS-3 Satellite] :

D_1 = 85 x 0.3 meters

D_2 = 40 x 0.3 meters

$\eta_1 = \eta_2 = 0.5$

(BW) = 360 kHz

τ = 1 sec

$T_{s_1} = T_{s_2} = 65°K$

$S_o \approx 2.77 \times 10^{-18}$ watts/m^2 The transponder output is 446 watts.

The signal to noise ratio will then be (For the ATS-3 Satellite Case):

$S/N \simeq 75$ db

Agassiz-Owens Valley Baseline [ATS-3 Satellite] :

D_1 = 84 x 0.3 meters

D_2 = 130 x 0.3 meters

$\eta_1 = \eta_2 = 0.5$

(BW) = 360 kHz

τ = 100 sec

$T_{s_1} = 350°K$

$T_{s_2} = 180°K$

$S_o = 2.77 \times 10^{-18}$ watts/m^2

$S/N \simeq 85$ db

Similar signal to noise ratio computations can be made for the case when the observed sources are quasars. Let us assume that a quasar of flux density 10 units is monitored at the two terminals.

Then S_0 = 10 flux units = 10^{-25} watts/m^2 .

For Rosman-Mojave baseline (integration time $\tau \simeq 100$ sec)

$$\frac{S}{N} \simeq 16 \text{ db}$$

For Agassiz-Owens Valley vaseline (integration time $\tau \simeq 100$ sec)

$$\frac{S}{N} \simeq 15 \text{ db.}$$

The use of the satellite transponder as a radio frequency source permits high resolution time-delay interferometry because the spectral energy density of the transmitted signal is extremely high compared to celestial sources. Flux densities correspond to an apparent source brightness about more than 100 db greater than the brightest quasar source at C-band.

Time-Delay Resolution Uncertainties: Significant timing errors are due to three principal causes:

1. clock epoch-alignment errors between the two stations.

2. long-term phase drifts in the atomic frequency standards used at the two stations.

3. recording-bandwidth limitations.

The clock-epoch alignment error (or the clock offset error) can be treated as an unknown while observing quasars and the time-delay observations from several sources will yield the clock offset parameter. While observing satellites, one has to resort to independent means for synchronizing clocks or accurately determining their relative offset. In our experiments, both the procedures were adapted. Clock synchronization experiments were conducted using the dual transponders of the ATS-3 and ATS-1 satellites and the clocks were synchronized to within 10 nanoseconds. Also, extensive quasars observations from the same sites also yielded the clock offset as a solution from the time-delay equations.

Over sufficiently long observing periods, phase drifts in the atomic frequency standards also produce significant timing errors. Both rubidium-vapor and hydrogen maser frequency standards are employed in the VLBI experiments. Recent data indicate that a stability figure of 1 part in 10^{-12} is achieved with rubidium standards; hydrogen masers are about 1.5 to 2.0 orders

of magnitude better stability. Over a 24 hour period, the maximum accumulated time-error with a rubidium standard can be expected to be around 0.1 μ sec.

The time-delay resolution of the VLBI recording system is given by the formula:

$$\epsilon_{\Delta\tau} \simeq \frac{1}{2\pi(BW)\sqrt{S/N}} \cdot \frac{1}{\nu} \qquad (38)$$

Where S/N is in the signal-to-noise ratio, (BW) is the recording badnwidth ($\sim$ 360 kHz) and ν is the number of independent observations. Thus the factors affecting the precision of the VLBI measurements are the overall signal-to-noise ratio, the instantaneous recording bandwidth, the stability of the reference local oscillator and the unknown atmospheric and instrumental phase fluctuations.

Based on the equation for $\epsilon_{\Delta\tau}$, it is possible to compute the time-delay resolution for the case of satellites and quasars. A nominal recording bandwidth of 360 kHz is assumed for both the cases.

For the ATS-3 Satellite Case:

$S/N \approx 75$ db $\approx 3 \times 10^7$

$\nu = 1$

Then, $\epsilon_{\Delta\tau} \approx 0.1$ nsec

In practice, however, the time-delay resolution that is achieved is limited by the frequency stability of the reference oscillator. The attainable time-delay resolution is of the order of 5 nanoseconds.

For quasars ($\sim$ 10 flux units):

$S/N \simeq 15$ db

$\nu = 1$

$\epsilon_{\Delta\tau} \simeq 75$ nsec.

It is therefore possible to develop the overall system resolution criteria for the Rosman-Mojave and Agassiz-Owens Valley baselines. The following table (Table 3) summaries the criteria.

TABLE 3

VLBI System Resolution Criteria

Criterion	Parameter	Satellite (ATS-3)	Quasar (10 F.U.)
Signal-to-Noise Ratio	Time-Delay	5 nsec	75 nsec
	Fringe-Rate	500-1000 μHz	5-10 mHz
Stability of the Reference Frequency Standard ~ 1 Part in 10^{13}	Time-Delay	5 nsec	10 nsec
	Fringe-Rate	200 μHz	1 mHz

Expected System Resolution		
Parameter \ Source	ATS-3 Satellite	Quasar
Time-Delay	5 nsec	75 nsec
Fringe-Rate	100 - 500 μHz	5 mHz

5. DATA ANALYSIS

5.1 OBSERVATION ROUTINE

A basic observation routine was followed in which one station (usually Rosman) transmitted an uplink carrier signed with a preselected modulation. The recording bandwidth in the experiment was 360 KHz. Increased recording bandwidth improves the measured time-delay resolution. However, marked improvement can be achieved with narrowband (360 KHz) recording if signal of specific spectral distributions are transmitted/received to/from the spacecraft transponder. Several modulation schemes were utilized as VLBI beacon signals to test their effect on the cross-correlation function. The modulations utilized in the experiment are listed in the following table.

TABLE 4

Signal Modulations

Modulation	Description
Noise Translation	Frequency translated broadband noise. Noise bandwidth 12 MHz
FM Noise	Frequency modulated carrier using 0-12 MHz bandwidth Marconi noise generator
Spacecraft Noise	Front-end noise emitted by the ATS-3 transponder at 4178 MHZ
PRS	Pseudorandom sequency modulation using clock-rates of 500 k bits/sec 1000 k bits/sec, 2 M bits/sec, 4 M bits/sec
Range Tones	Ensemble of range tones simultaneously used to modulate the carrier. The tones are 160 Hz, 4KHz, 20 KHz, 100 KHz and 500 KHz

The basic observation routine called for Rosman to transmit an uplink signal at 6301 MHz with a preselected modulation. The signal is transponded back to the earth from one of the ATS-3 transponders (Transponder #2, 6301

MHz uplink/4178 MHz downlink). The downlink signal is received at Rosman and Mojave. Both stations recorded the data simultaneously for 9 minutes. A variety of modulation schemes were utilized in a daily routine. Immediately before and after each VLBI recording, SHF ranging (R and $\dot{R}$) was conducted simultaneously from Rosman and Mojave using the dual transponders on the spacecraft. The ranging duration was normally three minutes. The ranging data is utilized to compute independently the spacecraft orbit for comparison with the orbital elements computed from the VLBI data. It also provides rough estimates of time-delay (τ_g) and fringe-rate (ν_f) for the intervening VLBI recording period. It would also have been desirable to conduct a systematic test on the effect of varying SNR on the precision of τ_g and ν_f (VLBI parameters). This however turned out to be not feasible since the spacecraft transponders are hard limited and there is little flexibility in varying the output power of the transponders.

A typical experiment schedule is shown in Table 5.

5.2 CLOCK-SYNCHRONIZATION

The VLBI clock at Mojave was set by a portable cesium clock and was also regularly monitored by a microwave relay signal both derived from the neighboring JPL/Goldstone Echo-Site. The Rosman clock was checked by monitoring Loran-C transmissions from Cape Fear, North Carolina.

The synchronization between the Rosman and Mojave clocks was achieved by the simultaneous exchange of microwave signal pulses of 10 μsec duration and a very sharp rise-time via the dual transponders of the ATS-3 or ATS-1 satellites. A precision of 10 nanoseconds was accomplished using this synchronization technique. More details of this time-synchronization experiment can be found in the report "VLBI clock synchronization tests conducted via the ATS Satellites" by J. Ramasastry et. al., NASA/GSFC, X-553-71-514, November 1971.

5.3 ATMOSPHERIC PARAMETERS

Both the troposphere and the ionosphere are significant sources of error in the measurement of the time-delay and fringe-rate parameters. The ionospheric error can be large at L-band (1600 MHz) and even at S-band (2200 MHz). At C-band (4000 MHz) which is the frequency that was used in our experiments, the ionospheric influence is extermely small. The atmospheric error becomes large at low elevation angles. Table 6 summarizes the ionospheric and atmospheric time-delay errors at various zenith angles.

TABLE 5

Typical Daily Experiment Schedule

Stations: Rosman & Mojave Source: ATS-3 Statellite

	Time (GMT)	Duration (min)	Transition (min)	Stations	Mode of Operation	Comments
First Session	T+0	10	5	R/M	Time synchronization test	Dual SHF transponders used
	T+15	3	2	R/M	(R) - VHF Ranging (M) - SHF Ranging	Two frequency ionospheric calibration
	T+20	3	2	M/R	(M) - VHF Ranging (R) - SHF Ranging	
	T+25	3	2	R/M	SHF Ranging	Simultaneous
	T+30	6	4	R/M	VLBI Recording	Rosman Xmit. noise translation
	T+40	3	2	R/M	SHF Ranging	Simultaneous
	T+45	6	4	R/M	VLBI Recording	Rosman Xmit. noise translation
	T+55	3	2	R/M	SHF Ranging	Simultaneous
	T+60	6	4	R/M	VLBI Recording	Rosman Xmit. FM noise
	T+70	3	2	R/M	SHF Ranging	Simultaneous
	T+75	6	4	R/M	VLBI Recording	Rosman Xmit. FM noise
	T+85	3	2	R/M	SHF Ranging	Simultaneous
	T+90	6	4	R/M	VLBI Recording	No Xmission Spacecraft noise
	T+100	3	2	R/M	SHF Ranging	Simultaneous
	T+105	6	4	R/M	VLBI Recording	No Xmission Spacecraft noise
	T+115	3	2	R/M	SHF Ranging	Simultaneous

TABLE 5 (cont.)

	Time (GMT)	Duration (min)	Transition (min)	Stations	Mode of Operation	Comments
First Session	T+120	6	4	R/M	VLBI Recording	Rosman Xmit PRS 500 kbit/ sec
	T+130	3	2	R/M	SHF Ranging	Simultaneous
	T+135	6	4	R/M	VLBI Recording	Rosman Xmit. Prs. 500 kbit/ sec
	T+145	3	2	R/M	SHF Ranging	Simultaneous
	T+150		60		Intermission	
Second Session	T+210	10	5	R/M	Time synchronization test	ATS-3 dual transponders used
	T+225	3	2	R/M	SHF Ranging	Simultaneous
	T+230	6	4	R/M	VLBI Recording	Rosman Xmit. noise trans- lation
	T+240	3	2	R/M	SHF Ranging	Simultaneous
	T+245	6	4	R/M	VLBI Recording	Rosman Xmit. Noise trans- lation
	T+255	3	2	R/M	SHF Ranging	Simultaneous
	T+260	6	4	R/M	VLBI Recording	Rosman Xmit. Noise trans- lation
	T+270	3	2	R/M	SHF Ranging	Simultaneous
	T+275	6	4	R/M	VLBI Recording	Rosman Xmit. FM noise
	T+285	3	2	R/M	SHF Ranging	Simultaneous
	T+290	6	4	R/M	VLBI Recording	Rosman Xmit. FM Noise
	T+300	3	2	R/M	SHF Ranging	Simultaneous

TABLE 5 (cont.)

	Time (GMT)	Duration (min)	Transition (min)	Stations	Mode of Operation	Comments
Second Session	T+305	6	4	R/M	VLBI Recording	Rosman Xmit. FM noise
	T+315	3	2	R/M	SHF Ranging	Simultaneous
	T+320	6	4	R/M	VLBI Recording	No Xmission. Spacecraft noise
	T+330	3	2	R/M	SHF Ranging	Simultaneous
	T+335	6	4	R/M	VLBI Recording	No Xmission. Spacecraft noise
	T+345	3	2	R/M	SHF Ranging	Simultaneous
	T+350	6	4	R/M	VLBI Recording	No Xmission. Spacecraft noise
	T+360		60		Intermission	
Third Session	T+420	3	2	R/M	SHF Ranging	Simultaneous
	T+425	6	4	R/M	VLBI Recording	Rosman Xmit. Noise translation
	T+435	3	2	R/M	SHF Ranging	Simultaneous
	T+440	6	4	R/M	VLBI Recording	Rosman Xmit. Noise translation
	T+450	3	2	R/M	SHF Ranging	Simultaneous
	T+455	6	4	R/M	VLBI Recording	Rosman Xmit. Noise Translation
	T+465	3	2	R/M	SHF Ranging	Simultaneous
	T+480	3	2	R/M	(R) - VHF Ranging (M) - SHF Ranging	Two Frequency
	T+485	3	12	R/M	(r) SHF Ranging (M) - VHF Ranging	Ionospheric Calibration
	T+500	15	—	R/M	Time Synchronization Test	Dual transponders on ATS-3 used
	T+515	—	—	—	End	

TABLE 6

Typical Values of Refractive Bias
(Ref: Refractive Corrections in High-Accuracy Radio Interferometry: D.F. Dickinson, M.D. Grossi & M. R. Pearlman, J. Geophy. Res. 75 (8), 1619-1622, March 1970)

Zenith Angle	Medium	X-band 10 GHZ (meters)	C-band 5 GHZ (meters)	L-band 1.5 GHZ (meters)
0°	Atmospheric	-2.3	-2.3	-2.3
	Ionospheric	0.1	0.3	3.3
	Total	-2.2	-2.0	1.0
45°	Atmospheric	-3.2	-3.2	-3.2
	Ionospheric	0.1	0.4	4.4
	Total	-3.1	-2.8	1.2
90° (Horizon)	Atmospheric	-86.6	-86.6	-86.6
	Ionospheric	0.2	1.0	11.0
	Total	-86.4	-85.6	-75.6

Atmospheric data from various sources were collected for correction of propagation effects on VLBI observables. The temperature, pressure and humidity were measured at both stations with hydrothermograph and microbarograph and monitored continuously by strip-chart recordings. These data are used to calculate surface refractivity and then to predict the tropospheric correction along the line of sight.

Several means were employed to obtain ionospheric data. A very accurate technique was utilized during our VLBI experiment. On several occasions during the VLBI experiment each day, the electron content along the line-of-sight was determined directly by conducting a two-frequency differential delay measurement via the ATS-3 satellite. This was accomplished by performing in rapid sequence SHF and VHF ranging from the two stations. Only a small extrapolation was needed to account for the non-simultaneity of the two ranging operations and bring both of them into a common time-frame. The difference between the VHF and SHF range measurements at any particular time gives the ionospheric propagation delay. This technique, though useful and precise was not always accessible. Furthermore, observations at Mojave were regularly made during the later afternoon when the electron content changes rapidly. It was therefore deemed desirable to have other ionospheric measurements. Faraday rotation measurements of ATS-1 and 3 VHF signals

were acquired at geographically favorable locations by us and other experimenters during the VLBI experiment. The Faraday polarization angle is directly related to the line of sight total electron content.

Table 7 gives details about the tropospheric and ionospheric data collected during the experiment.

TABLE 7

Atmospheric Data Monitored During the VLBI Experiment

Medium	Parameter	Method/ Instrumentation	Site(s)	Space-craft
Troposphere	Humidity Temperature Pressure	Hydrothermograph Microbarograph	Rosman Mojave	
Ionosphere	Actual Ionospheric Delay	Two Frequency (VHF/SHF) Simultaneous Ranging	Rosman Mojave	ATS-3
	Total Electron Content	FHF Faraday Rotation/Polarimeter	JPL/Goldstone Stanford Rosman Wallops-Island	ATS-1, ATS-3 ATS-3 ATS-3 ATS-3
	Ionospheric Differential Delay	Global Ionospheric Modeling/Ground Based Ionosonde Data Dr. Rodney Bent DBA Systems Inc.		

Figure 12a shows the time-delay corrections as applicable to a frequency of 4178 MHz for the Rosman-Mojave baseline for the quasar 3C-273 for June 3, 1971. Shown are the ionospheric and tropospheric delay corrections. Also shown in the figure are the universal time versus elevation angle on the star for both Mojave and Rosman for June 3, 1971. Figure 12b gives the multiplicative factor for computing the ionospheric correction for any other frequency larger than 1 GHz.

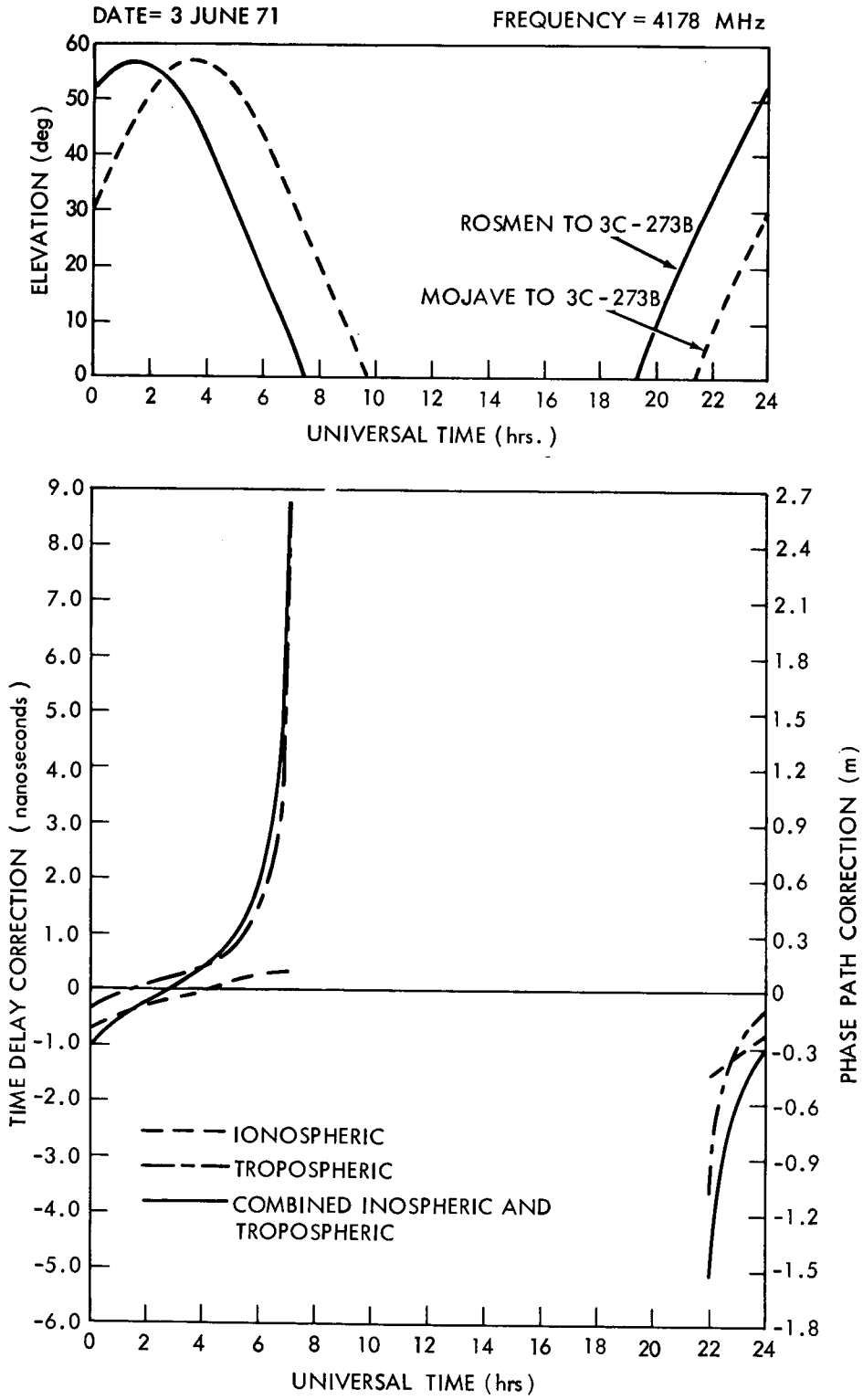

Figure 12a. Ionospheric and Tropospheric Corrections for the Quasar 3C-273B Observations from Rosman and Mojave

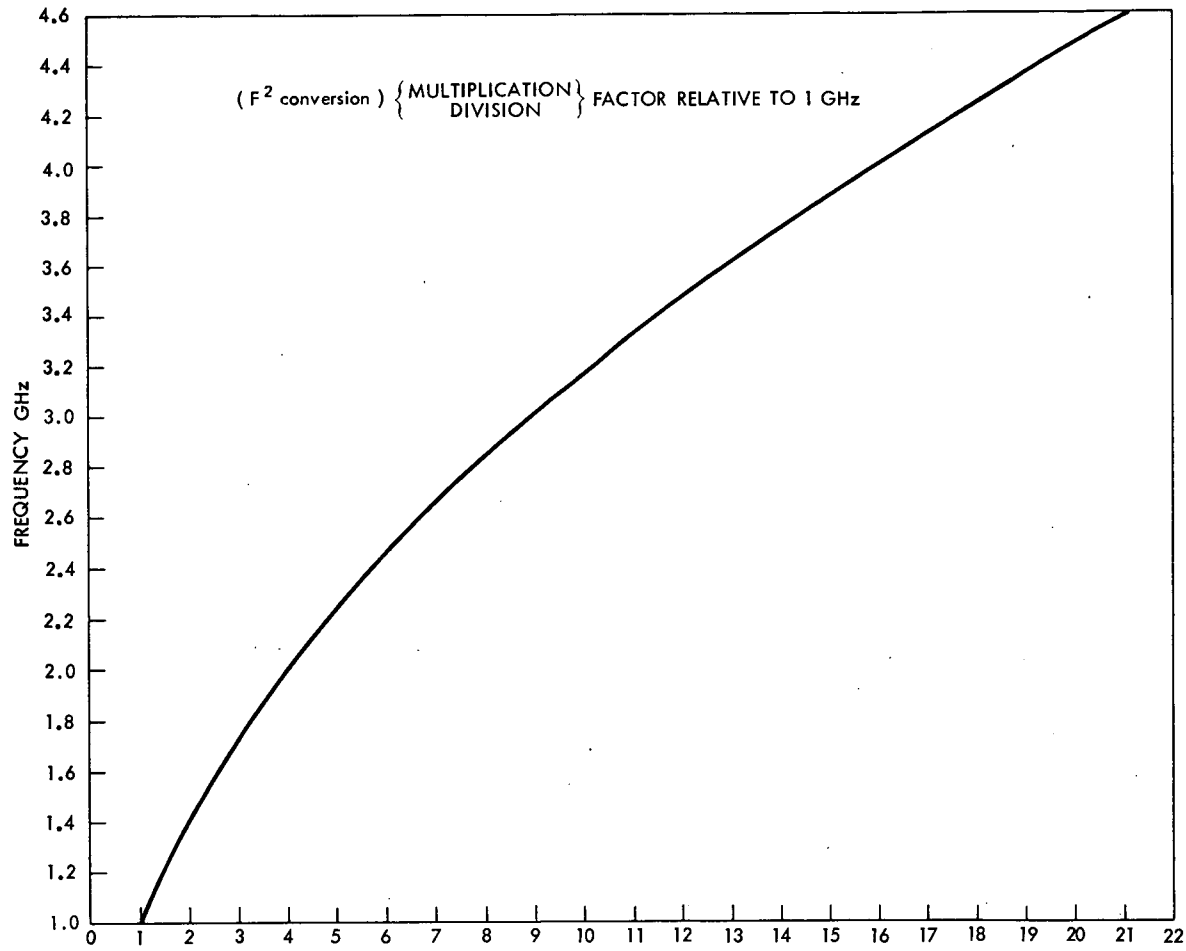

Figure 12b. Multiplication Factor for Ionospheric Corrections for Frequencies >1 GHz

Figure 12c shows the time-delay corrections as applicable to a frequency of 4178 MHz for the Rosman-Mojave baseline for the ATS-3 satellite for May 26, 1971. Also shown in the figure are the elevation angles of the satellite from both Mojave and Rosman. Figures 12a and c show sample results. The ionospheric and tropospheric time-delay corrections are stored in the computer for correcting the VLBI data.

5.4 SHF RANGE & RANGE-RATE TRACKING

An independent check on the accuracy of the VLBI parameters [namely, time-delay, τ_g , and fringe-rate, ν_f] can be obtained from C-band

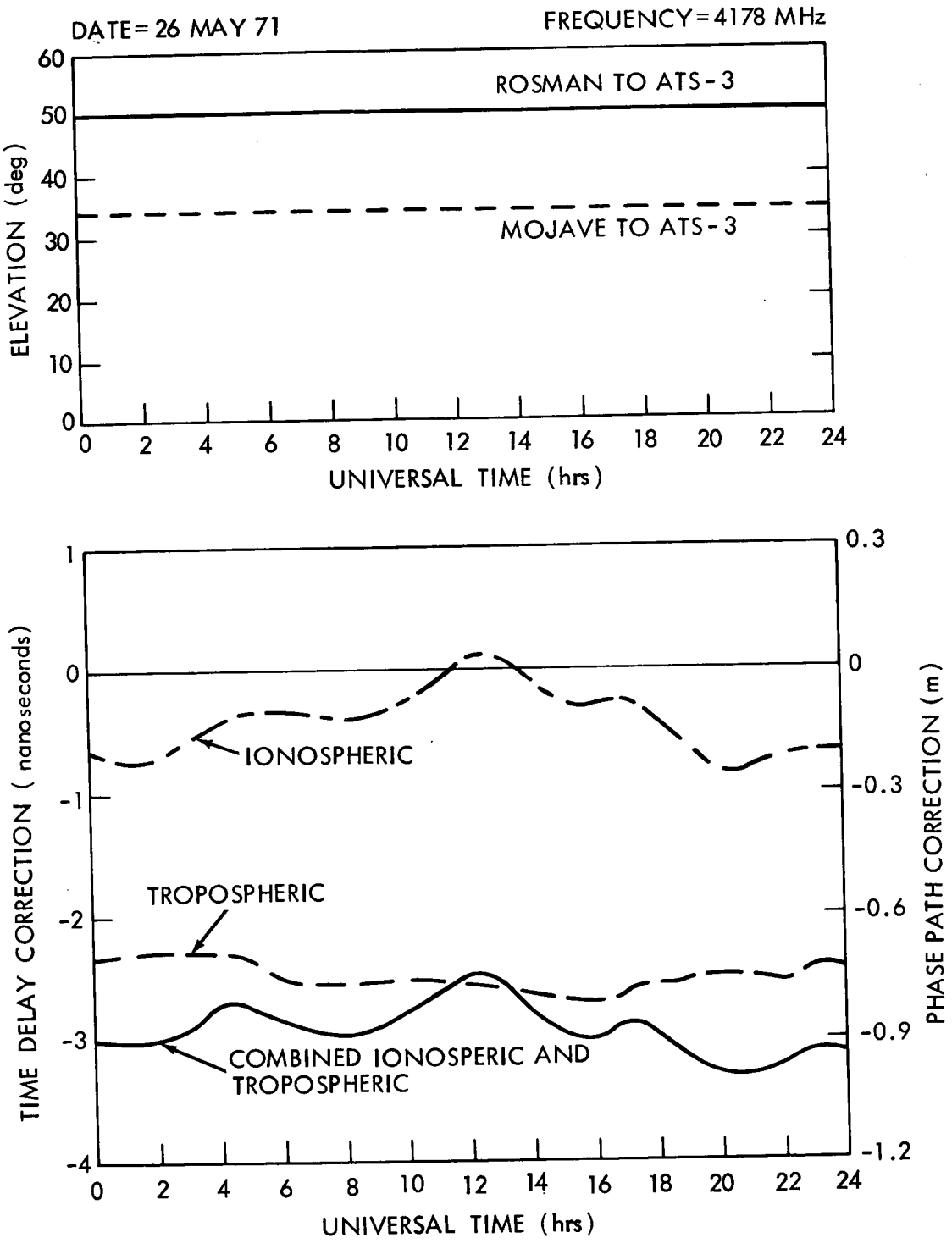

Figure 12c. Ionospheric and Tropospheric Corrections for ATS-3 Observations from Rosman and Mojave

tracking data. The VLBI parameters have a simple relation with the range and rate measurements made at the same frequency. They are given by

$$\tau_g = \frac{R_{Mojave} - R_{Rosman}}{c} \tag{39}$$

and

$$\nu_f = \frac{\dot{R}_{Mojave} - \dot{R}_{Rosman}}{\lambda} \tag{40}$$

where c is the speed of light and λ is the wavelength of the radio signals. R and $\dot{R}$ denote the ground to spacecraft range and range-rate. Determining τ_g and ν_f by R and $\dot{R}$ tracking is also of value in approximately predicting the VLBI parameters. This saves computer time in the initial search process, even though it is not essential for processing VLBI data. SHF range and range-rate measurements are also used to compute the orbital elements independently for later comparison with the orbital elements derived from the VLBI data. It is for the various reasons cited above that R and $\dot{R}$ measurements from both Mojave and Rosman were incorporated in the observation routine (Table 5).

5.5 VLBI TAPE PROCESSING PROCEDURES

The recording of the high bit-rate ($\sim$ 720 kbits/sec) is done by using the Ampex VR-660C helical scan video tape recorders which have a high density bit packing capacity. The reels of video tape used in the experiment store up to 96 minutes of observational data ($\sim$720 kbits/sec) as against individual 2400 feet 9-track tapes which can only record 3 minutes worth of the same data.

At the conclusion of the observation phase of the experiment, the tapes along with the recorders were transported to the Central processing facility where the playback system is used to transcribe the data on video tapes on to 9 track digital tapes. The cross-correlation and fringe-fitting is accomplished in the general purpose high-speed computers, the IBM 360/95 at the Goddard Space Flight Center and the CDC-6400 at the Smithsonian Astrophysical Observatory.

Seven computer programs are available to process the data. First is a pre-processor which does a quality check and realignment of the nine-track data tapes and transcribes the data to seven-track tapes. One of two fringe processors is used to do the correlations and determine delay and doppler for each pair of tapes. One fringe processor is used on satellite data, the other on stellar data. Also in use are two pairs of least-squares analysis programs. Each pair consists of a program which uses delay data and the other one which uses

delay-rate data. One pair is for stellar data and the other is for satellite data. Brief descriptions of all these programs are provided below. More details about these programs may be found in the publication "Documentation of Computer Programs Used in Very Long Baseline Interferometry Experiments," S. Ross and Company, November 1971, NASA Contract NAS-5-20247.

5.5.1 Garbage Collection Program - Tapes

The digitized data is recorded at the observing stations on Ampex VR-660C helical-scan videotape recorders. These video tapes are played back and the data is transferred to nine-track computer tapes. Along with the data on both video and computer tapes are recorded timing and synchronization codes. The data on the nine-track tapes are processed to align these codes on the proper word boundaries, inserting or deleting bits where necessary. This operation is performed by the Garbage Collection program. Incidental to this operation is the transcription to seven-track tapes. This is done because the SAO computer cannot handle pairs of nine-track tapes. The nine track tapes are used in GSFC computers.

5.5.2 Stellar Fringe Processor - VLBI1

The Fringe Processor does a two dimensional search for a peak fringe amplitude. The inputs consist of parameters describing the searches in the time-delay offset domain and the fringe frequency offset domain. Also required is the integration interval and certain parameters related to the recording system. The brunt of the computing is spent doing the bit-by-bit cross-correlation of the two data strings. The program computes delay and delay rate from the VLBI geometry and shifts one of the data strings to compensate. As the integration proceeds, the predicted phase difference is adjusted by the predicted doppler frequency. These compensations cancel out the known offsets. The two dimensional search around these predicted offsets allows the analyst to ascertain errors in the predictions. These errors are used at a later stage in the computations.

5.5.3 Satellite Fringe Processor - VLBI2

This program operates in much the same way as VLBI1 except that the time delay due to the geometry is not computed by the program, but rather is input in microseconds.

5.5.4 Stellar Least Squares Analysis Program for Delay Data - POSTPR.

This program does an analysis of the time delay errors from the Stellar Fringe Processor into corrections of source and baseline declination, baseline length, clock error, and baseline hour angle minus source hour angle. At least three sources must be used with at least three observations of each at different times of the day. The Least Squares technique is applied at two stages in the program, once on the data from each source and once on the results from the first stage.

5.5.5 Stellar Least Squares-Analysis Program for Delay Rate Data - POSTDR.

The Least Squares technique is used on the corrections to the predicted doppler frequency as ascertained by the stellar Fringe Processor. The assumption is made, for purposes of this program, that there are no errors in source coordinates. The data from at least three observations of natural sources is input and corrections to the hour angle and equatorial component of the baseline, as well as the clock drift rate are computed. An error propagation analysis has been added to this program to compute the likely errors in the corrections.

5.5.6 Satellite Least Squares Analysis for Delay Data - DELAY.

A sinusoid is fit to the delay offset data using the Least Squares technique. This program also produces a CALCOMP plot of the curve superimposed over the data points so that a visual check of the quality of the data can be made. Nine unknowns are estimated.

5.5.7 Satellite Least Squares Analysis Program for Delay-Rate Data - DELRT.

This program is analogous to the previous one except that the sinusoid is fit to the doppler offset data. Three unknowns are estimated.

Figure 13 is a schematic diagram which outlines the data processing procedure. In processing satellite data, it was found sufficient to integrate only one record-length of data (= 200 msec) to obtain unambiguous time-delay and fringe-rate values. However, the number of records integrated was increased to five (200 msec x 5 = 1 sec) since the sampling rate is identical to that of the range and range-rate data. The following table (Table 8) illustrates the fact that there was not much to gain by integrating more records. This is due to the fact that the signal-to-noise ratio (SNR) is so high in the case of satellites that one record of integration is sufficient to achieve strong correlation.

TABLE 8

VLBI Parameters as a Function of Number of Records Integrated

Satellite ATS-3 Run No. 159:22:11 (Year 1971)

Records Integrated Over	Doppler Search Interval (Hz)	Fringe Frequency at Peak Correlation	Maximum Corralation Amplitude
1	0.005	7.855	0.399981
5	0.005	7.855	0.398210
10	0.005	7.855	0.420594
20	0.005	7.850	0.411054
50	0.005	7.850	0.407456

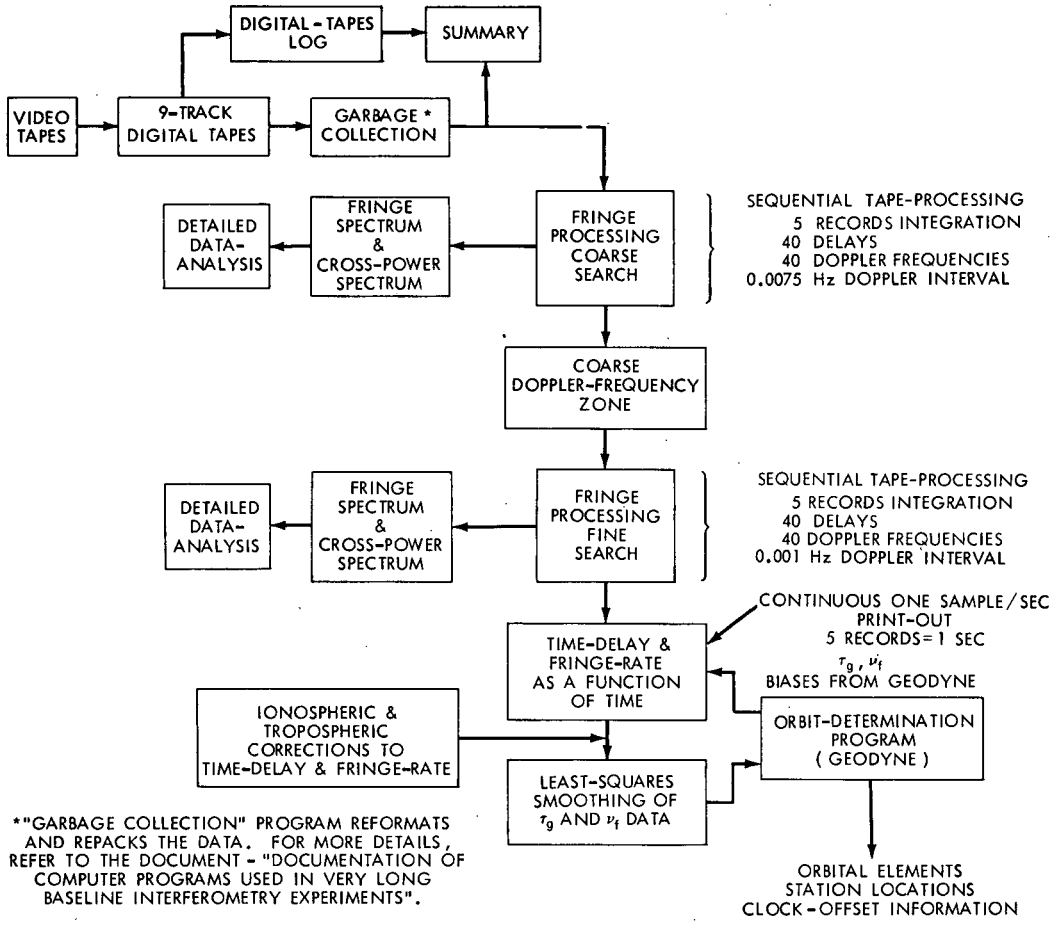

Figure 13. VLBI Data Processing Scheme

5.6 FRINGE PROCESSING RESULTS

Four types of signal modulation were employed during the experiment session. The objective was to determine whether any particular modulation scheme would be especially advantageous for VLBI application. The modulation types were:

1. Spacecraft Noise. Constant density analog noise transmitted from the spacecraft transponder front-end

2. Noise Translation. Flat-noise spectrum having 12 MHz bandwidth

3. Sidetone ensemble. A harmonic sidetone ensemble, using all of the ATS range tones turned on simultaneously.

4. Pseudo-random Sequence. A pseudo-random sequence code using 2047 sequences repeated at rates of 500 kbits/sec, 1 Mbits/sec and 2 Mbits/sec.

Figures 14-22 show the results from processing sample data from typical runs of each type. The "a" figures show the correlation function amplitude and phase as a function of number of delay bits, where the center of abscissa scale (usually between points 20 and 21) indicates zero relative excess shift. Each "a" plot is for a specific doppler frequency. Each bit is of length 1.4 μ seconds. This bit offset is in addition to the geometric delay offset which corresponds to the zero offset (between points 20 and 21) in these figures. The additional offset bits where the correlation function maximizes are added algebraically to the geometric delay to get the true time-delay, τ_g . However, this technique gives time-delay resolution equivalent to the bit-length which is 1.4 μ sec. An alternate technique which involves taking the slope of the phase versus frequency curve of the power spectrum gives a resolution for time-delay which is 2 orders of magnitude better than that obtained by using integral number of bits from the correlation plot. This technique will be discussed later on.

The "b" figures show the amplitude and phase of the power spectrum corresponding to the "a" figures. The amplitude spectrum is characteristic of the power spectrum of the received signals and is a reliable indicator of true correlation. The phase versus frequency plot is the most important plot of the set. It gives indications of phase noise in the system (random phase excursions and jumps).

The "c" figures show the "fringe spectrum." Shown in the figure are the peak correlation and power amplitudes as a function of the doppler frequency. The "a" and "b" figures are for one specific doppler frequency and each have a corresponding peak correlation and power amplitude. The "c" figure shows the distribution of the peak amplitudes with a doppler scan. One may see the $\frac{\sin x}{x}$ distribution in doppler space which is in line with the theory. The doppler frequency at which the peak correlation and power amplitudes maximize is the true doppler frequency (or fringe-rate) for that run.

The slope of the power spectrum phase curve (i.e. "fringe phase") can be used to determine with great precision the excess shift required to produce a peak in the correlation function. It is done in the following manner.

Total fringe phase,

$$\Delta\phi = (\Delta\phi_o + \Delta\phi_E) = f\left[\Delta\tau_o + \Delta\tau_E\right]$$

and, $$\Delta\phi_o = f\,\Delta\tau_o \qquad (41)$$

Therefore $$\Delta\phi_E = f\,\Delta\tau_E$$

Where $\Delta\phi$ is the total fringe phase, $\Delta\phi_0$ is the geometrical fringe-phase, $\Delta\phi_E$ is the excess fringe phase shown in the power spectrum phase plot, f is the RF frequency, $\Delta\tau_0$ is the constant geometric-delay and $\Delta\tau_E$ is the excess time-delay that one needs to determine accurately. The total delay $\Delta\tau = \Delta\tau_0 + \Delta\tau_E$ is then easily computed.

From the above expression:

$$\frac{d(\Delta\phi_E)}{df} = \sigma = \Delta\tau_E \qquad (42)$$

Where σ denotes the slope of the fringe-phase curve. In other words, the slope of the phase curve is equal to the relative excess time-delay ("excess" here refers to the amount in variance with the geometric delay. The variance may be positive or negative.) This is important because one can measure the phase/frequency slope to greater accuracy (one to two orders of magnitude improved resolution) than is possible by extracting the bit-offset from the correlation amplitude curve. For instance, if the fringe-phase traces n cycles linearly across a frequency band of m Hertz, the relative excess-delay would be n/m seconds. A least squares fit gives this slope with a standard deviation ($\sim$ resolution) of the order of 10 nanoseconds. The correlation amplitude curve will show a maximum around this computed excess-delay but at integral number of bits and the resolution is limited by the bit length which is 1.4 μsec for the present case. So, the correlation plots are never used to compute the excess delays. They are only used to check the sign and magnitude of the computed excess-delay.

As is evident from the accompanying figures, each of the modulations used during the experiment exhibited its characteristic forms. Figures 14, 15, 16 and 17 are examples of the noise translation and spacecraft noise modulations on the received signal. In the power spectra corresponding to these cases (Figures 14b, 15b, 16b and 17b), the shape of the bandpass filter and the flat noise spectra can be seen. The spectral phase curves are remarkably linear which is indicative of the extraordinary time-delay resolution. Figures 14 and 16 are the cases where the bit offset is relatively large which is evidenced by the number of cycles in the corresponding spectral phase plots. Figures 15 and 17 are for cases where the bit offset is not more than one bit. This is evidenced by less than a cycle of phase change in the spectral phase plots. Figures 15c and 17c show the typical $\frac{\text{Sin } x}{x}$ profiles for the "fringe spectrum."

Figures 18, 19, and 20 are typical of the pseudorandom sequence modulation. Figures 18a and 18b are the correlation function and power spectrum respectively of the 500 kbit/sec rate PRS modulation. The sixbit width of the

159-22-11 ATS 3 N=x

SEARCH FREQUENCY NUMBER 1
SEARCH FREQUENCY 7.9500
MAXIMUM AMPLITUDE .428865

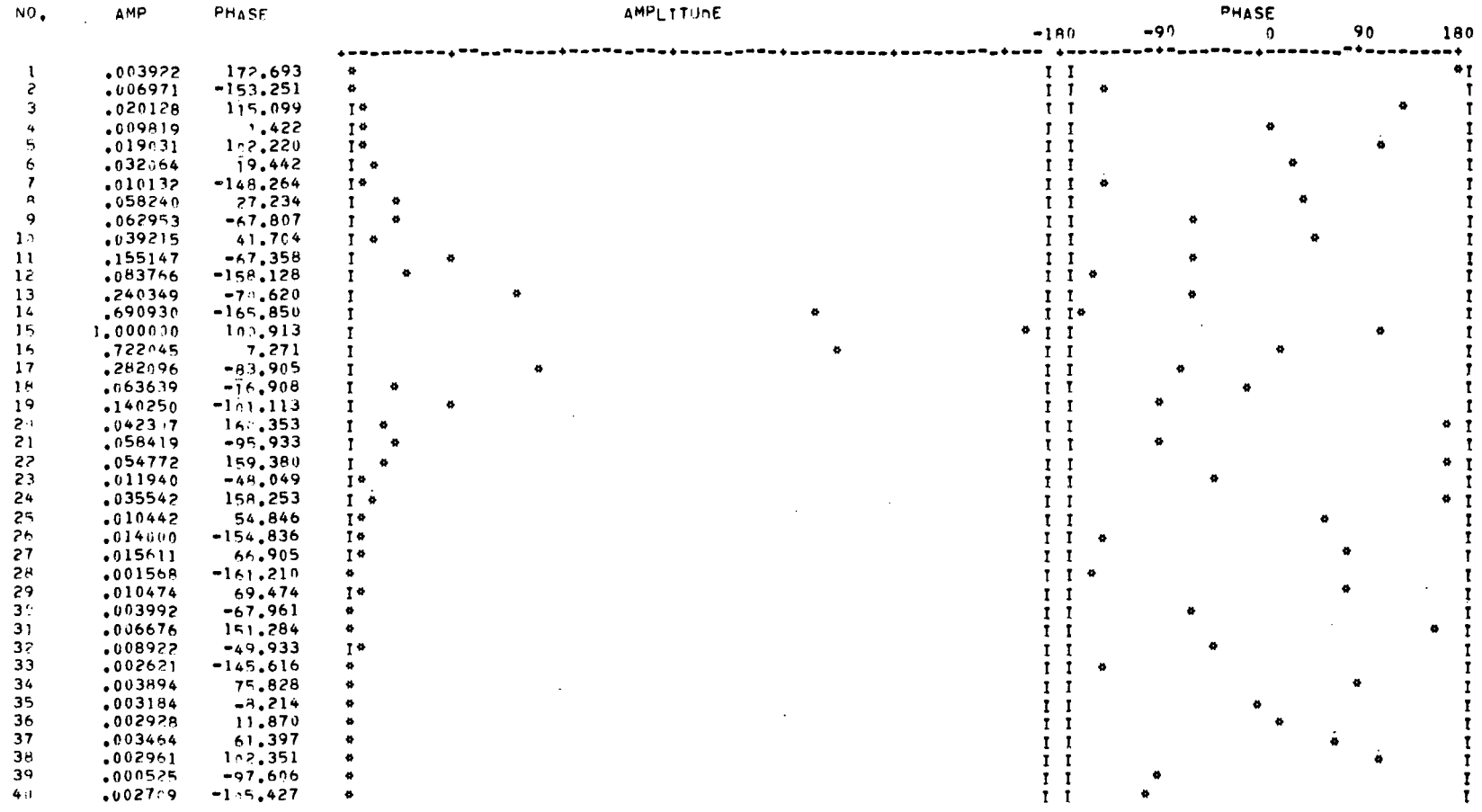

Figure 14a. Correlation Function Versus Delay Offset for Noise Modulation – Case of Large Delay Residual

PLOT OF FREQUENCY SPECTRUM, PEAK VALUE = 1.118286

NO.	AMP	PHASE
1	.040767	99.749
2	.043592	76.216
3	.062479	49.098
4	.119745	18.165
5	.228706	-9.888
6	.377994	-35.370
7	.540731	-63.075
8	.687655	-91.118
9	.795756	-118.594
10	.861132	-145.801
11	.901450	-172.906
12	.934623	161.662
13	.963012	134.693
14	.981952	108.235
15	.990176	81.171
16	.990391	54.048
17	.989099	27.269
18	.990923	1.118
19	.994677	-24.757
20	.998289	-51.239
21	1.000000	-78.213
22	.994189	-104.909
23	.979791	-131.642
24	.968285	-158.875
25	.965830	174.200
26	.963311	147.939
27	.952281	121.389
28	.938254	94.139
29	.930755	66.877
30	.932077	40.077
31	.936839	13.349
32	.937113	-14.265
33	.925022	-43.160
34	.884864	-71.968
35	.791609	-98.996
36	.636324	-124.272
37	.448188	-148.880
38	.277005	-173.520
39	.157946	161.408
40	.113960	134.590

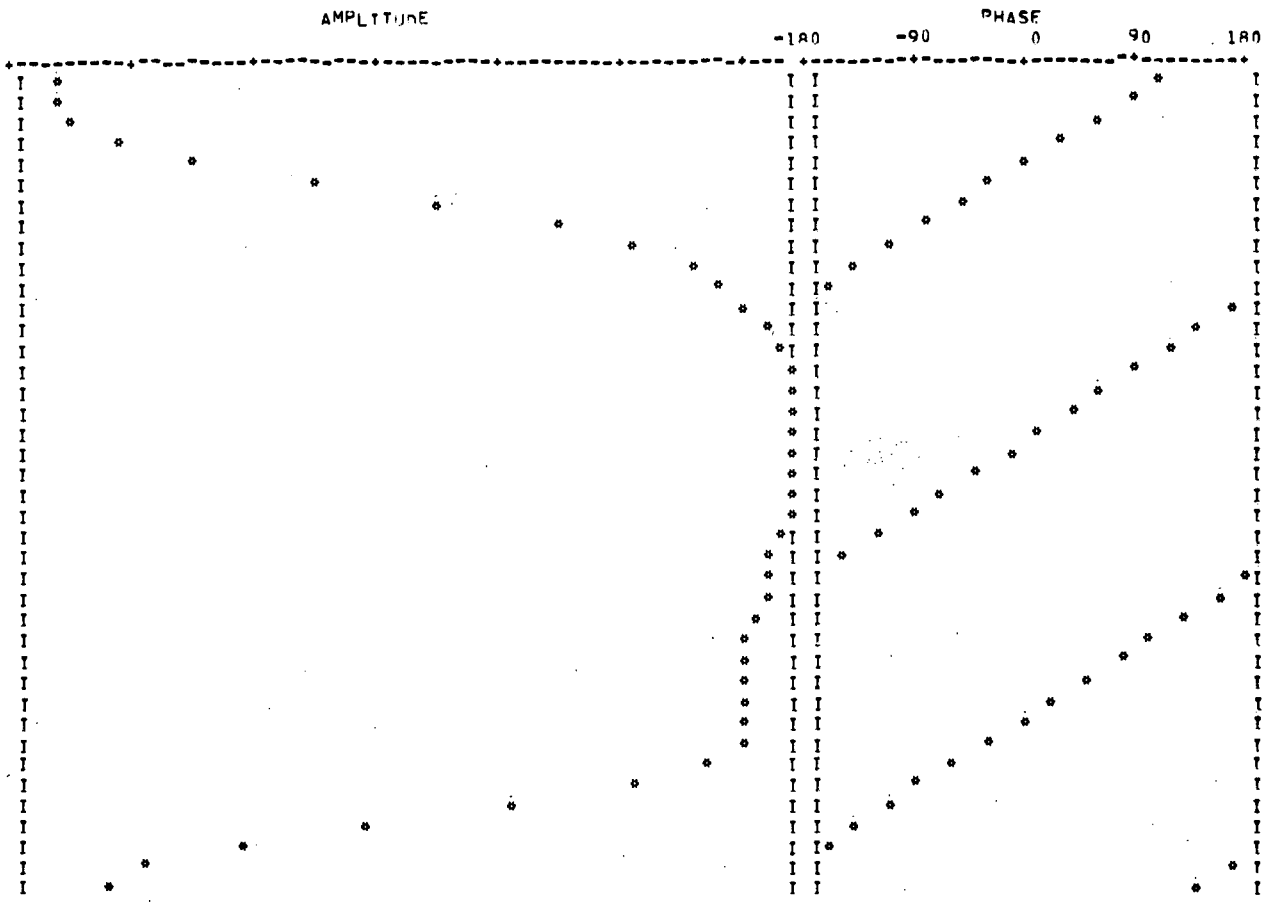

Figure 14b. Power Spectrum for Noise Modulation – Case of Large Geometrical Delay Residual

159-13-35 ATS-3 N-X

SEARCH FREQUENCY NUMBER 8
SEARCH FREQUENCY 12.2000000
MAXIMUM AMPLITUDE 0.42556408005624

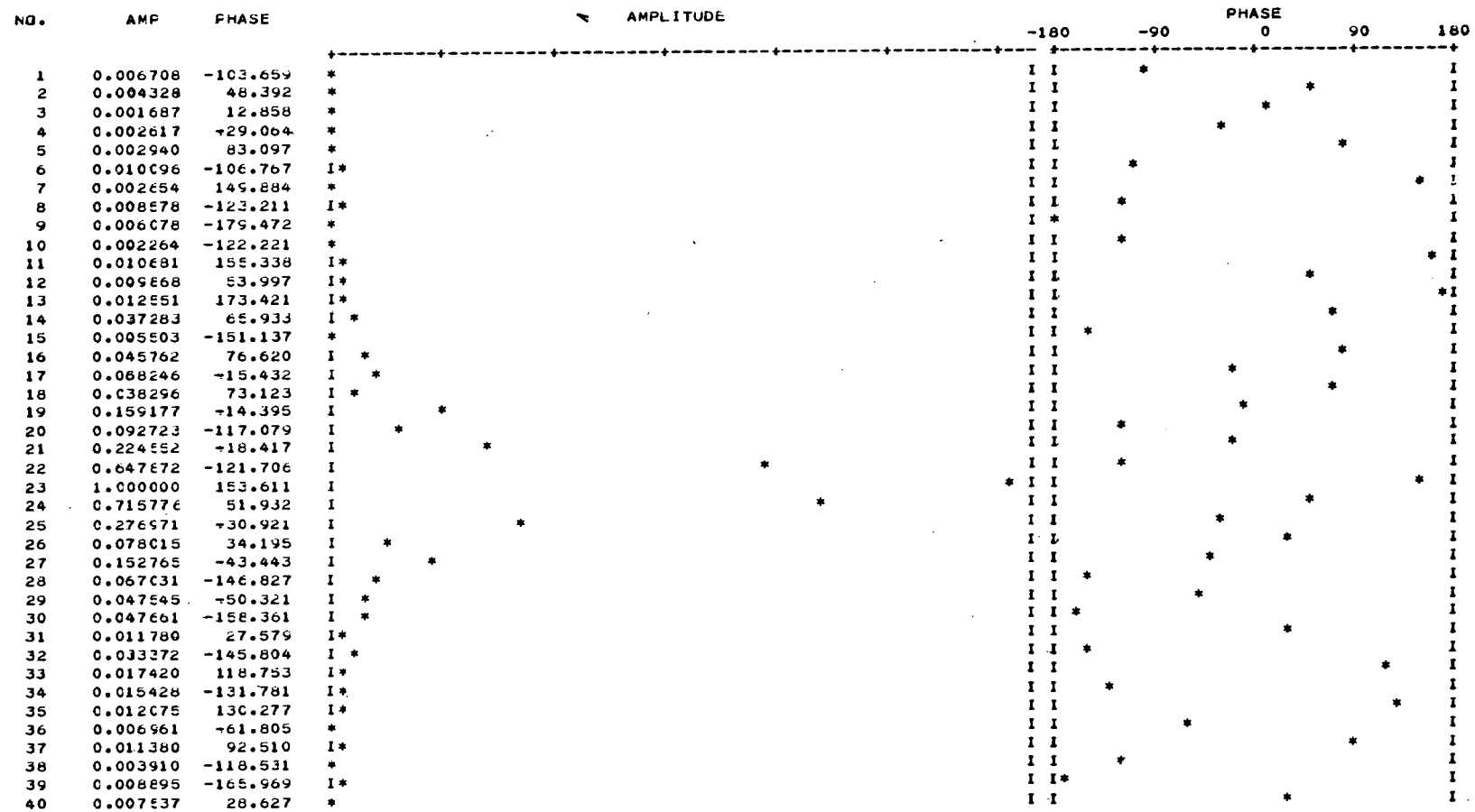

NO.	AMP	PHASE
1	0.006708	-103.659
2	0.004328	48.392
3	0.001687	12.858
4	0.002617	+29.064
5	0.002940	83.097
6	0.010C96	-106.767
7	0.002654	149.884
8	0.008578	-123.211
9	0.006C78	-179.472
10	0.002264	-122.221
11	0.010681	155.338
12	0.009868	53.997
13	0.012551	173.421
14	0.037283	65.933
15	0.005503	-151.137
16	0.045762	76.620
17	0.068246	+15.432
18	0.C38296	73.123
19	0.159177	+14.395
20	0.092723	-117.079
21	0.224552	+18.417
22	0.647672	-121.706
23	1.000000	153.611
24	0.715776	51.932
25	0.276571	+30.921
26	0.078C15	34.195
27	0.152765	-43.443
28	0.067C31	-146.827
29	0.047545	+50.321
30	0.047661	-158.361
31	0.011780	27.579
32	0.033372	-145.804
33	0.017420	118.753
34	0.015428	-131.781
35	0.012C75	130.277
36	0.006961	+61.805
37	0.011380	92.510
38	0.003910	-118.531
39	0.008895	-165.969
40	0.007537	28.627

Figure 15a. Correlation Function for Noise Modulation - Case of Small Delay Residual

PLOT OF FREQUENCY SPECTRUM. PEAK VALUE = 1.081797

NO.	AMP	PHASE
1	0.047750	146.718
2	0.051370	159.148
3	0.070629	160.768
4	0.127209	170.451
5	0.238679	-177.506
6	0.395752	-168.334
7	0.563458	-160.527
8	0.707130	-152.700
9	0.813223	-144.128
10	0.887834	-134.623
11	0.941106	-124.743
12	0.975970	-115.281
13	0.992705	-106.139
14	0.998080	+96.484
15	1.000000	+86.168
16	0.996685	+75.985
17	0.983841	+66.317
18	0.968485	-56.925
19	0.961240	+47.787
20	0.960139	+38.862
21	0.956595	+29.700
22	0.951278	+20.352
23	0.951379	-11.520
24	0.958375	-2.994
25	0.967204	6.301
26	0.971242	16.269
27	0.965983	25.782
28	0.956068	34.775
29	0.954159	44.109
30	0.962620	53.659
31	0.966806	62.681
32	0.956242	71.306
33	0.933769	79.881
34	0.890977	88.213
35	0.798601	96.639
36	0.642261	106.437
37	0.452049	118.513
38	0.280303	131.501
39	0.161711	141.299
40	0.117982	146.407

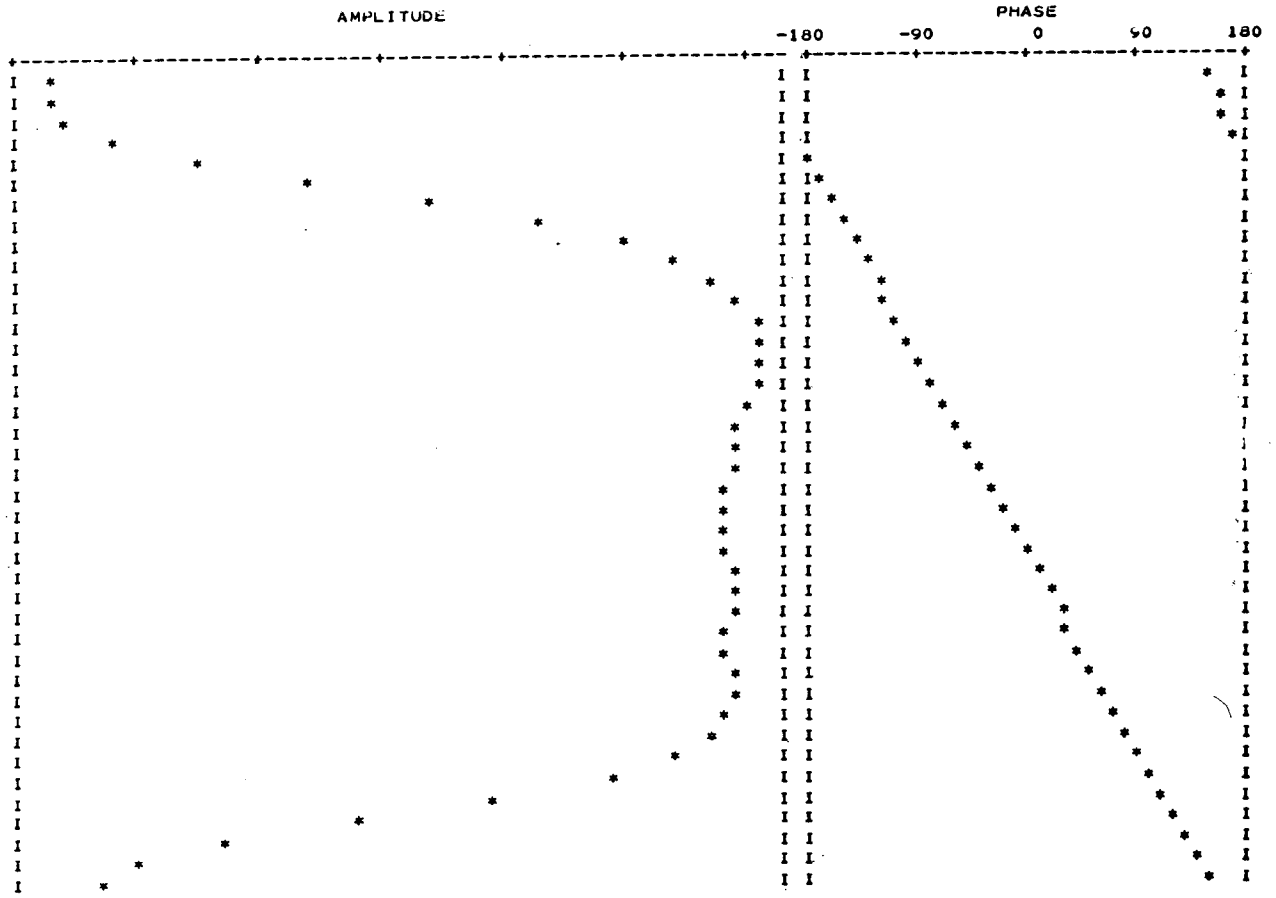

LEAST SQUARES FOR PHASE (IN CYCLES) VS FREQUENCY (IN HZ)

PHASE = (0.287667238D-05) * NO. + 0.371246456D 00
SIGMA IN PHASE = 0.436388509D-02
SIGMA IN SLOPE = 0.785746268D-08

Figure 15b. Power Spectrum for Noise Modulation - Case of Small Delay Residual

```
RUN     159-21-10       NO. REC.=   3       S.REC.NO.E=   2
SOURCE ATS-3 N-X        NO. PTS.=  40       S.REC.NO.W=   4

                                                    VLBI230 VAR230/VAM230 SAT-C
          GEOM. DELAY =     4112.21
          INST. DELAY =      -39130

DAY= 159 TIME=   21.0000    10.0000    31.4172

     FREQ          AMPLITUDE          TAU          CORREL AMPL     CORRELATION AMPLITUDE
 1 10.6000000  0.0ee037191121 -2.956e31491987  0.025878143525 I*                        I
 2 10.7000000  0.1002ab011181 -1.51815311 054  0.034802924756 I *                      I
 3 10.8000000  0.1096e5041134 -1.722979120289  0.054619795888 I  *                     I
 4 10.9000000  0.218312739197 -1.811504790037  0.073652910975 I    *                   I
 5 11.0000000  0.26e2c5054545 -1.85ab1b929301  0.087430159443 I     *                  I
 6 11.1000000  0.285206145439 -1.882340551109  0.093421025157 I     *                  I
 7 11.2000000  0.2e3230011445 -1.89e894996494  0.099019253313 I     *                  I
 8 11.3000000  0.2583410775821 -1.901549164729  0.07042540315 I    *                   I
 9 11.4000000  0.1568e9359285 -1.887022113704  0.0e0328477932 I   *                    I
10 11.5000000  0.115460930406 -1.724390503756  0.038024452394 I *                      I
11 11.6000000  0.0993e9e022e7 -1.46057220c07b  0.045396000151 I  *                     I
12 11.7000000  0.225097940681 -1.913606097944  0.093185794693 I     *                  I
13 11.8000000  0.3635e9642164 -1.947957147020  0.149060455740 I         *              I
14 11.9000000  0.506277328324 -1.959302736784  0.207535724165 I            *           I
15 12.0000000  0.650e94526111 -1.964442206911  0.265360138426 I               *        I
16 12.1000000  0.782270769182 -1.966999001915  0.318780122494 I                  *     I
17 12.2000000  0.897595955183 -1.970344621512  0.3e0954491120 I                    *   I
18 12.3000000  0.993614599393 -1.975423700373  0.395541724029 I                     *  I
19 12.4000000  1.06520d052916 -1.979c0e807e0e  0.417471932043 I                      * I
20 12.5000000  1.10e843727001 -1.978e32257268  0.431151963812 I                      *I
21 12.6000000  1.10e80e077951 -1.977226361100  0.428422545385 I                      *I
22 12.7000000  1.0719c9899e79 -1.977790588592  0.408640037062 I                     *  I
23 12.8000000  1.004922046988 -1.980222304609  0.377595726430 I                   *    I
24 12.9000000  0.913534723635 -1.981419920896  0.338952718113 I                 *      I
25 13.0000000  0.79822720c482 -1.980e96197369  0.291699138235 I               *        I
26 13.1000000  0.662723453e96 -1.979d7b2b4480  0.236455067296 I            *           I
27 13.2000000  0.517441982699 -1.979614e44597  0.177011734889 I         *              I
28 13.3000000  0.37206102e213 -1.978836150903  0.119731e84353 I      *                 I
29 13.4000000  0.22ee2375e068 -1.975326277ed9  0.077584609793 I   *                    I
30 13.5000000  0.1016e7167959 -2.053e07e23891  0.045e9023e2e8 I *                      I
31 13.6000000  0.10e362596651 -1.80945ee75116  0.038538192556 I *                      I
32 13.7000000  0.167e22444438 -1.953926153149  0.064277459708 I    *                  I
33 13.8000000  0.24221407c9e6 -1.946035057178  0.082119747161 I      *                I
34 13.9000000  0.2e656e310160 -1.946472539404  0.089485628224 I       *               I
35 14.0000000  0.2e6c24302585 -1.938707599753  0.08e0e5461242 I      *                I
36 14.1000000 -0.247101e74097 -1.924e99443996  0.074918143186 I      *                I
37 14.2000000  0.2062133e2742 -1.904213004256  0.056419815928 I   *                   I
38 14.3000000  0.15e752422483 -1.889957324644  0.035227108458 I *                      I
39 14.4000000  0.106136e6e109 -7.359019796942  0.023e40541130 I*                       I
40 14.5000000  0.132233480455 -2.46ee1e551525  0.038291267047 I *                      I
```

TAU

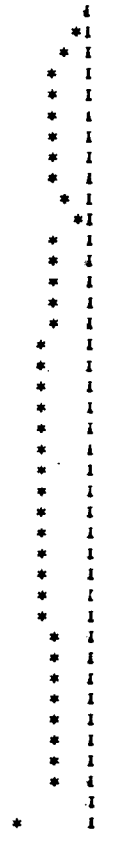

Figure 15c. Fringe Spectrum for Noise Modulation

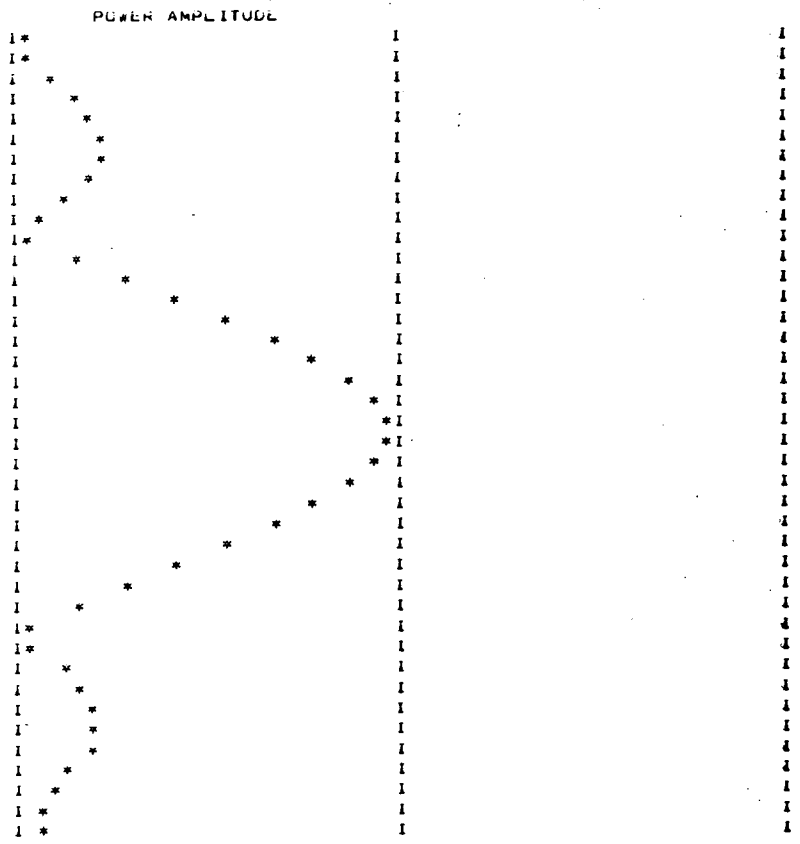

Figure 15c. Continued

159-22-27 S/C NOISE

SEARCH FREQUENCY NUMBER 15
SEARCH FREQUENCY 6.7000
MAXIMUM AMPLITUDE .378901

NO.	AMP	PHASE
1	.005928	-57.367
2	.013484	-144.798
3	.002767	108.553
4	.025837	-90.630
5	.031533	158.355
6	.014129	-68.433
7	.075021	172.915
8	.048988	72.523
9	.075683	174.799
10	.171214	75.522
11	.050871	-17.602
12	.330176	71.625
13	.814730	-21.660
14	1.000000	-116.873
15	.684444	152.000
16	.211966	60.201
17	.098011	136.686
18	.136712	43.184
19	.019328	-68.928
20	.070235	46.988
21	.043460	-59.917
22	.019511	61.633
23	.033386	-46.667
24	.011199	140.805
25	.018797	-30.934
26	.017699	-124.836
27	.003661	177.727
28	.002653	-146.989
29	.004883	84.625
30	.013853	-104.182
31	.003468	113.461
32	.003343	-24.857
33	.006086	179.530
34	.003536	13.777
35	.003886	83.169
36	.006995	111.881
37	.002279	-24.719
38	.001884	-17.112
39	.002234	123.249
40	.005662	-179.713

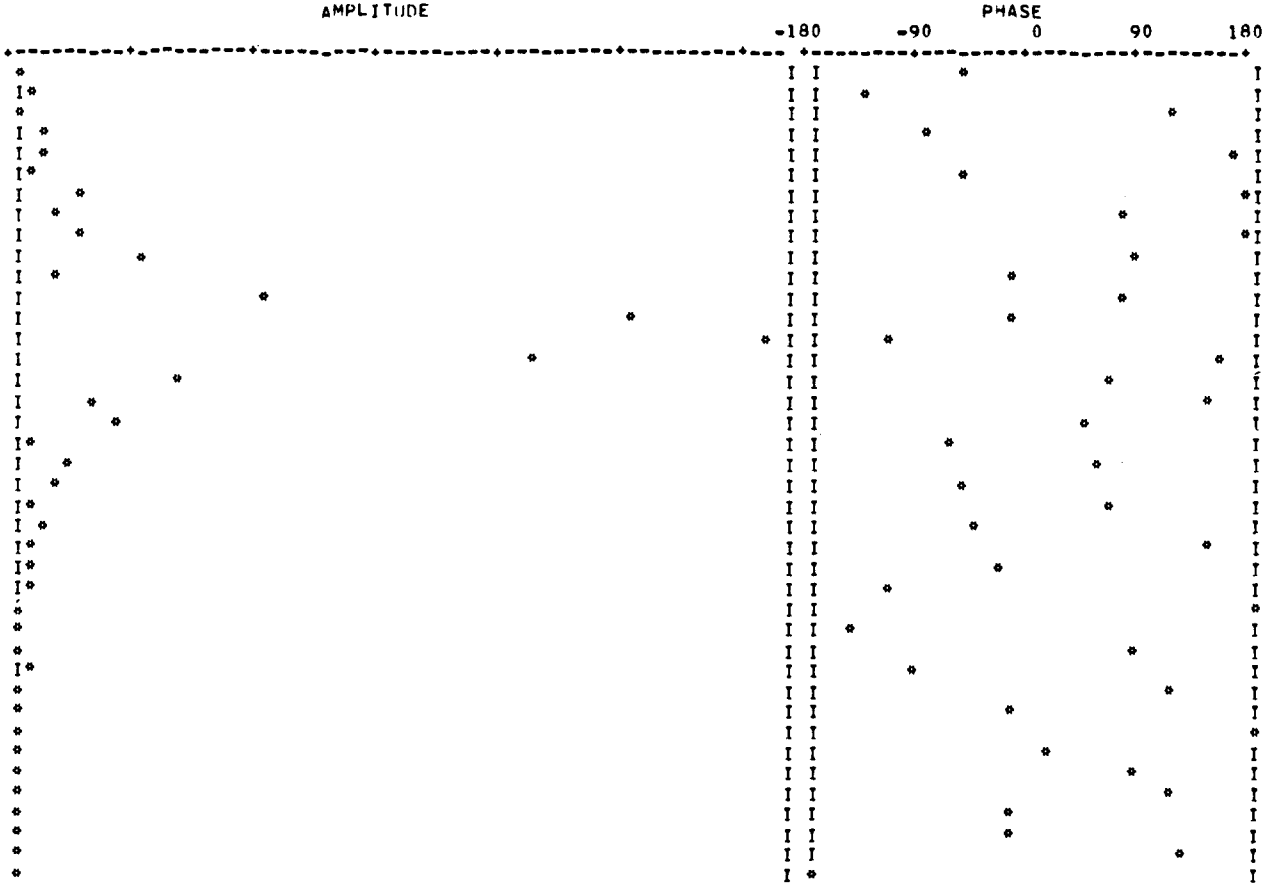

Figure 16a. Correlation Function for Broadband Spacecraft Noise - Case of Large Delay Residual

PLOT OF FREQUENCY SPECTRUM. PEAK VALUE = 1.023789

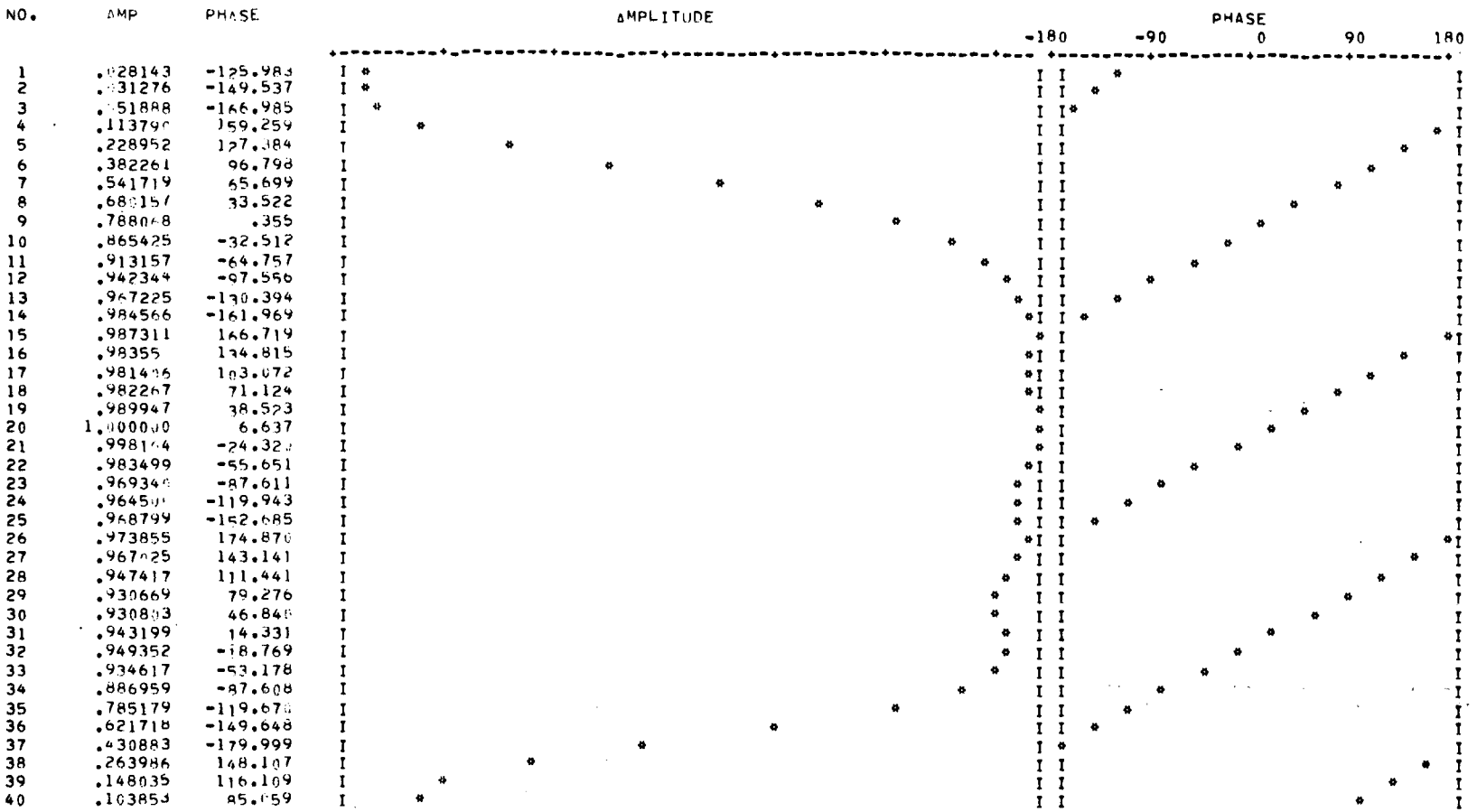

Figure 16b. Power Spectrum for Broadband Spacecraft Noise - Case of Large Delay Residual

159-21-45 ATS-3 S-N

SEARCH FREQUENCY NUMBER 25
SEARCH FREQUENCY 10.0000000
MAXIMUM AMPLITUDE 0.36332314548290

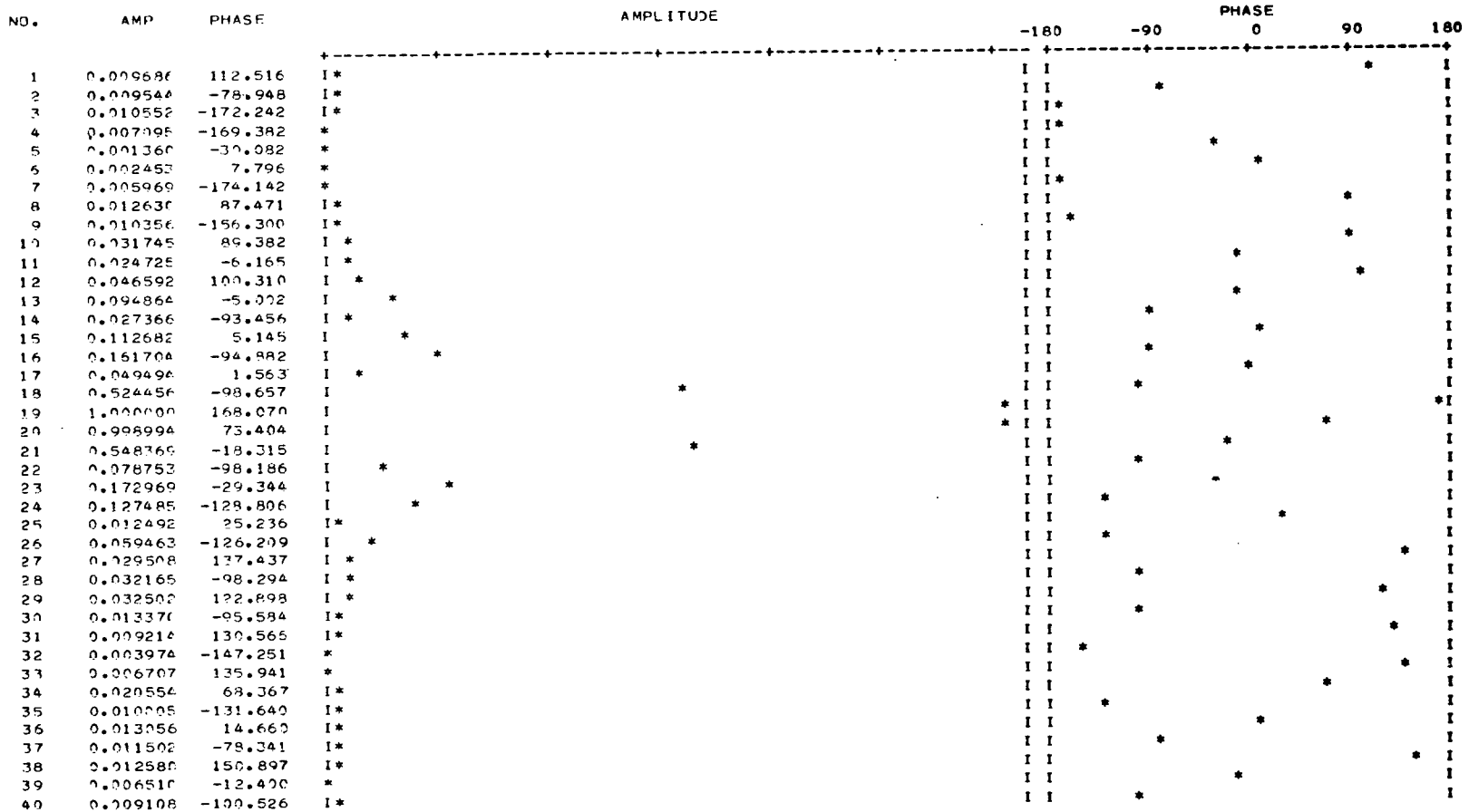

Figure 17a. Correlation Function for Broadband Spacecraft Noise - Case of Small Delay Residual

PLOT OF FREQUENCY SPECTRUM. PEAK VALUE = 1.043227

NO.	AMP	PHASE
1	0.032659	117.677
2	0.039563	96.080
3	0.064404	95.517
4	0.122013	99.263
5	0.229085	93.906
6	0.381578	86.211
7	0.547448	79.307
8	0.689330	72.464
9	0.793393	64.799
10	0.869049	55.692
11	0.925677	49.213
12	0.961624	42.786
13	0.974486	37.196
14	0.971990	32.094
15	0.969667	25.754
16	0.978628	20.402
17	0.994205	13.498
18	1.000000	7.318
19	0.989265	1.864
20	0.976294	-4.456
21	0.975833	-12.424
22	0.979166	-20.571
23	0.969217	-27.693
24	0.952753	-34.381
25	0.950504	-41.358
26	0.958658	-48.114
27	0.953374	-54.318
28	0.935656	-60.657
29	0.935451	-67.367
30	0.961299	-73.557
31	0.981111	-79.309
32	0.968681	-86.170
33	0.934586	-94.898
34	0.887027	-103.700
35	0.796627	-110.573
36	0.636932	-115.834
37	0.438143	-120.790
38	0.265786	-126.412
39	0.155689	-132.889
40	0.116934	-140.419

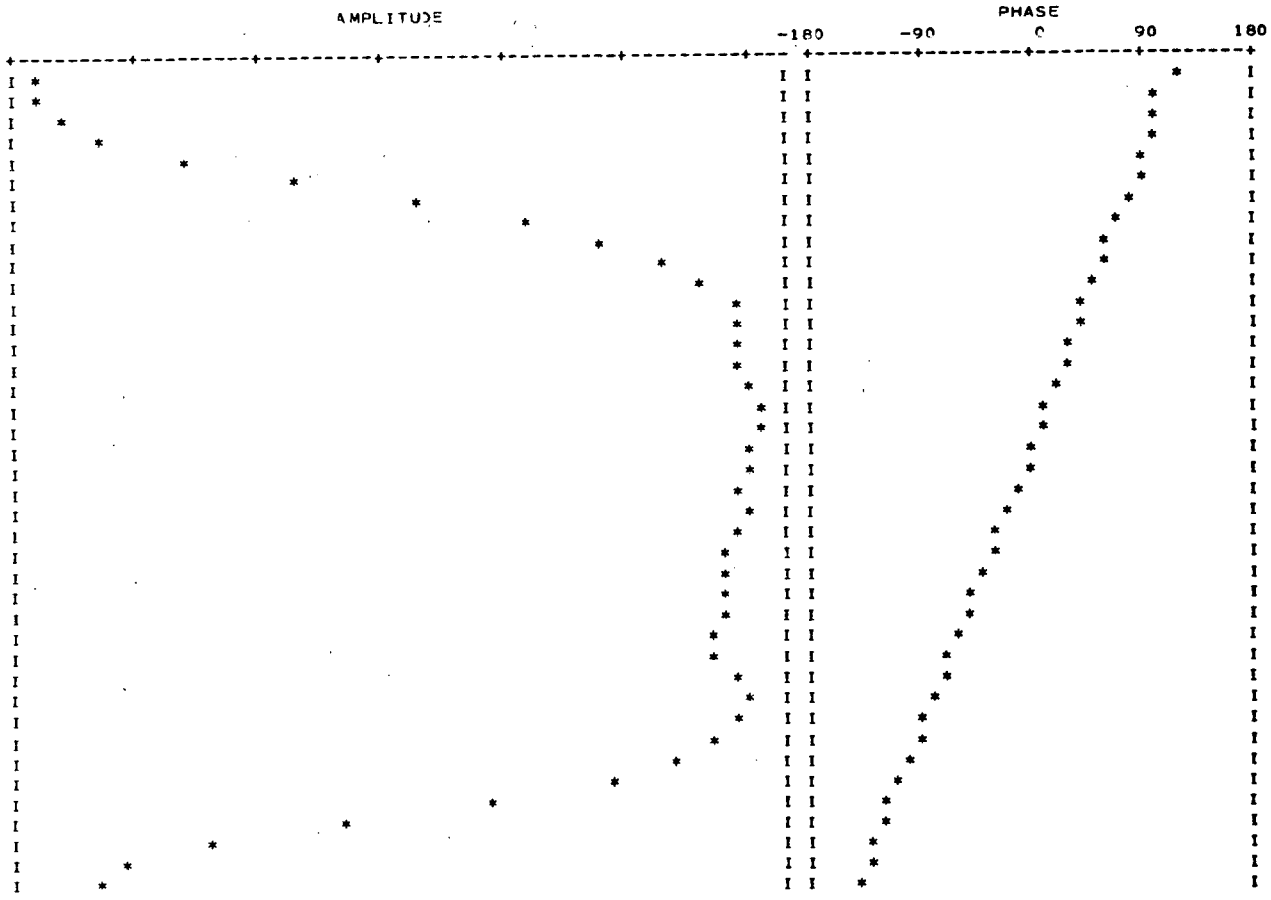

LEAST SQUARES FOR PHASE (IN CYCLES) VS FREQUENCY (IN HZ)

PHASE = (-.2060445380-05) * NO. + 0.3496940560 00
SIGMA IN PHASE = 0.4504756590-02
SIGMA IN SLOPE = 0.9583113610-08

Figure 17b. Power Spectrum for Broadband Spacecraft Noise - Case of Small Delay Residual

RUN 159-21-45 NO. REC.= 5 S.REC.NO.E= 2
SOURCE ATS-3 S-N NO. PTS.= 40 S.REC.NO.W= 1

VLBI233 VAR233/VAM233 SAT-C

GEOM. DELAY = 4118.00
INST. DELAY = 61670

DAY= 159 TIME= 21.0000 45.0000 1.2276

	FREQ	AMPLITUDE	TAU	CORREL AMPL	CORRELATION AMPLITUDE TAU
1	7.6000000	0.221266690378	-2.068557935192	0.069486373679	
2	7.7000000	0.216225123219	-2.071395266307	0.069432214241	
3	7.8000000	0.191091213078	-2.073475817508	0.063936747105	
4	7.9000000	0.147110565189	-2.075149220268	0.051576502757	
5	8.0000000	0.087198743985	-2.074414984860	0.033429181060	
6	8.1000000	0.039241215072	-5.911133554668	0.014478161606	
7	8.2000000	0.095015118297	-2.082364771348	0.039120268437	
8	8.3000000	0.168038231942	-2.074506084183	0.063601971182	
9	8.4000000	0.235566043995	-2.073546439094	0.085001634265	
10	8.5000000	0.290826710421	-2.073117496230	0.101263738472	
11	8.6000000	0.330701802714	-2.072538071954	0.110651498322	
12	8.7000000	0.346688132445	-2.071650834229	0.115522056282	
13	8.8000000	0.335096184413	-2.070563618221	0.111413659077	
14	8.9000000	0.294164361632	-2.069420237789	0.102492840566	
15	9.0000000	0.224114683015	-2.068356793189	0.080429241151	
16	9.1000000	0.128084297515	-2.070835626088	0.048599659261	
17	9.2000000	0.048393448443	-2.298071231816	0.022927065591	
18	9.3000000	0.173835443035	-2.096670221994	0.071044144494	
19	9.4000000	0.319644001905	-2.080064012215	0.123046176708	
20	9.5000000	0.469027580599	-2.075084644807	0.175601668671	
21	9.6000000	0.616483617990	-2.072776115090	0.226215386557	
22	9.7000000	0.759123673731	-2.070671798266	0.273010878522	
23	9.8000000	0.884381889213	-2.067212696702	0.313473520753	
24	9.9000000	0.980795949660	-2.063020444143	0.344084478499	
25	10.0000000	1.043227087496	-2.060445377340	0.363323145493	
26	10.1000000	1.074352039891	-2.060236458239	0.375172250674	
27	10.2000000	1.076689905532	-2.059565116324	0.377237959336	
28	10.3000000	1.045940276723	-2.055662428293	0.367260060985	
29	10.4000000	0.978381945866	-2.049527633775	0.343335706412	
30	10.5000000	0.879621959615	-2.043798666410	0.307538283239	
31	10.6000000	0.758525712360	-2.038709442630	0.266893182703	
32	10.7000000	0.625864064307	-2.031449726224	0.222135298823	
33	10.8000000	0.490728155674	-2.018782256772	0.174244432871	
34	10.9000000	0.352289765929	-1.996408703220	0.125155118623	
35	11.0000000	0.218565852740	-1.947447361081	0.077514481903	
36	11.1000000	0.097347196269	-1.742339141569	0.034219259492	
37	11.2000000	0.063149222571	-2.521790619380	0.024920378635	
38	11.3000000	0.148329051109	-2.195286754723	0.053837767195	
39	11.4000000	0.207254264861	-2.138929730372	0.072688046800	
40	11.5000000	0.238811160460	-2.113871464888	0.081232034966	

Figure 17c. Fringe Spectrum for Broadband Spacecraft Noise.

Figure 17c. Continued

159-22-39 ATS 3 P-R

SEARCH FREQUENCY NUMBER 14
SEARCH FREQUENCY 5.6500
MAXIMUM AMPLITUDE .377265

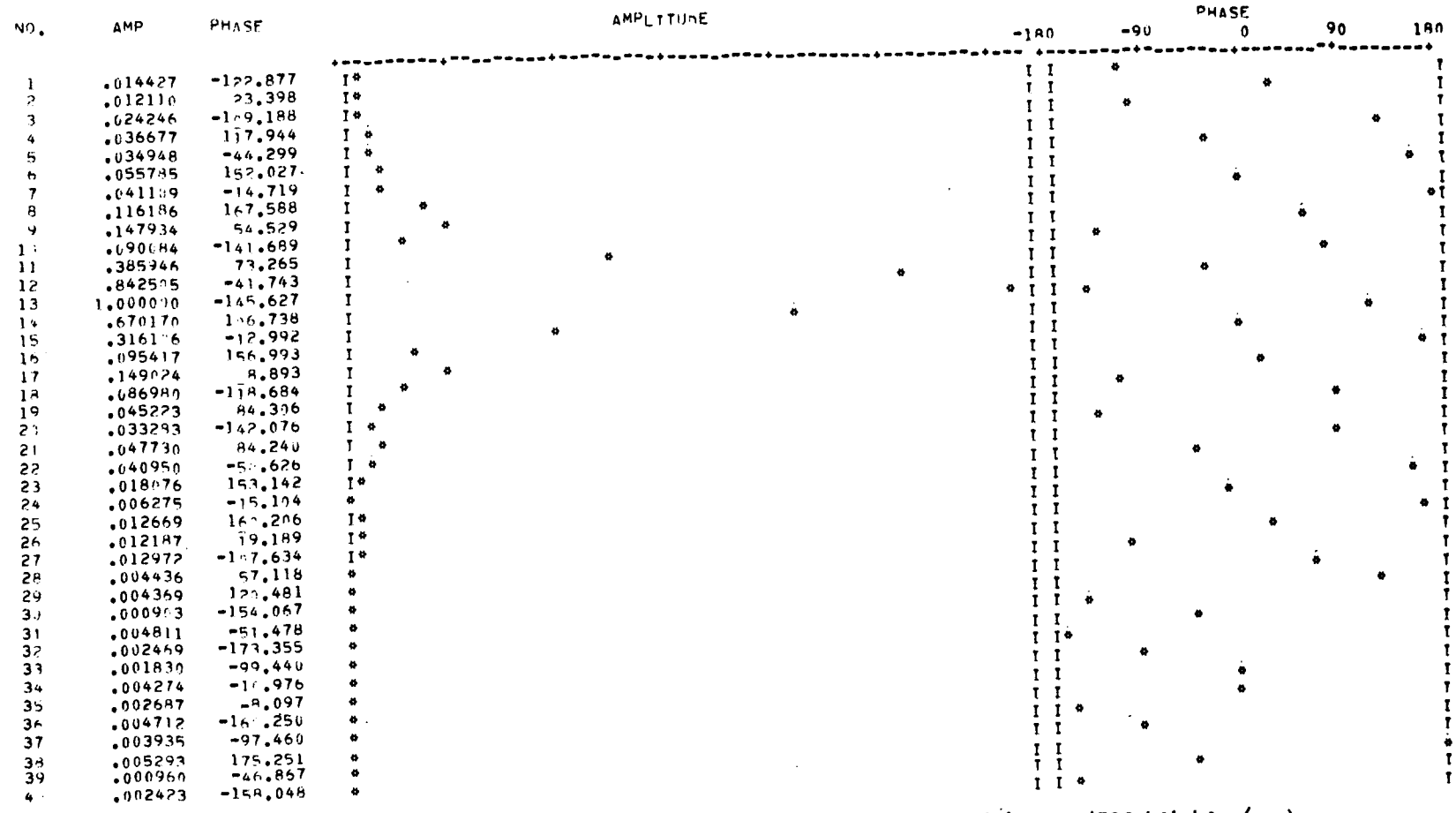

Figure 18a. Correlation Function for Pseudo Random Sequence Modulation (500 kilobits/sec) - Case of Large Delay Residual

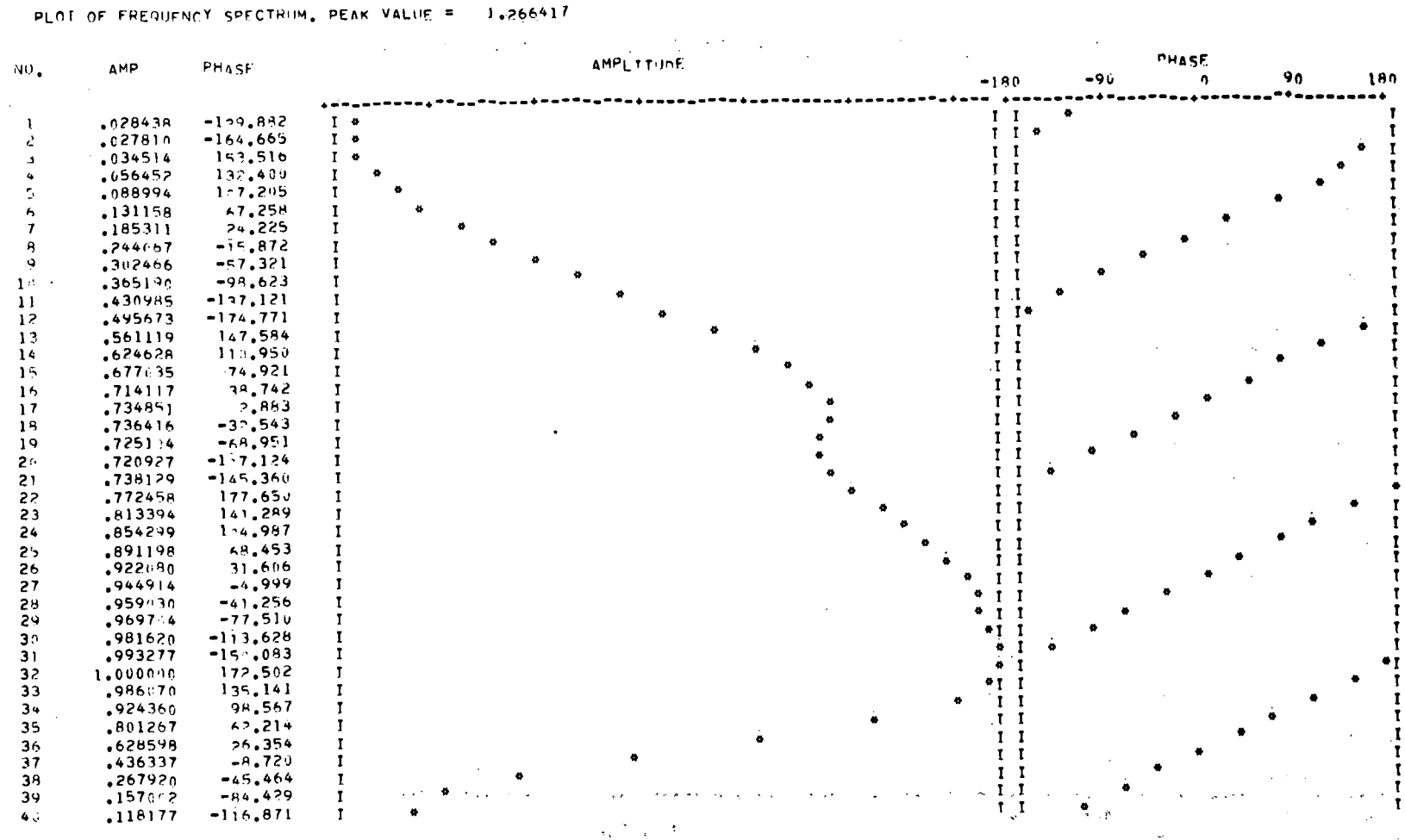

Figure 18b. Power Spectrum for Pseudo Random Sequence Modulation (500 kilobits/sec) - Case of Large Delay Residual

159-21-33 ATS 3 P-R

SEARCH FREQUENCY NUMBER 11
SEARCH FREQUENCY 11.0000
MAXIMUM AMPLITUDE .394213

NO.	AMP	PHASE
1	.021139	95.358
2	.022672	-52.322
3	.021817	158.303
4	.026001	18.808
5	.021414	-124.610
6	.015429	73.603
7	.024499	-61.181
8	.025894	132.191
9	.012337	-44.420
10	.026148	107.479
11	.057093	-38.531
12	.096115	176.781
13	.118491	20.753
14	.167402	-141.346
15	.214529	64.433
16	.319284	-99.237
17	.590920	119.067
18	.931024	-7.387
19	1.000000	-130.266
20	.701060	105.584
21	.402572	-27.325
22	.235488	172.149
23	.188701	9.562
24	.141117	-154.915
25	.100853	48.664
26	.067548	-97.373
27	.044808	162.987
28	.028584	-103.791
29	.040047	79.970
30	.037104	-58.122
31	.021793	171.179
32	.021263	15.083
33	.022064	-146.942
34	.025560	61.600
35	.013575	-96.042
36	.007224	131.264
37	.006424	49.638
38	.008132	-67.661
39	.009464	142.446
40	.010800	-.117

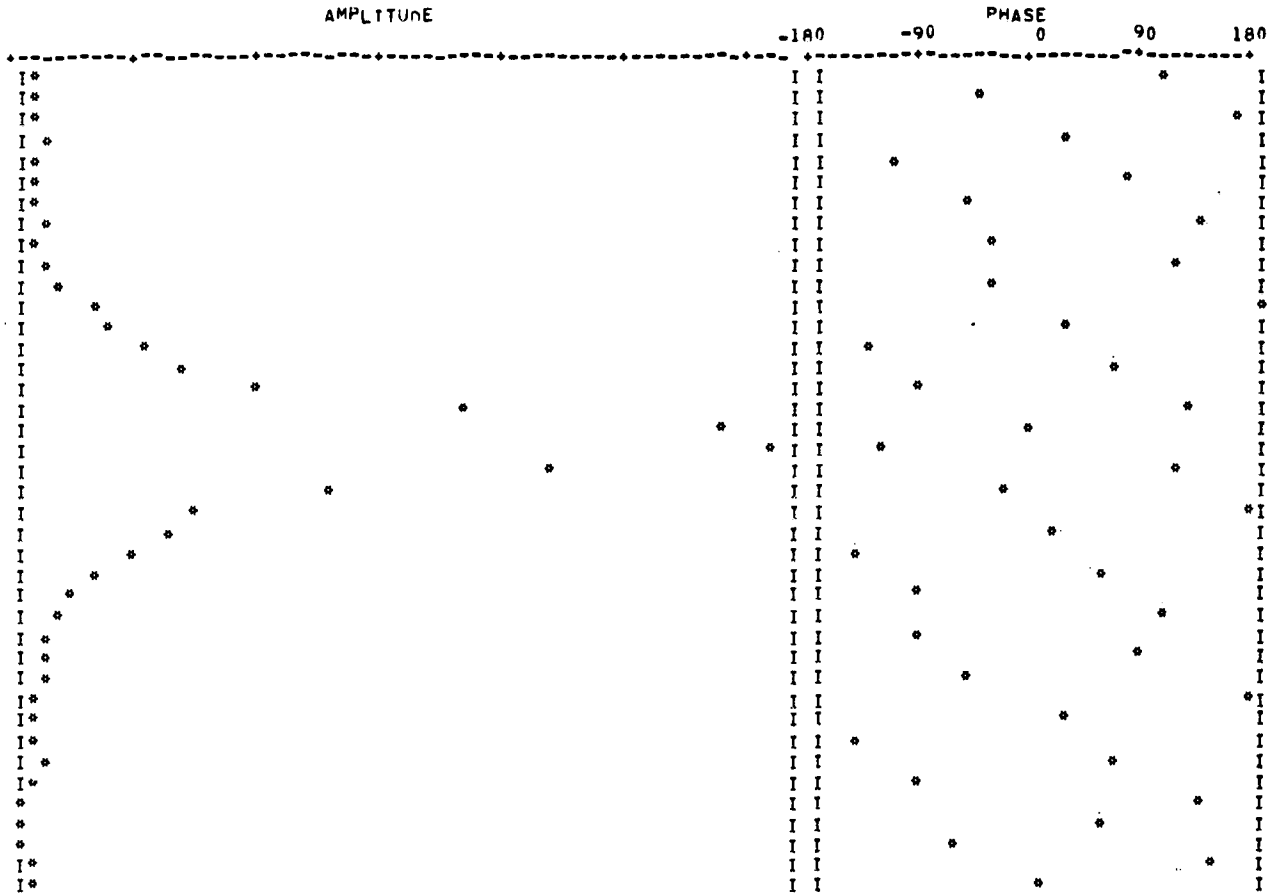

Figure 19a. Correlation Function for Pseudo Random Sequence Modulation (1 Mbit/sec) - Case of Large Delay Residual

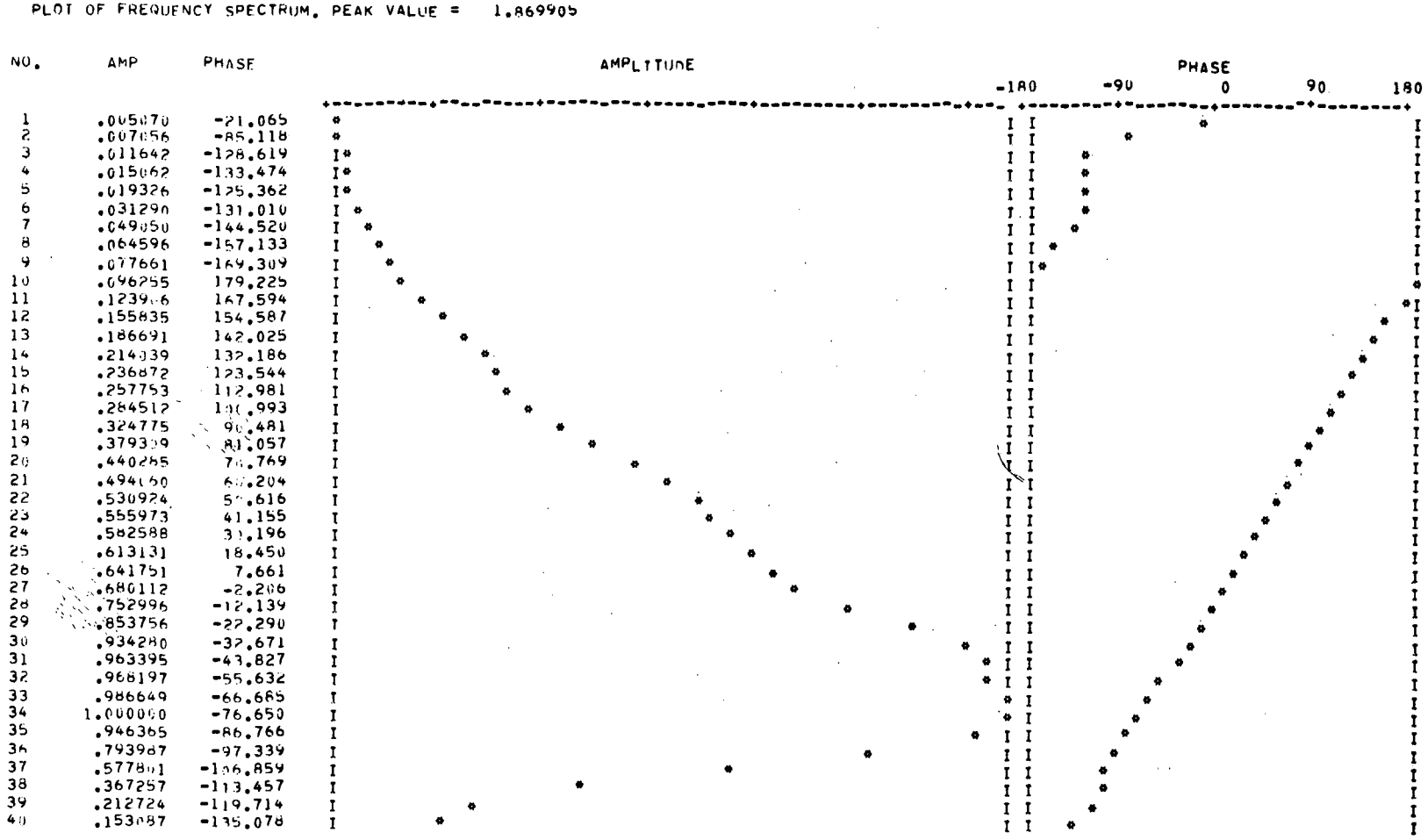

Figure 19b. Power Spectrum for Pseudo Random Sequence Modulation (1 Mbit/sec) – Case of Large Delay Residual

159-21-33 ATS-3 P-S

SEARCH FREQUENCY NUMBER 19
SEARCH FREQUENCY 11.0000000
MAXIMUM AMPLITUDE 0.341805489350 64

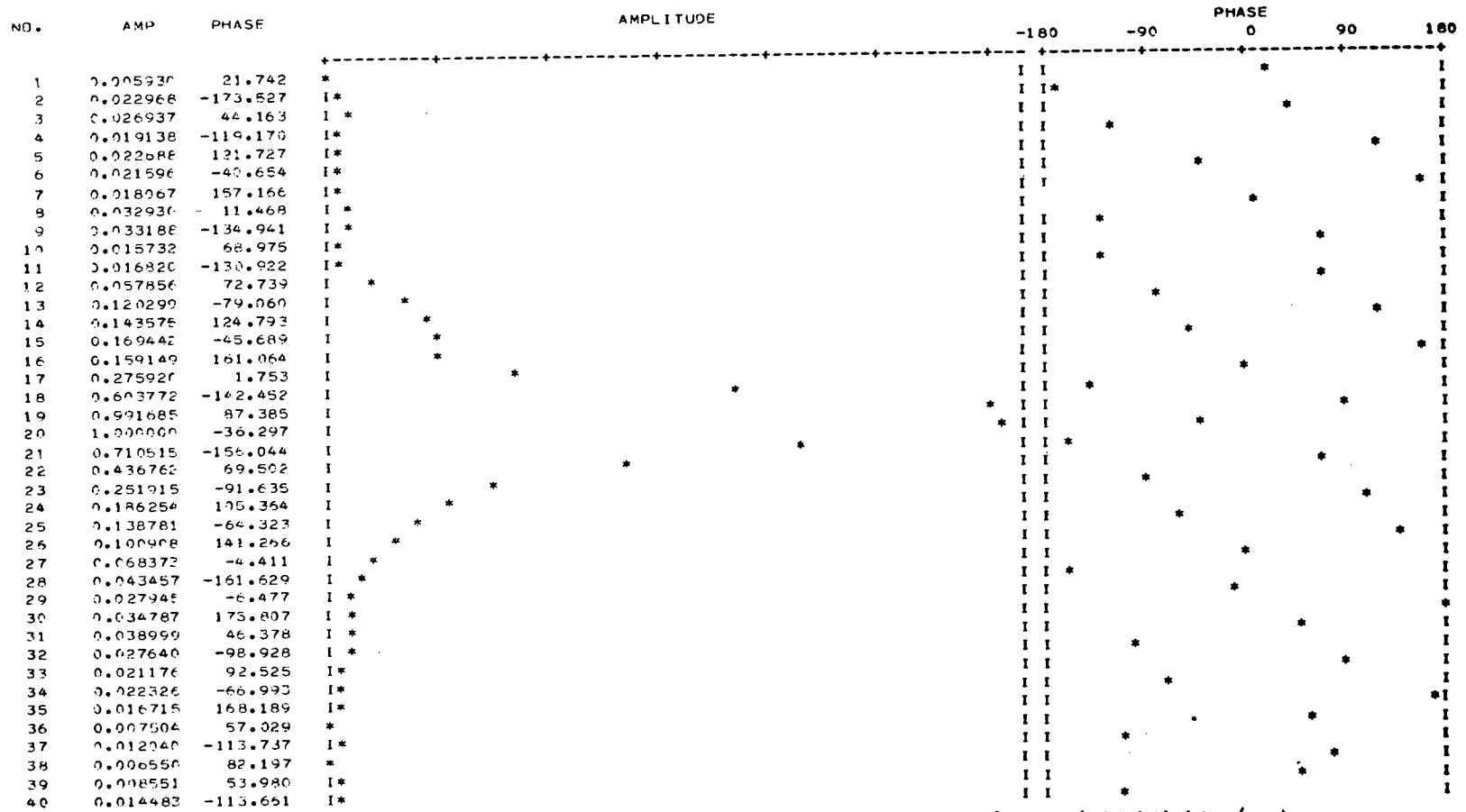

Figure 20a. Correlation Function for Pseudo Random Sequence Modulation (500 kilobits/sec) – Case of Small Delay Residual

PLOT OF FREQUENCY SPECTRUM. PEAK VALUE = 1.655398

NO.	AMP	PHASE
1	0.007451	-24.644
2	0.009352	-21.905
3	0.011337	-26.469
4	0.012646	-28.416
5	0.019968	-14.061
6	0.035527	-13.596
7	0.053862	-22.199
8	0.069934	-31.375
9	0.084192	-36.543
10	0.100547	-40.632
11	0.123651	-49.600
12	0.154860	-60.718
13	0.187813	-67.827
14	0.213575	-71.511
15	0.232155	-76.222
16	0.253199	-83.849
17	0.285465	-91.232
18	0.331706	-96.467
19	0.391609	-101.808
20	0.459057	-108.647
21	0.517928	-115.676
22	0.554484	-121.842
23	0.574581	-127.532
24	0.595013	-133.387
25	0.619941	-139.306
26	0.644510	-145.065
27	0.680087	-150.692
28	0.746727	-155.976
29	0.835679	-160.936
30	0.905189	-166.261
31	0.932374	-172.437
32	0.944605	-178.951
33	0.974603	175.176
34	1.000000	169.613
35	0.956482	163.401
36	0.809746	156.799
37	0.595240	151.484
38	0.384950	149.178
39	0.228292	147.179
40	0.166511	136.326

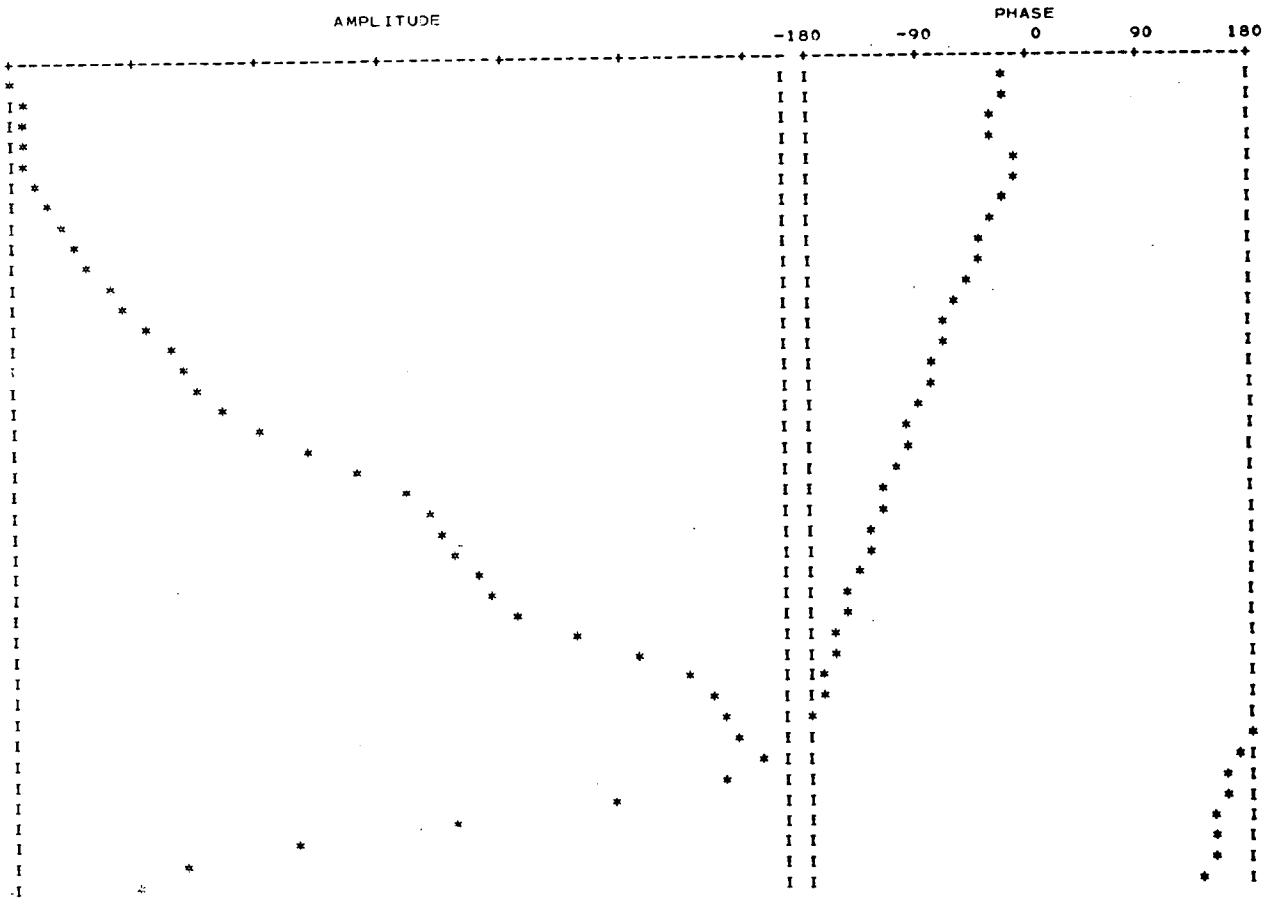

LEAST SQUARES FOR PHASE (IN CYCLES) VS FREQUENCY (IN HZ)

PHASE = (-.1902807690-05) * NO. + 0.4643599540-01
SIGMA IN PHASE = 0.7213377390-02
SIGMA IN SLOPE = 0.1534529980-07

Figure 20b. Power Spectrum for Pseudo Random Sequence Modulation (500 kilobits/sec) - Case of Small Delay Residual

RUN 159-21-22 NO. REC.= 5 S.REC.NO.s= 1
SOURCE ATS-3 P-R NO. PTS.= 40 S.REC.NO.w= 1

VLBI231 VAR231/VAM231 SAT-C

GEOM. DELAY = 4114.20
INST. DELAY = -5530

DAY= 159 TIME= 21.[illegible] 22.[illegible] 1.1412

	FREQ	AMPLITUDE	TAU	CORREL AMPL	CORRELATION AMPLITUDE	TAU
1	9.9000000	0.[illegible]47461864	-1.[illegible]1916247[illegible]	0.[illegible]195418486	I* I	* I
2	10.0000000	0.[illegible]1187358	-3.[illegible]17989849	0.[illegible]255649366	I* I	I
3	10.1000000	0.131462[illegible]28969	-1.4157131[illegible]009	0.[illegible]6804378	I * I	* I
4	10.2000000	0.199121[illegible]67619	-1.482186924675	0.[illegible]599918183	I * I	* I
5	10.3000000	0.257449496226	-1.475157581691	0.[illegible]891424411	I * I	* I
6	10.4000000	0.287717781913	-1.481753703471	0.[illegible]51523317756	I * I	* I
7	10.5000000	0.288536676285	-1.486698960197	0.[illegible]9167265523[illegible]	I * I	* I
8	10.6000000	0.2582[illegible]5256792	-1.488073175477	0.[illegible]51823324793	I * I	* I
9	10.7000000	0.19[illegible]76[illegible]52936	-1.495834175527	0.[illegible]6112160676[illegible]	I * I	* I
10	10.8000000	0.11[illegible]647049517	-1.[illegible]6[illegible]489946651	0.[illegible]31748169120	I * I	* I
11	10.9000000	0.1[illegible]5[illegible]1380317	-1.[illegible]4[illegible]4569933327	0.[illegible]23926691497	I * I	* I
12	11.0000000	0.2516289[illegible]785	-1.4616[illegible]118967	0.[illegible]6829590[illegible]63	I * I	* I
13	11.1000000	0.3694667362[illegible]	-1.5[illegible]38[illegible]4562	0.122848953351	I * I	* I
14	11.2000000	0.[illegible]8[illegible]2464[illegible]811	-1.[illegible]43226[illegible]7572	0.18[illegible]933739923	I * I	* I
15	11.3000000	0.761[illegible]71[illegible]63116	-1.[illegible]5[illegible]15037[illegible]7515	0.23[illegible]5[illegible]736[illegible]2	I * I	* I
16	11.4000000	0.[illegible]31[illegible]0[illegible]1[illegible]69[illegible]69	-1.[illegible]5[illegible]4[illegible]5[illegible]2[illegible]4418	0.[illegible]2513[illegible]3[illegible]5[illegible]274	I * I	* I
17	11.5000000	1.[illegible]81[illegible]3[illegible]9[illegible]9441	-1.[illegible]5[illegible]8[illegible]221178932	0.337241723422	I * I	* I
18	11.6000000	1.20504421[illegible]79	-1.[illegible]5[illegible]1595[illegible]8[illegible]435	0.[illegible]37[illegible]43[illegible]3[illegible]1[illegible]	I * I	* I
19	11.7000000	1.2943[illegible]5521[illegible]98	-1.[illegible]5[illegible]1[illegible]1[illegible]9978[illegible]3	0.[illegible]4[illegible][illegible]49[illegible]3[illegible]271	I * I	* I
20	11.8000000	1.341[illegible]3[illegible]342990	-1.497046[illegible]39895	0.[illegible]420219717147	I * I	* I
21	11.9000000	1.343[illegible]6[illegible]99[illegible]1	-1.495[illegible]4[illegible]3[illegible]2[illegible]89	0.[illegible]41814117[illegible]40	I * I	* I
22	12.0000000	1.3[illegible]2[illegible]61[illegible]2[illegible]526	-1.[illegible]5[illegible]76[illegible]4[illegible]98579	0.[illegible]4[illegible]5[illegible]8[illegible]78[illegible]2[illegible]8	I * I	* I
23	12.1000000	1.223379539313	-1.51476312[illegible]681	0.38[illegible]3[illegible]4[illegible]13574	I * I	* I
24	12.2000000	1.1[illegible]6[illegible]64[illegible]96686	-1.[illegible]7552977[illegible]6[illegible]	0.[illegible]35[illegible]711[illegible]94718	I * I	* I
25	12.3000000	0.[illegible]5[illegible]43[illegible]97[illegible]3[illegible]4	-1.497335[illegible]6[illegible]797	0.[illegible]3[illegible]5789229618	I * I	* I
26	12.4000000	0.[illegible]7[illegible]852[illegible]21232	-1.49365[illegible]336792	0.[illegible]252[illegible]343[illegible]82[illegible]15	I * I	* I
27	12.5000000	0.[illegible]5[illegible]7[illegible]49[illegible]92155	-1.49[illegible]3[illegible]5[illegible]1[illegible]5730	0.[illegible]1[illegible]6[illegible]58[illegible]066[illegible]25[illegible]	I * I	* I
28	12.6000000	0.[illegible]4[illegible]9[illegible]33[illegible]84646	-1.484[illegible]76417747	0.[illegible]13947547[illegible]224	I * I	* I
29	12.7000000	0.23[illegible]3[illegible]5[illegible]354757	-1.[illegible]45[illegible]3[illegible]9[illegible]9[illegible]5[illegible]66	0.[illegible]8447979[illegible]9[illegible]7	I * I	* I
30	12.8000000	0.[illegible]7[illegible]8427[illegible]25122	-1.[illegible]9[illegible]4[illegible]9[illegible]71[illegible]6[illegible]53479	0.[illegible]3[illegible]6[illegible]6[illegible]7[illegible]6[illegible]78[illegible]19	I * I	*I
31	12.9000000	0.[illegible]1[illegible]9[illegible]33[illegible]6[illegible]3[illegible]9[illegible]89	-1.[illegible]5[illegible]8[illegible]71[illegible]74[illegible]3[illegible]2[illegible]84	0.[illegible]3[illegible]6[illegible]261[illegible]25[illegible]3[illegible]63	I * I	* I
32	13.0000000	0.[illegible]2[illegible]6[illegible]7[illegible]3[illegible]3[illegible]6[illegible]2[illegible]89	-1.[illegible]3[illegible]4[illegible]3[illegible]12[illegible]1[illegible]7[illegible]69[illegible]779	0.[illegible]6[illegible]14[illegible]7[illegible]8[illegible]8[illegible]9[illegible]721	I * I	* I
33	13.1000000	0.[illegible]3[illegible]1[illegible]7[illegible]55[illegible]4[illegible]7[illegible]8[illegible]14	-1.[illegible]5[illegible]7[illegible]6[illegible]9[illegible]8[illegible]1[illegible]8[illegible]648	0.[illegible]7[illegible]9[illegible]1[illegible]3[illegible]4[illegible]7[illegible]2[illegible]38	I * I	* I
34	13.2000000	0.[illegible]3[illegible]3[illegible]2[illegible]4[illegible]7[illegible]5[illegible]2[illegible]91	-1.[illegible]524[illegible]3[illegible]5[illegible]3[illegible]46123	0.[illegible]9[illegible]4[illegible]4[illegible]57[illegible]4[illegible]611	I * I	* I
35	13.3000000	0.[illegible]3[illegible]7[illegible]3[illegible]4[illegible]9[illegible]4[illegible]9[illegible]4[illegible]649	-1.[illegible]5[illegible]1[illegible]8[illegible]1[illegible]4[illegible]2[illegible]7[illegible]923	0.[illegible]9[illegible]9[illegible]7[illegible]4[illegible]4[illegible]2[illegible]3[illegible]7[illegible]313	I * I	* I
36	13.4000000	0.[illegible]3[illegible]5[illegible]5[illegible]7[illegible]7[illegible]4[illegible]2[illegible]942	-1.[illegible]5[illegible]1[illegible]2[illegible]8[illegible]7[illegible]5[illegible]4[illegible]5[illegible]261	0.[illegible]9[illegible]6[illegible]5[illegible]5[illegible]2[illegible]3[illegible]8[illegible]219	I * I	* I
37	13.5000000	0.[illegible]3[illegible]1[illegible]9[illegible]6[illegible]6[illegible]7[illegible]7[illegible]525	-1.[illegible]5[illegible]7[illegible]5[illegible]4[illegible]9[illegible][illegible]8[illegible]5[illegible]37	0.[illegible]8[illegible]5[illegible]9[illegible]1[illegible]2[illegible]9[illegible]6[illegible]3[illegible]319	I * I	* I
38	13.6000000	0.[illegible]2[illegible]5[illegible]7[illegible]3[illegible]1[illegible]4[illegible]8[illegible]5[illegible]038	-1.[illegible]4[illegible]9[illegible]9[illegible]5[illegible]5[illegible]6[illegible]5[illegible]3[illegible]6[illegible]6	0.[illegible]0[illegible]9[illegible]5[illegible]1[illegible]0[illegible]2[illegible]2[illegible]9[illegible]6[illegible]42	I * I	* I
39	13.7000000	0.[illegible]1[illegible]8[illegible]3[illegible]6[illegible]2[illegible]9[illegible]8[illegible]2[illegible]6[illegible]131	-1.[illegible]4[illegible]2[illegible]3[illegible]5[illegible]6[illegible]4[illegible]8[illegible]1[illegible]3[illegible]7[illegible]6[illegible]9	0.[illegible]3[illegible]4[illegible]9[illegible]6[illegible]5[illegible]7[illegible]7[illegible]8[illegible]3[illegible]2[illegible]49	I * I	* I
40	13.8000000	0.[illegible]1[illegible]4[illegible]5[illegible]8[illegible]5[illegible]5[illegible]3[illegible]6[illegible]1[illegible]9[illegible]0	-1.[illegible]4[illegible]3[illegible]3[illegible]8[illegible]6[illegible]9[illegible]5[illegible]3[illegible]6[illegible]5[illegible]73	0.[illegible]0[illegible]2[illegible]8[illegible]2[illegible]7[illegible]5[illegible]1[illegible]6[illegible]5[illegible]703	I * I	* I

Figure 20c. Fringe Spectrum for Pseudo Random Sequence Modulation

159-21-56 SIDET ENS

SEARCH FREQUENCY NUMBER 7
SEARCH FREQUENCY 9.2600
MAXIMUM AMPLITUDE .414657

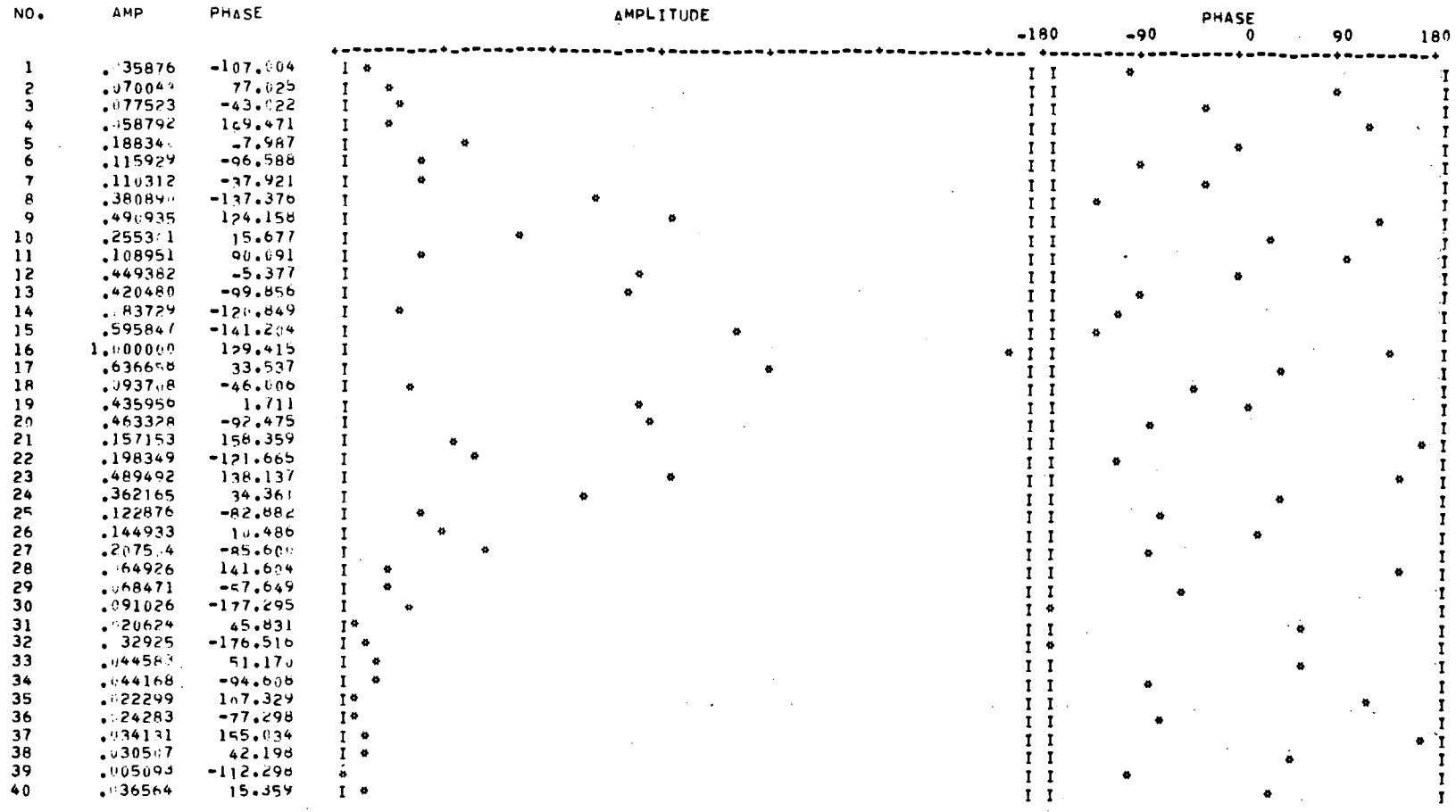

Figure 21a. Correlation Function for Sidetone Ensemble Modulation - Case of Large Delay Residual

PLOT OF FREQUENCY SPECTRUM. PEAK VALUE = 2.419238

NO.	AMP	PHASE
1	.011852	-11.932
2	.024950	143.031
3	.060931	95.13
4	.105186	56.917
5	.122214	34.874
6	.089363	19.927
7	.051559	-14.886
8	.087272	-47.763
9	.235196	-54.626
10	.484328	-75.818
11	.770916	-98.331
12	.975097	-119.154
13	1.000000	-140.661
14	.859563	-165.395
15	.636765	168.248
16	.396158	144.933
17	.188664	124.116
18	.069747	89.681
19	.060283	69.521
20	.132230	62.532
21	.237983	41.659
22	.327552	16.516
23	.361445	-8.501
24	.334148	-35.461
25	.272194	-62.854
26	.203370	-85.909
27	.137937	-102.561
28	.078577	-116.829
29	.045260	-140.985
30	.077573	172.292
31	.205621	175.366
32	.429273	156.189
33	.708017	134.115
34	.932778	106.477
35	.952122	87.143
36	.720219	49.352
37	.384299	47.746
38	.135842	12.196
39	.035898	34.369
40	.020035	79.696

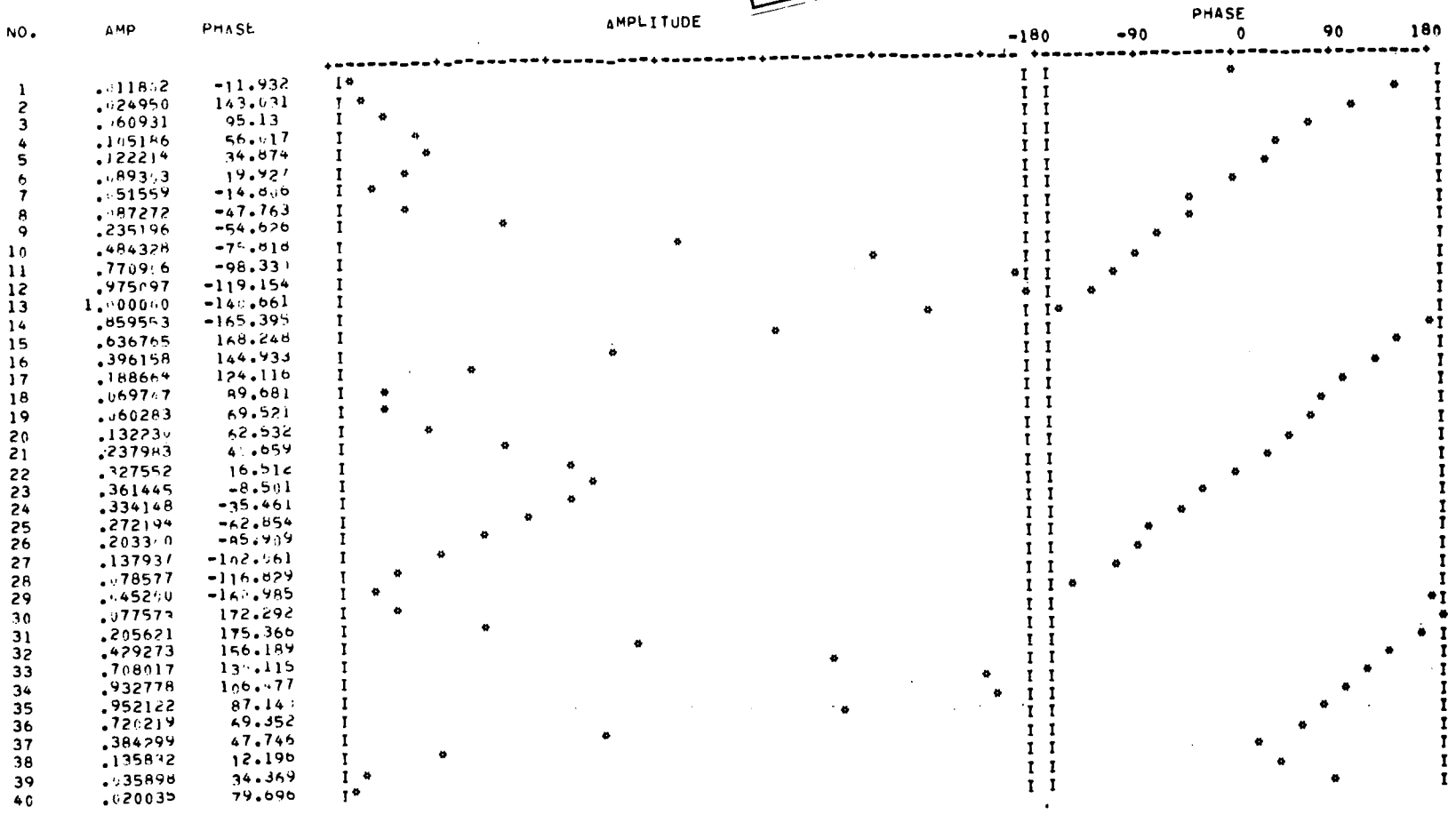

Figure 21b. Power Spectrum for Sidetone Ensemble Modulation – Case of Large Delay Residual

```
169-21-56 ATS-3 S-E

SEARCH FREQUENCY NUMBER   20
SEARCH FREQUENCY          9.2500300
MAXIMUM AMPLITUDE         0.5905222004547328
```

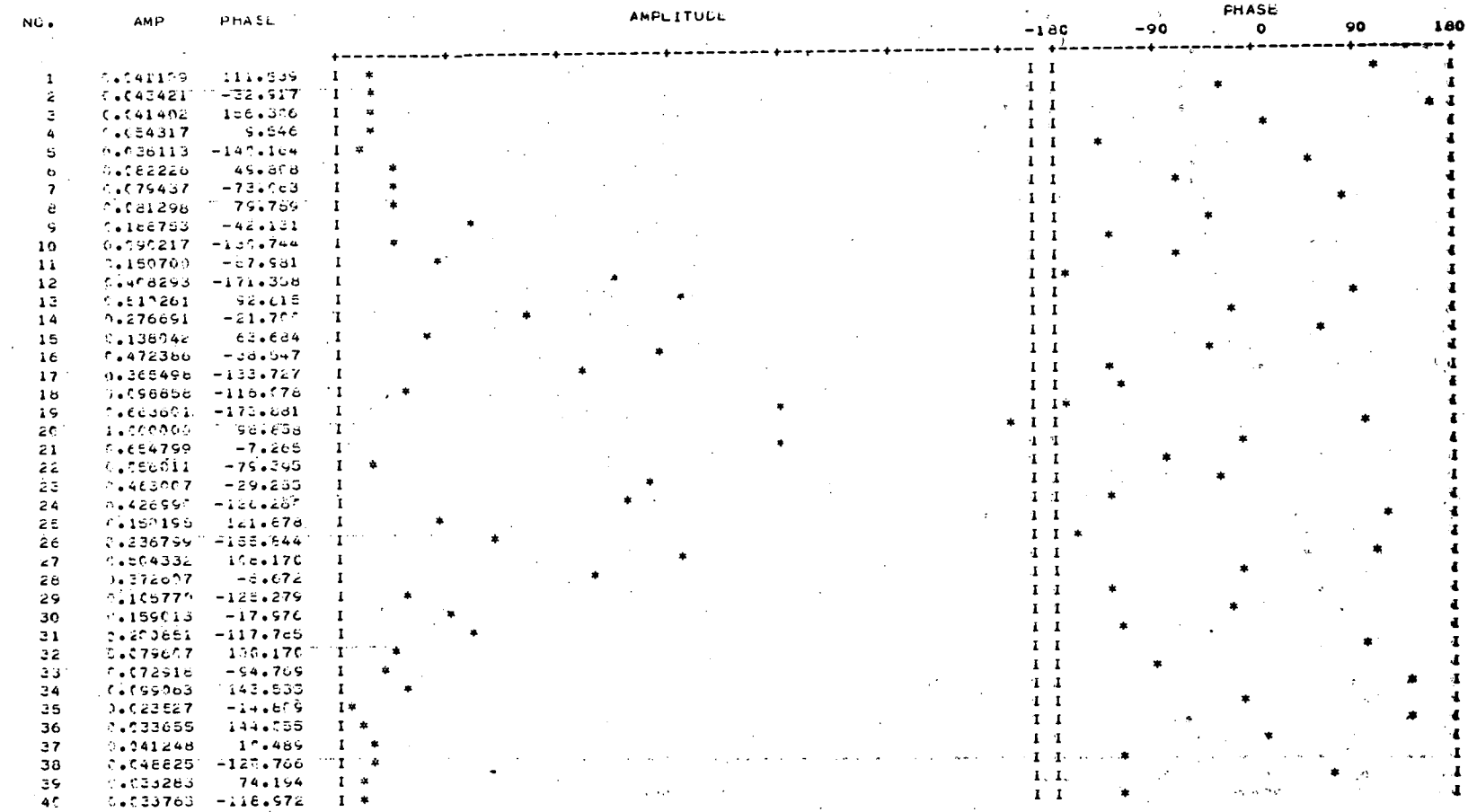

Figure 22a. Correlation Function for Sidetone Ensemble Modulation – Case of Small Delay Residual

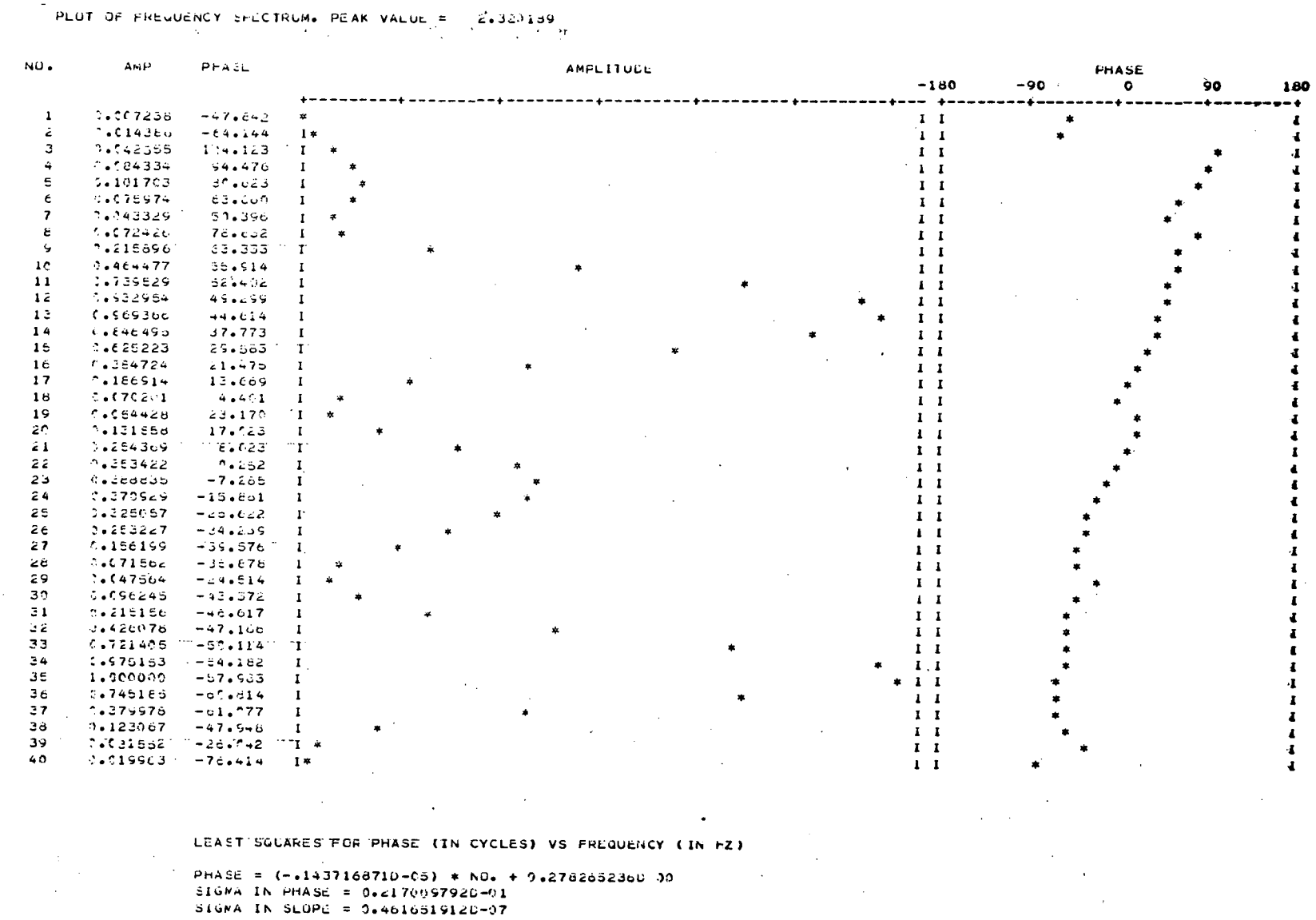

LEAST SQUARES FOR PHASE (IN CYCLES) VS FREQUENCY (IN HZ)

PHASE = (-.1437168710-05) * NO. + 0.2782652360 00
SIGMA IN PHASE = 0.2170097920-01
SIGMA IN SLOPE = 0.4616519120-07

Figure 22b. Power Spectrum for Sidetone Ensemble Modulation – Case of Small Delay Residual

RUN 159-21-56 NO. REC.= 5 S.REC.NO.e= 7
SOURCE ATS-3 S-E NO. PTS.= 40 S.REC.NO.w= 6

VLB1234 VAR234/VAM234 SAT-C

GEOM. DELAY = 4119.60
INST. DELAY = -39139

DAY= 159 TIME= 21.0000 56.0000 32.1760

	FREQ	AMPLITUDE	TAU	CORREL AMPL	CORRELATION AMPLITUDE	TAU
1	7.3000000	0.092712279747	-1.123102460497	0.017572994727	I*	I * I
2	7.4000000	0.201338223449	-1.302034131449	0.029361083258	I *	I * I
3	7.5000000	0.332371258128	-1.348530295335	0.053278174493	I *	I * I
4	7.6000000	0.456939496360	-1.374082277704	0.075273540521	I *	I * I
5	7.7000000	0.542484091593	-1.391713034439	0.092188276289	I *	I * I
6	7.8000000	0.594333700380	-1.405986788744	0.101936869953	I *	I * I
7	7.9000000	0.596969095181	-1.417920943503	0.102827033800	I *	I * I
8	8.0000000	0.544130163590	-1.429948464740	0.093949444361	I *	I * I
9	8.1000000	0.432833812776	-1.444755835143	0.074845785912	I *	I * I
10	8.2000000	0.286861949475	-1.463790092714	0.049307071616	I *	I * I
11	8.3000000	0.082437491459	-6.440164139240	0.018456359721	I*	I * I
12	8.4000000	0.275869961317	-1.259871421639	0.048054552525	I *	I * I
13	8.5000000	0.582269489686	-1.374460447316	0.099854645341	I *	I * I
14	8.6000000	0.908791106836	-1.397659692479	0.156908498645	I *	I * I
15	8.7000000	1.233479682743	-1.410221729231	0.211229389000	I *	I * I
16	8.8000000	1.544306201818	-1.419793395576	0.265866244561	I *	I * I
17	8.9000000	1.782102824717	-1.422127110211	0.309261404094	I *	I * I
18	9.0000000	2.053246314513	-1.425694887318	0.349505465549	I *	I * I
19	9.1000000	2.223560199666	-1.433794594053	0.373577963426	I *	I * I
20	9.2000000	2.320186787384	-1.437108713422	0.390582866473	I *	I * I
21	9.3000000	2.347916779437	-1.435818660612	0.395505637159	I *	I * I
22	9.4000000	2.301085578758	-1.445961956834	0.386525929316	I *	I * I
23	9.5000000	2.174488563859	-1.451820846342	0.366634049617	I *	I * I
24	9.6000000	1.968228466854	-1.451106946751	0.331699088532	I *	I * I
25	9.7000000	1.742235303493	-1.459055949108	0.291586387056	I *	I * I
26	9.8000000	1.483561863628	-1.468669386427	0.241191045074	I *	I * I
27	9.9000000	1.139111272574	-1.476658499356	0.187609083234	I *	I * I
28	10.0000000	0.818602348935	-1.493309699327	0.134184522408	I *	I * I
29	10.1000000	0.501883462145	-1.527530398575	0.085535668891	I *	I * I
30	10.2000000	0.220088797957	-1.634150152815	0.054086737532	I *	I * I
31	10.3000000	0.073144955538	-2.990514294563	0.057445732006	I *	I * I
32	10.4000000	0.269961879044	-1.311550181161	0.079567832608	I *	I * I
33	10.5000000	0.468418876203	-1.368479986826	0.099867854574	I *	I * I
34	10.6000000	0.457406166753	-1.396038530197	0.111810956963	I *	I * I
35	10.7000000	0.527082219814	-1.412972716562	0.114302832177	I *	I * I
36	10.8000000	0.503907088052	-1.425503325128	0.107815328192	I *	I * I
37	10.9000000	0.433394525954	-1.437967334293	0.093338206849	I *	I * I
38	11.0000000	0.326937491311	-1.454920089408	0.072940932981	I *	I * I
39	11.1000000	0.214666449425	-1.493155323429	0.049383430232	I *	I * I
40	11.2000000	0.093231857574	-5.094274429045	0.027629835034	I *	I * I

Figure 22c. Fringe Spectrum for Sidetone Ensemble Modulation

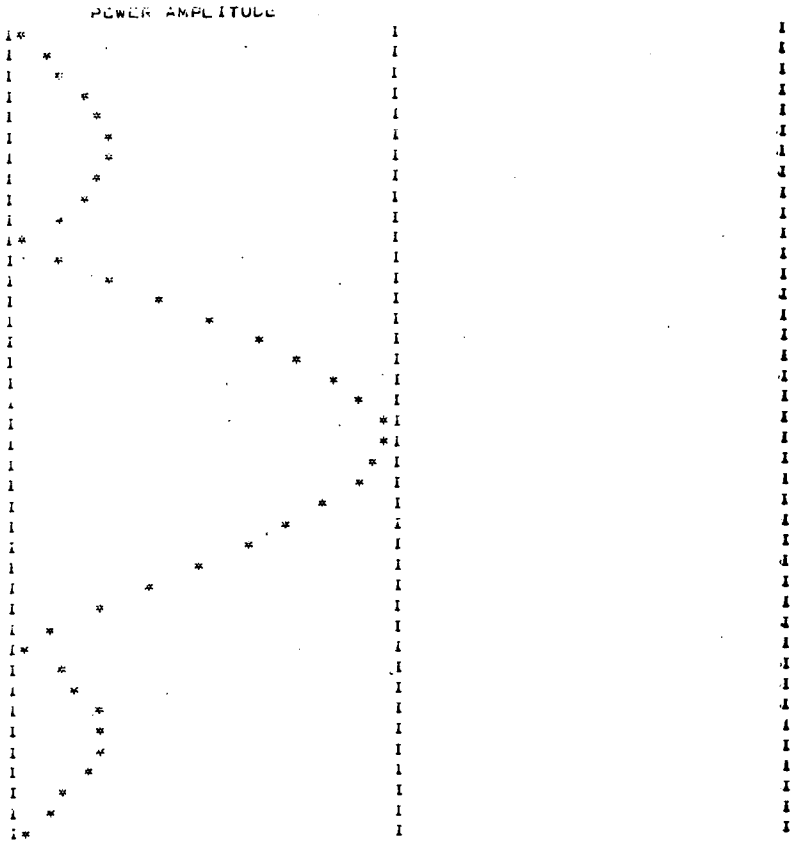

Figure 22c. Continued

central correlation peak with small side peaks is a characteristic of this modulation. Figure 19a is the correlation function of the 1 Mbit/sec rate PRS. This modulation exhibits a very broad peak with negligible side peaks. The expected bias towards higher frequencies can be seen in both the spectra (Figures 18b and 19b). Figures 20a, b and c correspond to the case of PRS modulation where the bit offset is once again less than one. However, the typical features of the correlation function and power spectrum are identical to those of Figures 18 and 19. Figures 21 and 22 are the results of a sidetone ensemble run. The range tones are clearly visible as can be seen in the spectral plots. The correlation function exhibits the strong side lobes that are characteristic of this modulation.

Analysis of the characteristics of the five types of modulation show that broadband noise, either the spacecraft front end noise (this is the noise generate by the transponder front end when it is turned on; the transponder is not triggered by any ground emitted signal) or the transponded noise spectrum whicl is originated on ground is the most advantageous type of modulation. This is predictable theoretically since a broadband noise signal contains the most frequencies within a given passband, and one expects this to make the central fringe stand out most prominently. In practice, this was confirmed, first by the fact that the fringe phase slopes for these two types consistently showed the least amount of jitter and secondly that the correlation peaks in these two types stand out strongly from the background.

In our data processing scheme, a standard integration schedule of 5 records was followed. Each digital tape has approximately 3 minutes or 900 records. In cross-correlating a pair of tapes, averaging is done over 5 records and the whole tape is processed in sequence of 5 records. Thus one has a delay and delay rate parameter approximately every second (5 records). The delay and delay-rate (fringe-rate or differential doppler) are printed out and plotted with all the accessory information. Figures 23,24, 25, and 26 show samples of the processed runs. The data (time-delay and fringe-rate) shown in these runs are smoothed and used as inputs to the orbit determination program.

Table 9 shows a sample list of satellite runs that were processed. The time delay and the doppler correspond to the time of the run. The format of the run indicates the day of the year, hours, minutes and seconds of universal time. Also, indicated in the table are the various signal modulations corresponding to the data run.

RUN 158-21-07 ROSMAN - MOJAVE
SOURCE ATS-1 N-X NREC = 5

DAY	HR	MIN	SECOND	DOPPLER	TAU
158	21	7	1.38600	-23.275	-8250.467147
158	21	7	2.39400	-23.210	-8250.432625
158	21	7	3.40200	-23.225	-8250.504816
158	21	7	4.41000	-23.420	-8250.448057
158	21	7	5.41800	-23.180	-8250.572023
158	21	7	6.42600	-23.230	-8250.402141
158	21	7	7.43400	-23.300	-8250.346112
158	21	7	8.44200	-23.155	-8250.418295
158	21	7	9.45000	-23.280	-8250.365575
158	21	7	10.45800	-23.265	-8250.431055
158	21	7	11.46600	-23.225	-8250.454922
158	21	7	12.47400	-23.240	-8250.430142
158	21	7	13.48200	-23.230	-8250.379265
158	21	7	14.49000	-23.225	-8250.368872
158	21	7	15.49800	-23.165	-8250.423093
158	21	7	16.50600	-23.250	-8250.382744
158	21	7	17.51399	-23.260	-8250.416366
158	21	7	18.52199	-23.250	-8250.395283
158	21	7	19.53000	-23.175	-8250.389646
158	21	7	20.53799	-23.175	-8250.334162
158	21	7	21.54599	-23.210	-8250.340199
158	21	7	22.55399	-23.080	-8250.366431
158	21	7	23.56200	-23.355	-8250.349954
158	21	7	24.56999	-23.160	-8250.349741
158	21	7	25.57799	-22.205	-8250.335099
158	21	7	26.58600	-23.220	-8250.328867
158	21	7	27.59399	-23.180	-8250.291720
158	21	7	28.60199	-23.215	-8250.311933
158	21	7	29.60999	-23.230	-8250.314103
158	21	7	30.61800	-23.150	-8250.340545
158	21	7	31.62599	-23.235	-8250.313873
158	21	7	32.63399	-23.200	-8250.287036
158	21	7	33.64200	-23.245	-8250.303099
158	21	7	34.64999	-23.235	-8250.274545
158	21	7	35.65799	-23.210	-8250.235789
158	21	7	36.66599	-23.165	-8250.265948
158	21	7	37.67400	-23.095	-8250.274453
158	21	7	38.68199	-23.280	-8250.263706
158	21	7	39.68999	-23.170	-8250.250816
158	21	7	40.69800	-23.190	-8250.211225
158	21	7	41.70599	-23.295	-8250.258621
158	21	7	42.71399	-23.285	-8250.262143
158	21	7	43.72198	-23.140	-8250.279181
158	21	7	44.73000	-23.245	-8250.224839
158	21	7	45.73799	-23.225	-8250.181446
158	21	7	46.74599	-23.180	-8250.220312
158	21	7	47.75400	-23.245	-8250.220533
158	21	7	48.76199	-23.200	-8250.227134
158	21	7	49.76999	-23.215	-8250.222475
158	21	7	50.77800	-23.250	-8250.196163

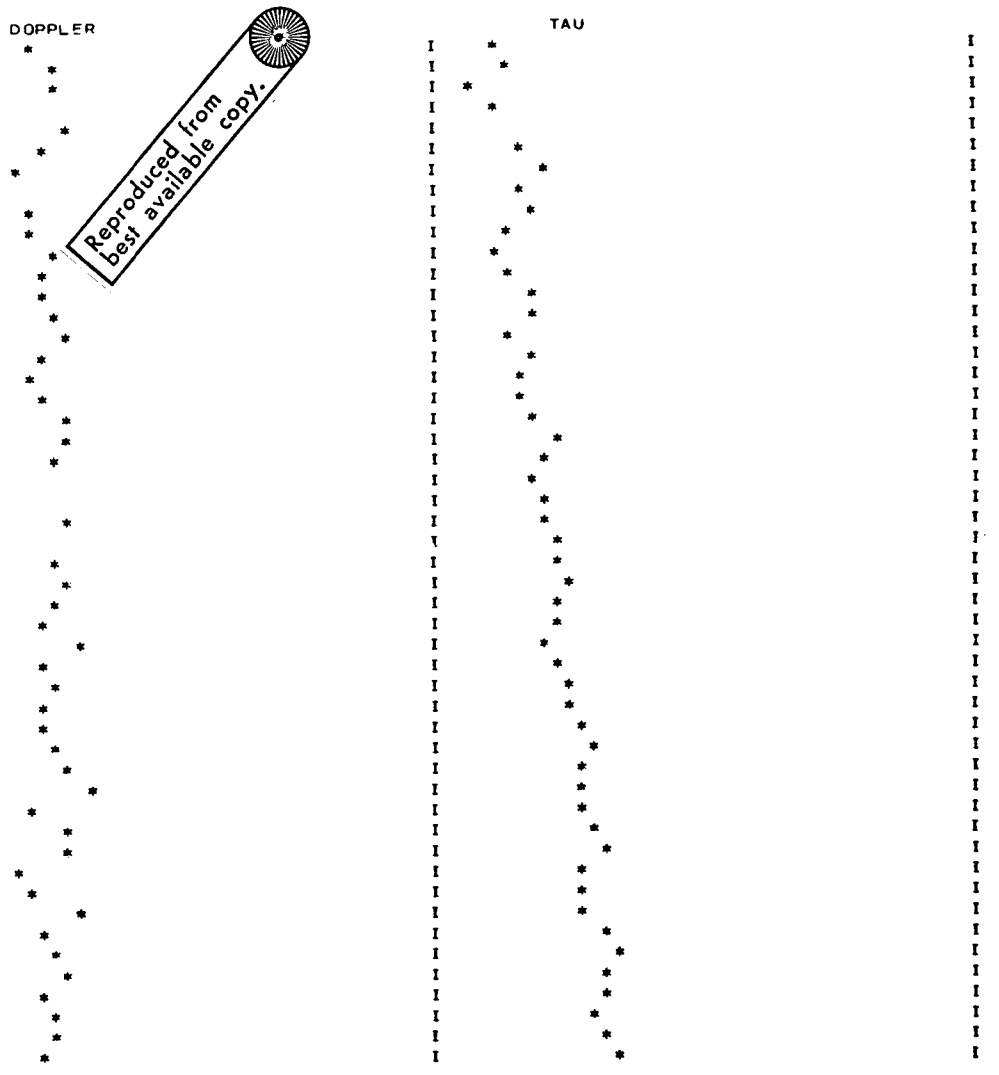

Figure 23. Fringe-Rate and Time-Delay Versus Time for the ATS-3 Satellite - Noise Modulation - Run No. 158-21-07. Rosman - Mojave Experiment . (Sheet 1 of 4)

RUN 158-21-07 ROSMAN - MOJAVE
SOURCE ATS-1 N-X NREC = 5

VLBI105 VARICS/VAM105 SAT-F

DAY	HR	MIN	SECOND	DOPPLER	TAU
158	21	7	51.78600	-23.260	-8250.189453
158	21	7	52.79399	-23.260	-8250.192312
158	21	7	53.80199	-23.225	-8250.115493
158	21	7	54.81000	-23.285	-8250.138456
158	21	7	55.81799	-23.125	-8250.217997
158	21	7	56.82599	-23.190	-8250.199666
158	21	7	57.83400	-23.265	-8250.146824
158	21	7	58.84200	-23.280	-8250.162272
158	21	7	59.84999	-23.175	-8250.157668
158	21	8	0.85800	-23.225	-8250.175164
158	21	8	1.86600	-23.270	-8250.099209
158	21	8	2.87400	-23.350	-8250.136883
158	21	8	3.88200	-23.225	-8250.123619
158	21	8	4.89000	-23.165	-8250.138154
158	21	8	5.89800	-23.215	-8250.102689
158	21	8	6.90600	-23.245	-8250.084732
158	21	8	7.91400	-23.285	-8250.131303
158	21	8	8.92200	-23.610	-8250.093811
158	21	8	9.93000	-22.990	-8250.106619
158	21	8	10.93800	-23.175	-8250.095109
158	21	8	11.94600	-23.210	-8250.090136
158	21	8	12.95400	-23.230	-8250.066274
158	21	8	13.96200	-23.160	-8250.088161
158	21	8	14.97000	-23.235	-8250.068465
158	21	8	15.97800	-23.230	-8250.038435
158	21	8	16.98599	-23.190	-8250.024096
158	21	8	17.99399	-23.235	-8250.037383
158	21	8	19.00200	-23.260	-8250.027823
158	21	8	20.00999	-23.150	-8250.077214
158	21	8	21.01799	-23.220	-8250.025287
158	21	8	22.02599	-23.225	-8250.003921
158	21	8	23.03400	-23.240	-8250.020638
158	21	8	24.04199	-23.245	-8250.038177
158	21	8	25.04999	-23.250	-8250.025805
158	21	8	26.05800	-23.305	-8250.004155
158	21	8	27.06599	-23.215	-8249.990673
158	21	8	28.07399	-23.200	-8249.984464
158	21	8	29.08199	-23.110	-8249.977929
158	21	8	30.09000	-23.235	-8249.938983
158	21	8	31.09799	-23.260	-8249.936927
158	21	8	32.10599	-23.220	-8249.932798
158	21	8	33.11400	-23.285	-8249.927960
158	21	8	34.12199	-23.135	-8249.971289
158	21	8	35.12999	-23.245	-8249.835959
158	21	8	36.13799	-23.215	-8249.954749
158	21	8	37.14600	-23.280	-8249.957031
158	21	8	38.15399	-23.250	-8249.940251
158	21	8	39.16199	-23.200	-8249.952807
158	21	8	40.17000	-23.250	-8249.944171
158	21	8	41.17799	-23.250	-8249.918626

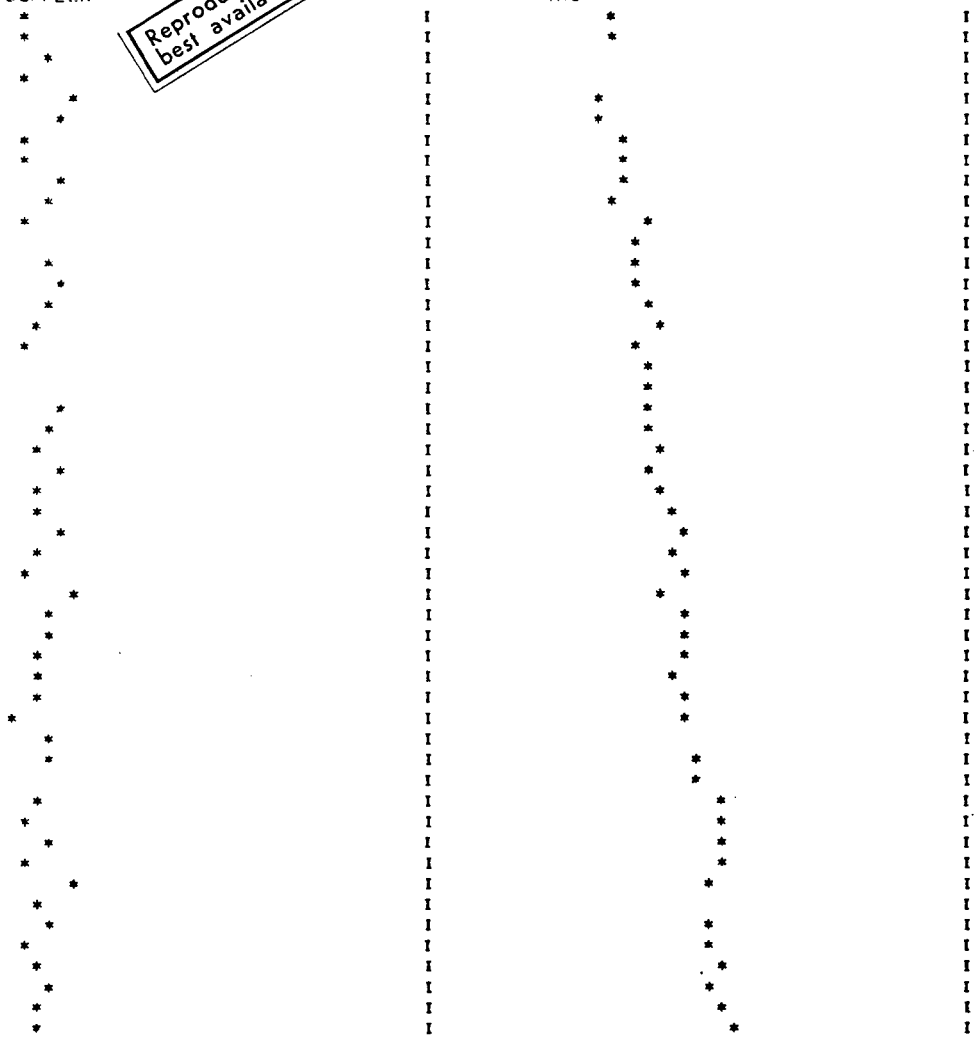

Figure 23. Sheet 2 of 4

RUN 158-21-07 ROSMAN - MOJAVE
SOURCE ATS-1 N-X NREC = 5

DAY	HR	MIN	SECOND	DOPPLER	TAU
158	21	8	42.18599	-23.215	-8249.927454
158	21	8	43.19398	-23.260	-8249.950538
158	21	8	44.20200	-23.115	-8249.968689
158	21	8	45.20999	-23.210	-8249.910492
158	21	8	47.04120	-23.105	-8249.877163
158	21	8	48.04919	-23.130	-8249.741037
158	21	8	49.05719	-23.095	-8249.879612
158	21	8	50.06519	-23.135	-8249.815328
158	21	8	51.07320	-23.195	-8249.848237
158	21	8	52.08119	-23.120	-8249.854231
158	21	8	53.08919	-23.145	-8249.791602
158	21	8	54.09720	-23.190	-8249.762766
158	21	8	55.10519	-23.035	-8249.867076
158	21	8	56.11319	-23.095	-8249.785703
158	21	8	57.12119	-23.100	-8249.816908
158	21	8	58.12920	-23.105	-8249.802294
158	21	8	59.13719	-23.150	-8249.855823
158	21	9	0.14520	-23.195	-8249.759422
158	21	9	1.15320	-23.050	-8249.808267
158	21	9	2.16120	-23.045	-8249.831695
158	21	9	3.16920	-23.155	-8249.768811
158	21	9	4.17720	-23.110	-8249.767219
158	21	9	5.18520	-23.085	-8249.773720
158	21	9	6.19320	-23.200	-8249.734080
158	21	9	7.20120	-23.100	-8249.721871
158	21	9	8.20920	-23.120	-8249.738602
158	21	9	9.21720	-23.130	-8249.773874
158	21	9	10.22520	-23.115	-8249.772961
158	21	9	11.23320	-23.055	-8249.689054
158	21	9	12.24120	-23.240	-8249.748276
158	21	9	13.24920	-23.165	-8249.713368
158	21	9	14.25720	-23.120	-8249.766289
158	21	9	15.26520	-23.120	-8249.685276
158	21	9	16.27319	-23.165	-8249.680372
158	21	9	17.28119	-23.110	-8249.727627
158	21	9	18.28920	-23.125	-8249.678133
158	21	9	19.29720	-23.105	-8249.709545
158	21	9	20.30519	-23.055	-8249.641583
158	21	9	21.31319	-23.095	-8249.718444
158	21	9	22.32120	-23.085	-8249.577391
158	21	9	23.32919	-22.790	-8249.748534
158	21	9	24.33719	-23.120	-8249.646797
158	21	9	25.34520	-23.110	-8249.625789
158	21	9	26.35320	-23.100	-8249.708323
158	21	9	27.36119	-23.025	-8249.596020
158	21	9	28.36919	-23.190	-8249.681846
158	21	9	29.37720	-23.105	-8249.644922
158	21	9	30.38519	-23.235	-8249.568676
158	21	9	31.39319	-23.085	-8249.597397
158	21	9	32.40120	-23.040	-8249.576299

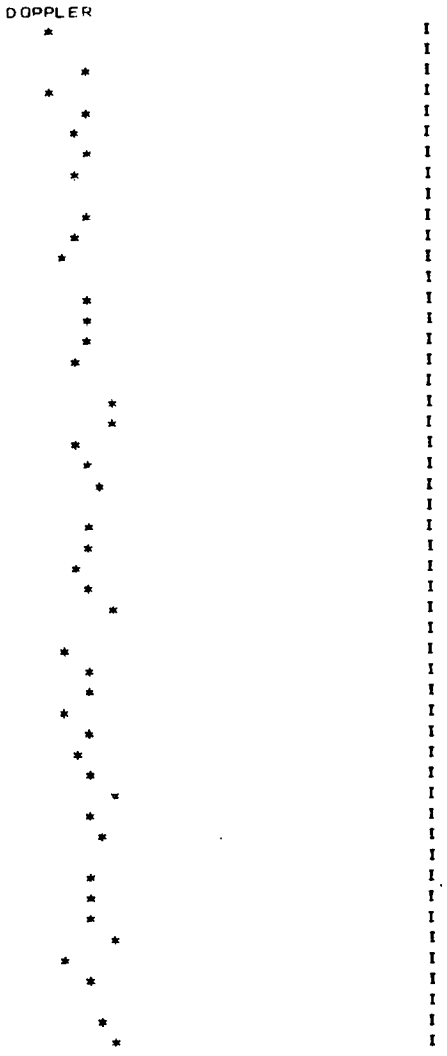

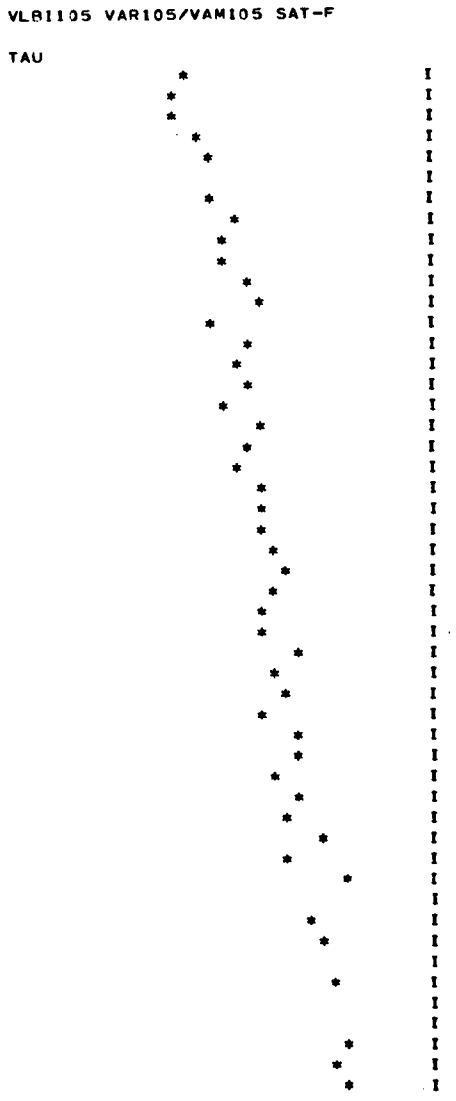

Figure 23. Sheet 3 of 4

RUN 158-21-07 ROSMAN - MOJAVE
SOURCE ATS-1 N-X NREC = 5

DAY	HR	MIN	SECOND	DOPPLER	TAU
158	21	9	33.40919	-23.080	-8249.599419
158	21	9	34.41719	-23.120	-8249.602616
158	21	9	35.42519	-23.120	-8249.583168
158	21	9	36.43320	-23.190	-8249.591261
158	21	9	37.44119	-23.145	-8249.606316
158	21	9	38.44919	-23.035	-8249.557936
158	21	9	39.45720	-23.190	-8249.586708
158	21	9	40.46519	-23.125	-8249.579126
158	21	9	41.47319	-23.135	-8249.604560
158	21	9	42.48119	-23.160	-8249.521478
158	21	9	43.48920	-23.095	-8249.537642
158	21	9	44.49719	-23.140	-8249.552743
158	21	9	45.50519	-23.125	-8249.547625
158	21	9	46.51320	-23.145	-8249.588591
158	21	9	47.52119	-23.020	-8249.556669
158	21	9	48.52919	-23.015	-8249.501072
158	21	9	49.53719	-23.080	-8249.595394
158	21	9	50.54520	-23.110	-8249.517330
158	21	9	51.55319	-23.150	-8249.495994
158	21	9	52.56119	-23.065	-8249.493973
158	21	9	53.56920	-23.080	-8249.406670
158	21	9	54.57719	-22.910	-8249.513061
158	21	9	55.58519	-23.165	-8249.425394

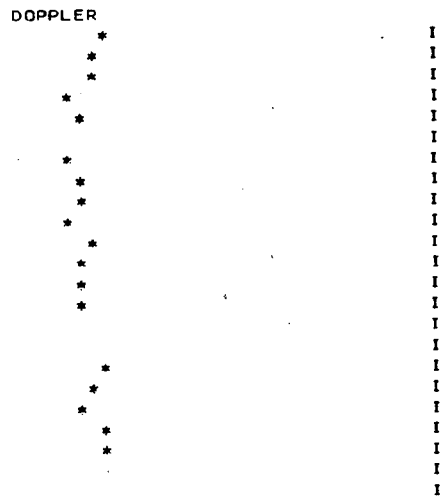

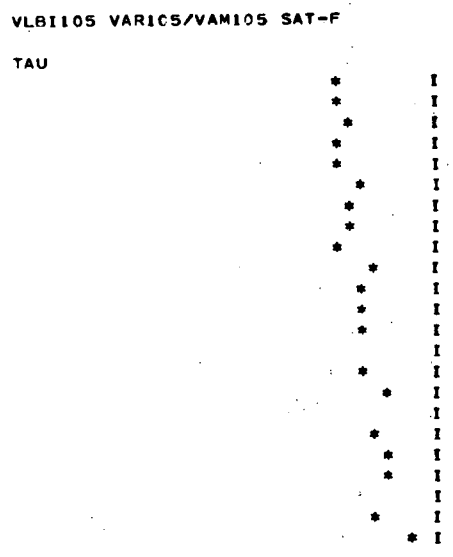

Figure 23. Sheet 4 of 4

RUN 158-21-55 ROSMAN - MOJAVE
SOURCE ATS-3 S-N NREC = 5

VLBI109 VAR109/VAM109 SAT-F

DAY	HR	MIN	SECOND	DOPPLER	TAU
158	21	55	1.34280	9.690	4115.623984
158	21	55	2.35080	9.580	4115.590431
158	21	55	3.35880	9.590	4115.597764
158	21	55	4.36680	9.710	4115.625825
158	21	55	5.37480	9.580	4115.593446
158	21	55	6.38280	9.660	4115.609596
158	21	55	7.39080	9.630	4115.597786
158	21	55	8.39880	9.750	4115.613519
158	21	55	9.40680	9.650	4115.594083
158	21	55	10.41480	9.630	4115.590443
158	21	55	11.42280	9.620	4115.583786
158	21	55	12.43080	9.650	4115.600968
158	21	55	13.43880	9.720	4115.585454
158	21	55	14.44680	9.600	4115.565635
158	21	55	15.45480	9.630	4115.578924
158	21	55	16.46280	9.620	4115.573385
158	21	55	17.47079	9.580	4115.622799
158	21	55	18.47879	9.620	4115.578403
158	21	55	19.48679	9.680	4115.559534
158	21	55	20.49480	9.590	4115.554882
158	21	55	21.50279	9.660	4115.576644
158	21	55	22.51079	9.570	4115.570495
158	21	55	23.51880	9.620	4115.583838
158	21	55	24.52679	9.670	4115.559469
158	21	55	25.53479	9.550	4115.546216
158	21	55	26.54279	9.600	4115.555859
158	21	55	27.55080	9.640	4115.553867
158	21	55	28.55879	9.570	4115.547409
158	21	55	29.56679	9.560	4115.551426
158	21	55	30.57480	9.540	4115.548226
158	21	55	31.58279	9.540	4115.547864
158	21	55	32.59079	9.610	4115.533741
158	21	55	33.59879	9.600	4115.529089
158	21	55	34.60680	9.640	4115.532552
158	21	55	35.61479	9.630	4115.527777
158	21	55	36.62279	9.570	4115.549421
158	21	55	37.63080	9.540	4115.541897
158	21	55	38.63879	9.620	4115.521003
158	21	55	39.64679	9.540	4115.537333
158	21	55	40.65479	9.570	4115.523888
158	21	55	41.66280	9.630	4115.547955
158	21	55	42.67079	9.530	4115.579289
158	21	55	43.67879	9.560	4115.502318
158	21	55	44.68680	9.640	4115.505334
158	21	55	45.69479	9.580	4115.524789
158	21	55	46.70279	9.590	4115.513336
158	21	55	47.71078	9.540	4115.508783
158	21	55	48.71880	9.650	4115.503632
158	21	55	49.72679	9.570	4115.508693
158	21	55	50.73479	9.610	4115.504333

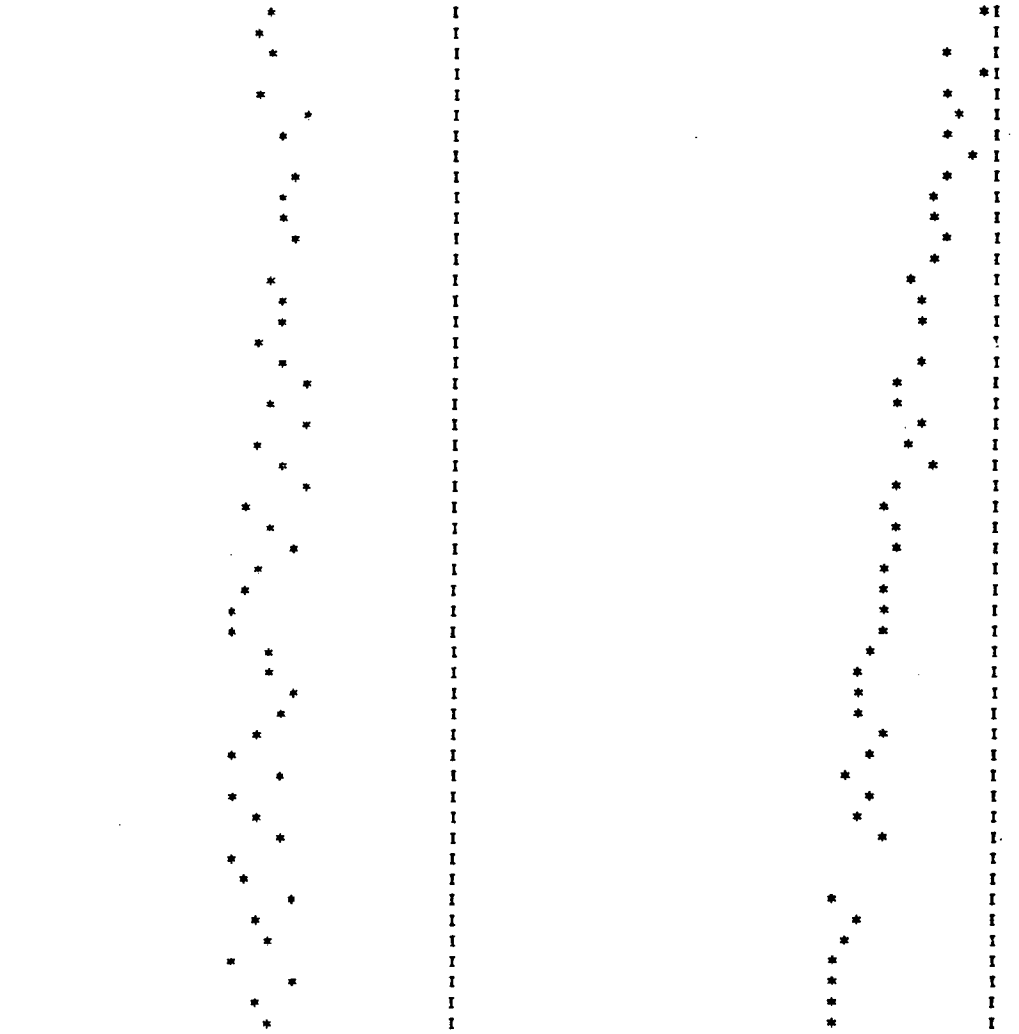

Figure 24. Fringe-Rate and Time-Delay Versus Time for the ATS-3 Satellite - Spacecraft Noise - Run No. 158-21-54. Rosman-Mojave Experiment. (Sheet 1 of 4)

RUN 158-21-55 ROSMAN - MOJAVE
SOURCE ATS-3 S-N NREC = 5

DAY	HR	MIN	SECOND	DOPPLER	TAU
158	21	55	51.74280	9.640	4115.503971I
158	21	55	52.75079	9.650	4115.501533I
158	21	55	53.75879	9.690	4115.544979I
158	21	55	54.76680	9.570	4115.485982I
158	21	55	55.77480	9.570	4115.494093I
158	21	55	56.78279	9.650	4115.479687I
158	21	55	57.79079	9.590	4115.521708I
158	21	55	58.79880	9.550	4115.471686I
158	21	55	59.80679	9.690	4115.487695I
158	21	56	0.81480	9.510	4115.476978I
158	21	56	1.82280	9.590	4115.466580I
158	21	56	2.83080	9.480	4115.499202I
158	21	56	3.83880	9.530	4115.473022I
158	21	56	4.84680	9.530	4115.542457I
158	21	56	5.85480	9.560	4115.476355I
158	21	56	6.86280	9.560	4115.458250I
158	21	56	7.87080	9.570	4115.458863I
158	21	56	8.87880	9.500	4115.456777I
158	21	56	9.88680	9.570	4115.448723I
158	21	56	10.89480	9.520	4115.452588I
158	21	56	11.90280	9.570	4115.491021I
158	21	56	12.91080	9.580	4115.472021I
158	21	56	13.91880	9.590	4115.453137I
158	21	56	14.92680	9.370	4115.420689I
158	21	56	15.93480	9.490	4115.450124I
158	21	56	16.94279	9.590	4115.448747I
158	21	56	17.95079	9.680	4115.442879I
158	21	56	18.95879	9.540	4115.436134I
158	21	56	19.96680	9.480	4115.449144I
158	21	56	20.97479	9.450	4115.415720I
158	21	56	21.98279	9.520	4115.436891I
158	21	56	22.99080	9.530	4115.416854I
158	21	56	23.99879	9.500	4115.458218I
158	21	56	25.00679	9.570	4115.431467I
158	21	56	26.01479	9.540	4115.467719I
158	21	56	27.02280	9.450	4115.413726I
158	21	56	28.03079	9.460	4115.444726I
158	21	56	29.03879	9.610	4115.418451I
158	21	56	30.04680	9.530	4115.426836I
158	21	56	31.05479	9.450	4115.428194I
158	21	56	32.06279	9.520	4115.428295I
158	21	56	33.07079	9.570	4115.420569I
158	21	56	34.07880	9.570	4115.403023I
158	21	56	35.08679	9.530	4115.417183I
158	21	56	36.09479	9.570	4115.396055I
158	21	56	37.10280	9.510	4115.410125I
158	21	56	38.11079	9.480	4115.390043I
158	21	56	39.11879	9.530	4115.418129I
158	21	56	40.12679	9.480	4115.395723I
158	21	56	41.13480	9.460	4115.396116I

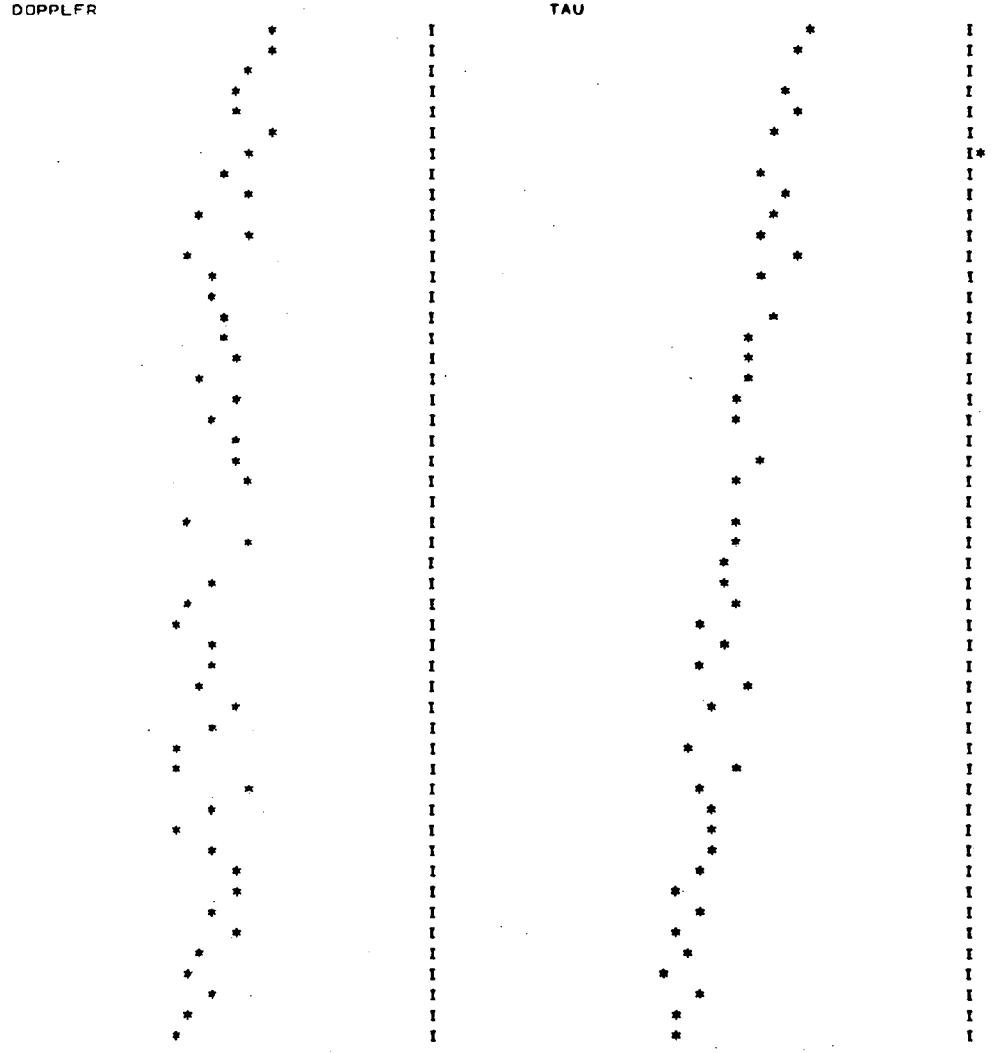

Figure 24. Sheet 2 of 4

RUN 158-21-55 ROSMAN - MOJAVE
SOURCE ATS-3 S-N NREC = 5

DAY	HR	MIN	SECOND	DOPPLER	TAU
158	21	56	42.14279	9.460	4115.403247I
158	21	56	43.15079	9.510	4115.385481I
158	21	56	44.15880	9.530	4115.376626I
158	21	56	45.16679	8.940	4115.375210I
158	21	56	46.17479	9.540	4115.401915I
158	21	56	47.18279	9.930	4115.398197I
158	21	56	48.19080	9.500	4115.374144I
158	21	56	49.19879	9.510	4115.358505I
158	21	56	50.20679	9.520	4115.370884I
158	21	56	51.21480	9.530	4115.357622I
158	21	56	52.22279	9.490	4115.371967I
158	21	56	53.23079	9.480	4115.358792I
158	21	56	54.23878	9.490	4115.364561I
158	21	56	55.24680	9.460	4115.378118I
158	21	56	56.25479	9.420	4115.360605I
158	21	56	57.26279	9.510	4115.372726I
158	21	56	58.27080	9.500	4115.358226I
158	21	56	59.27879	9.480	4115.368633I
158	21	57	0.28680	9.540	4115.343195I
158	21	57	1.29480	9.430	4115.351678I
158	21	57	2.30280	9.510	4115.330542I
158	21	57	3.31080	9.470	4115.329737I
158	21	57	4.31880	9.520	4115.321942I
158	21	57	5.32680	9.460	4115.334548I
158	21	57	6.33480	9.480	4115.323175I
158	21	57	7.34280	9.360	4115.345038I
158	21	57	8.35080	9.490	4115.340722I
158	21	57	9.35880	9.450	4115.369235I
158	21	57	10.36680	9.550	4115.261741I
158	21	57	11.37480	9.510	4115.325338I
158	21	57	12.38280	9.400	4115.303991I
158	21	57	13.39080	9.400	4115.337355I
158	21	57	14.39880	9.470	4115.331949I
158	21	57	15.40680	9.400	4115.321838I
158	21	57	16.41479	9.500	4115.301995I
158	21	57	17.42279	9.490	4115.336966I
158	21	57	18.43079	9.460	4115.312624I
158	21	57	19.43880	9.490	4115.320931I
158	21	57	20.44679	9.520	4115.299575I
158	21	57	21.45479	9.460	4115.307521I
158	21	57	22.46280	9.460	4115.302588I
158	21	57	23.47079	9.470	4115.312494I
158	21	57	24.47879	9.480	4115.296859I
158	21	57	25.48679	9.450	4115.292491I
158	21	57	26.49480	9.410	4115.317951I
158	21	57	27.50279	9.480	4115.303056I
158	21	57	28.51079	9.510	4115.278846I
158	21	57	29.51880	9.440	4115.270928I
158	21	57	30.52679	9.470	4115.277933I
158	21	57	31.53479	9.460	4115.277137I

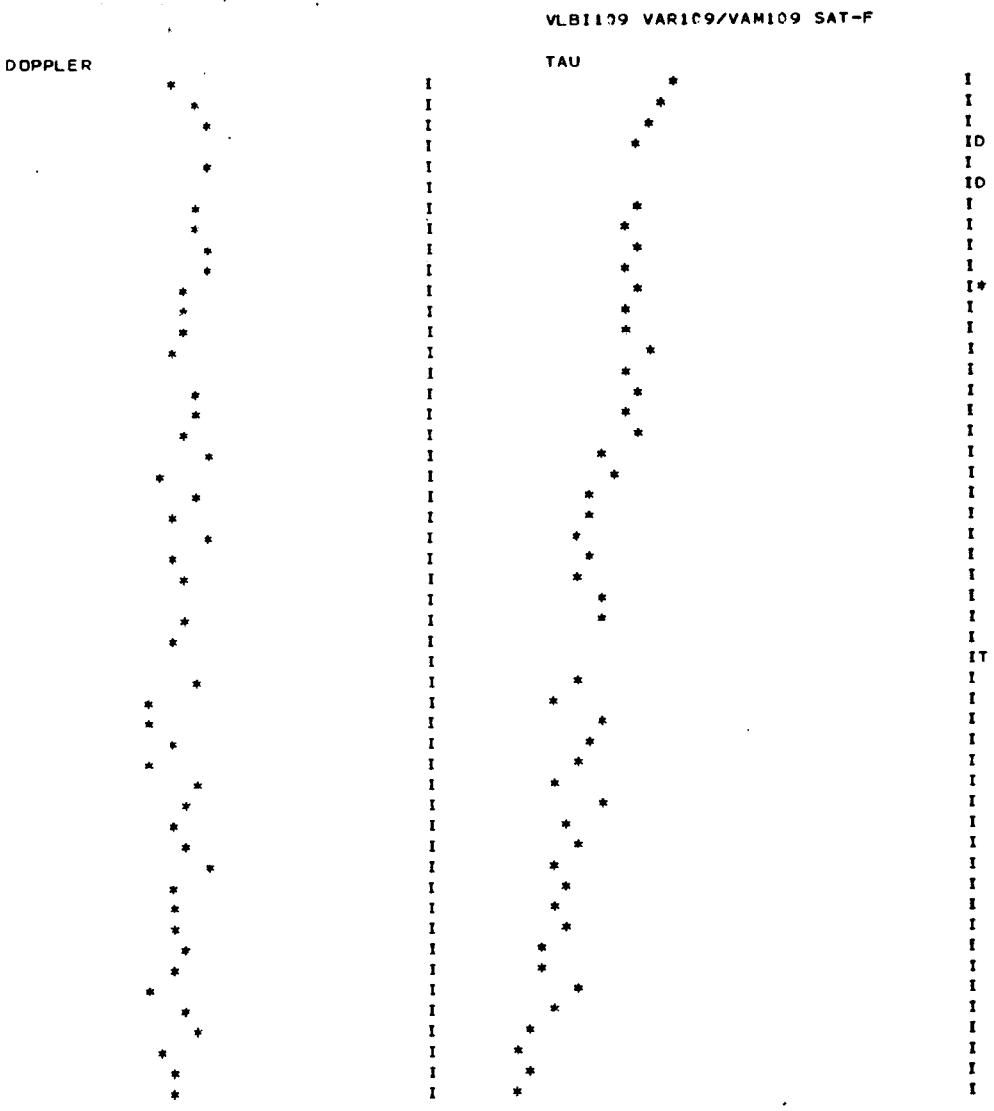

Figure 24. Sheet 3 of 4

RUN 158-21-55 ROSMAN - MOJAVE
SOURCE ATS-3 S-N NREC = 5

DAY	HR	MIN	SECOND	DOPPLER	TAU
158	21	57	32.54279	9.490	4115.274559
158	21	57	33.55080	9.370	4115.263459
158	21	57	34.55879	9.460	4115.312579
158	21	57	35.56679	9.390	4115.282032
158	21	57	36.57480	9.440	4115.281978
158	21	57	37.58279	9.510	4115.291795
158	21	57	38.59079	9.390	4115.270902
158	21	57	39.59879	9.480	4115.260992
158	21	57	40.60680	9.370	4115.299396
158	21	57	41.61479	9.450	4115.261681
158	21	57	42.62279	9.490	4115.250235
158	21	57	43.63080	9.420	4115.257158
158	21	57	44.63879	9.480	4115.257392
158	21	57	45.64679	9.440	4115.281169
158	21	57	46.65479	9.440	4115.251202
158	21	57	47.66280	9.470	4115.264763
158	21	57	48.67079	9.510	4115.245443
158	21	57	49.67879	9.480	4115.231919
158	21	57	50.68680	9.410	4115.247746
158	21	57	51.69479	9.400	4115.228423
158	21	57	52.70279	9.450	4115.230795
158	21	57	53.71078	9.270	4115.241834
158	21	57	54.71880	9.450	4115.254223
158	21	57	55.72679	9.420	4115.243106
158	21	57	56.73479	9.350	4115.230788
158	21	57	57.74280	9.400	4115.250276
158	21	57	58.75079	9.440	4115.213482

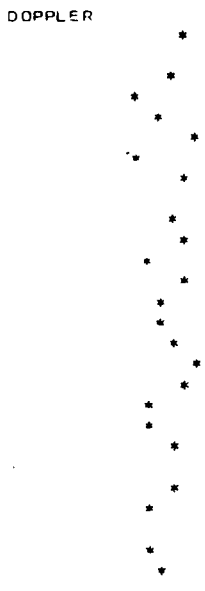

VLBI109 VAR109/VAM109 SAT-F

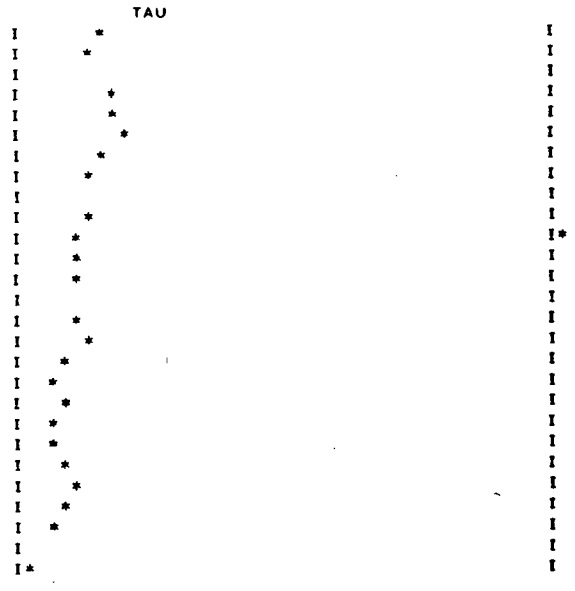

Figure 24. Sheet 4 of 4

RUN 159-21-10 ROSMAN - MOJAVE
SOURCE ATS-3 M-X NREC = 5

DAY	HR	MIN	SECOND	DOPPLER	TAU
159	21	10	32.42519	12.550	4110.200277I
159	21	10	33.43320	12.545	4110.194005I
159	21	10	34.44119	12.605	4110.194824I
159	21	10	35.44919	12.570	4110.181345I
159	21	10	36.45720	12.590	4110.196359I
159	21	10	37.46519	12.560	4110.181890I
159	21	10	38.47319	12.610	4110.255084I
159	21	10	39.48119	12.590	4110.168909I
159	21	10	40.48920	12.625	4110.183083I
159	21	10	41.49719	12.575	4110.165085I
159	21	10	42.50519	12.610	4110.171875I
159	21	10	43.51320	12.535	4110.163683I
159	21	10	44.52119	12.625	4110.152982I
159	21	10	45.52919	12.575	4110.165716I
159	21	10	46.53719	12.665	4110.148427I
159	21	10	47.54520	12.570	4110.148042I
159	21	10	48.55319	12.625	4110.147472I
159	21	10	49.56119	12.560	4110.152925I
159	21	10	50.56920	12.645	4110.148578I
159	21	10	51.57719	12.535	4110.139117I
159	21	10	52.58519	12.590	4110.153673I
159	21	10	53.59319	12.595	4110.134305I
159	21	10	54.60120	12.580	4110.120698I
159	21	10	55.60919	12.575	4110.131706I
159	21	10	56.61719	12.620	4110.099343I
159	21	10	57.62520	12.555	4110.125608I
159	21	10	58.63319	12.635	4110.126709I
159	21	10	59.64119	12.575	4110.102456I
159	21	11	0.64920	12.510	4110.121283I
159	21	11	1.65720	12.600	4110.104657I
159	21	11	2.66520	12.540	4110.102912I
159	21	11	3.67320	12.545	4110.134553I
159	21	11	4.68120	12.595	4110.105936I
159	21	11	5.68920	12.555	4110.097133I
159	21	11	6.69720	12.595	4110.095418I
159	21	11	7.70520	12.570	4110.091333I
159	21	11	8.71320	12.615	4110.090466I
159	21	11	9.72120	12.545	4110.083154I
159	21	11	10.72920	12.525	4110.071383I
159	21	11	11.73720	12.555	4110.087642I
159	21	11	12.74520	12.545	4110.082775I
159	21	11	13.75320	12.585	4110.072953I
159	21	11	14.76120	12.560	4110.070808I
159	21	11	15.76920	12.485	4110.062731I
159	21	11	16.77719	12.595	4110.066109I
159	21	11	17.78519	12.490	4110.056662I
159	21	11	18.79320	12.590	4110.055377I
159	21	11	19.80119	12.515	4110.049314I
159	21	11	20.80919	12.520	4110.053746I
159	21	11	21.81720	12.540	4110.057808I

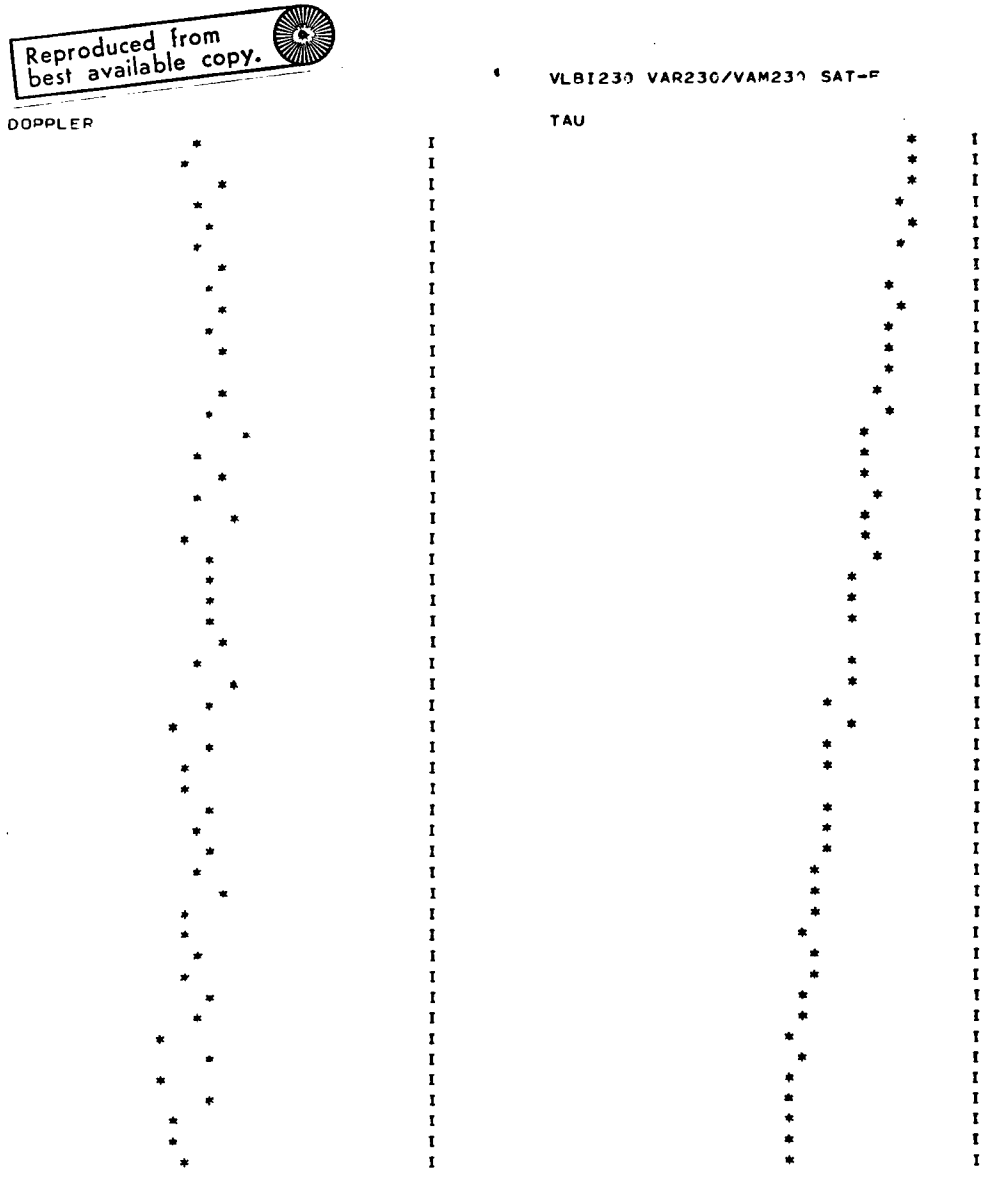

Figure 25. Fringe-Rate and Time-Delay Versus Time for ATS-3 Satellite - Noise Modulation - Run No. 159-21-10. Rosman-Mojave Experiment. (Sheet 1 of 4)

RUN 159-21-1C ROSMAN - MOJAVE
SOURCE ATS-3 N-X NREC = 5

DAY	HR	MIN	SECOND	DOPPLER	TAU
159	21	11	22.82520	12.630	4110.034206I
159	21	11	23.83319	12.470	4110.082932I
159	21	11	24.84119	12.555	4110.043666I
159	21	11	25.84920	12.600	4110.039965I
159	21	11	26.85719	12.530	4110.032924I
159	21	11	27.86519	12.560	4110.037119I
159	21	11	28.87320	12.585	4110.019264I
159	21	11	29.88120	12.510	4110.032322I
159	21	11	30.88919	12.590	4110.023152I
159	21	11	31.89719	12.620	4110.026993I
159	21	11	32.90520	12.440	4110.066735I
159	21	11	33.91319	12.590	4110.0654C2I
159	21	11	34.92119	12.510	4110.010619I
159	21	11	35.92920	12.560	4110.000263I
159	21	11	36.93719	12.120	4110.009809I
159	21	11	37.94519	12.580	4109.985963I
159	21	11	38.95319	12.595	4109.989881I
159	21	11	39.96120	12.535	4110.022845I
159	21	11	40.96919	12.495	4109.997440I
159	21	11	41.97719	12.535	4109.980641I
159	21	11	42.98520	12.545	4109.992666I
159	21	11	43.99319	12.545	4109.988772I
159	21	11	45.00119	12.585	4109.984757I
159	21	11	46.00919	12.480	4109.975127I
159	21	11	47.01720	12.520	4109.983172I
159	21	11	48.02519	12.550	4109.979283I
159	21	11	49.03319	12.475	4109.976812I
159	21	11	50.04120	12.565	4109.962920I
159	21	11	51.04919	12.585	4109.997834I
159	21	11	52.05719	12.525	4109.943791I
159	21	11	53.06519	12.540	4109.956067I
159	21	11	54.07320	12.470	4109.967738I
159	21	11	55.08119	12.585	4109.957996I
159	21	11	56.08919	12.840	4109.945341I
159	21	11	57.09720	12.535	4109.939862I
159	21	11	58.10519	12.515	4109.943121I
159	21	11	59.11319	12.580	4109.941196I
159	21	12	0.12120	12.515	4109.943835I
159	21	12	1.12920	12.515	4109.927535I
159	21	12	2.13720	12.510	4109.925627I
159	21	12	3.14520	12.485	4109.944806I
159	21	12	4.15320	12.545	4109.927261I
159	21	12	5.16120	12.510	4109.907709I
159	21	12	6.16920	12.500	4109.921782I
159	21	12	7.17720	12.445	4109.915011I
159	21	12	8.18520	12.640	4109.938405I
159	21	12	9.19320	12.485	4109.904229I
159	21	12	10.20120	12.445	4109.906002I
159	21	12	11.20920	12.575	4109.899923I
159	21	12	12.21720	12.460	4109.907762I

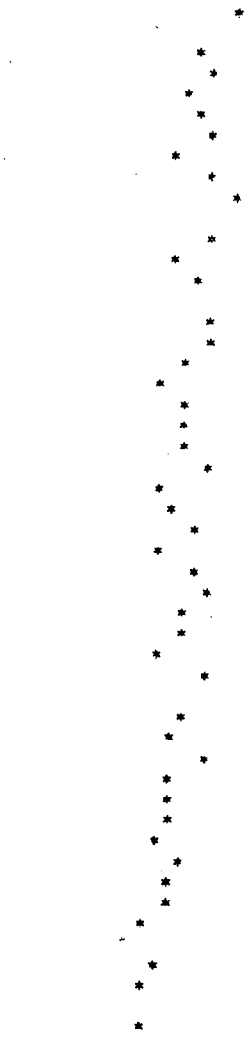

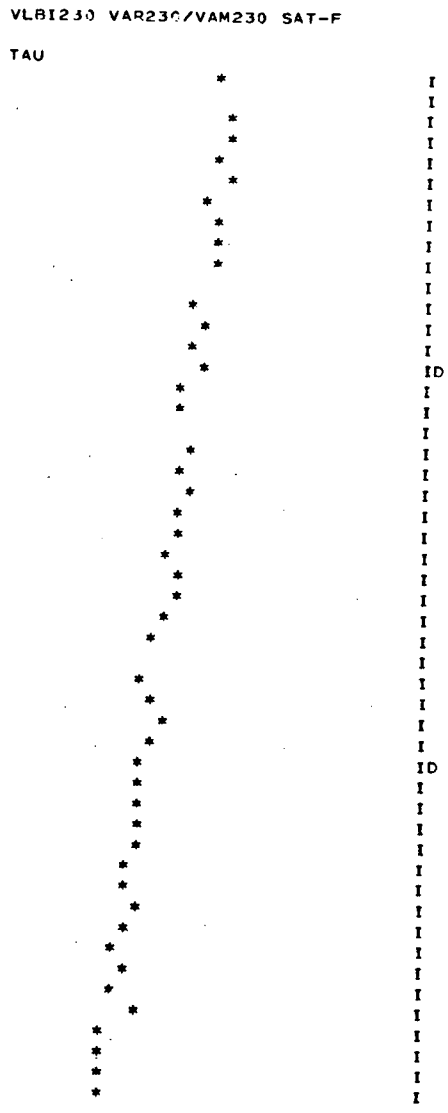

Figure 25. Sheet 2 of 4

RUN 159-21-10 ROSMAN - MOJAVE
SOURCE ATS-3 N-X NREC = 5

VLBI230 VAR230/VAM230 SAT-F

DAY	HR	MIN	SECOND	DOPPLER	TAU
159	21	12	13.22520	12.475	4109.902201
159	21	12	14.23320	12.515	4109.885326
159	21	12	15.24120	12.530	4109.873499
159	21	12	16.24919	12.425	4109.887144
159	21	12	17.25719	12.485	4109.884548
159	21	12	18.26520	12.455	4109.882827
159	21	12	19.27319	12.405	4109.876543
159	21	12	20.28119	12.485	4109.875076
159	21	12	21.28920	12.520	4109.858024
159	21	12	22.29720	12.470	4109.870498
159	21	12	23.30519	12.475	4109.878260
159	21	12	24.31319	12.465	4109.877673
159	21	12	25.32120	12.525	4109.848897
159	21	12	26.32919	12.455	4109.893846
159	21	12	27.33719	12.510	4109.874022
159	21	12	28.34520	12.440	4109.859022
159	21	12	29.35320	12.445	4109.840610
159	21	12	30.36119	11.930	4109.851557
159	21	12	31.36919	12.500	4109.853671
159	21	12	32.37720	12.770	4109.829956
159	21	12	33.38519	12.445	4109.837545
159	21	12	34.39319	12.470	4109.838652
159	21	12	35.40120	12.390	4109.846247
159	21	12	36.40919	12.360	4109.820301
159	21	12	37.41719	12.445	4109.828077
159	21	12	38.42519	12.470	4109.824225
159	21	12	39.43320	12.420	4109.827441
159	21	12	40.44119	12.425	4109.813477
159	21	12	41.44919	12.405	4109.819876
159	21	12	42.45720	12.460	4109.811718
159	21	12	43.46519	12.440	4109.798155
159	21	12	44.47319	12.475	4109.781057
159	21	12	45.48119	12.390	4109.803022
159	21	12	46.48920	12.475	4109.791313
159	21	12	47.49719	12.450	4109.801378
159	21	12	48.50519	12.460	4109.786886
159	21	12	49.51320	12.470	4109.794471
159	21	12	50.52119	12.505	4109.754077
159	21	12	51.52919	12.450	4109.772278
159	21	12	52.53719	12.430	4109.779011
159	21	12	53.54520	12.350	4109.770639
159	21	12	54.55319	12.420	4109.771381
159	21	12	55.56119	12.435	4109.793897
159	21	12	56.56920	12.400	4109.774992
159	21	12	57.57719	12.480	4109.761553
159	21	12	58.58519	12.435	4109.759375
159	21	12	59.59319	12.470	4109.759376
159	21	13	0.60120	12.375	4109.751320
159	21	13	1.60920	12.435	4109.746186
159	21	13	2.61720	12.395	4109.780475

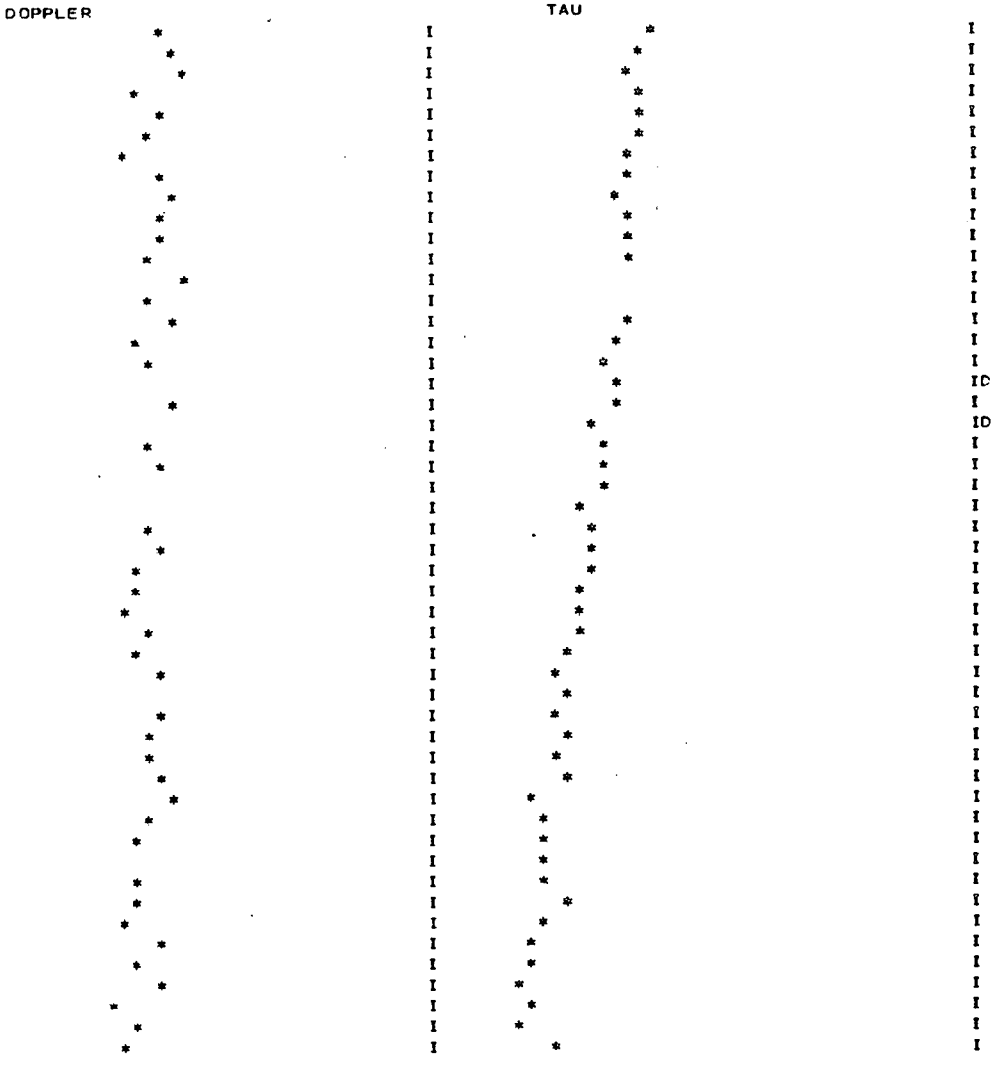

Figure 25. Sheet 3 of 4

RUN 159-21-10 ROSMAN - MOJAVE
SOURCE ATS-3 N-X NREC = 5

VLBI230 VAR230/VAM230 SAT-F

DAY	HR	MIN	SECOND	DOPPLER	TAU
159	21	13	3.62520	12.490	4109.754343
159	21	13	4.63320	12.440	4109.740098
159	21	13	5.64120	12.425	4109.746426
159	21	13	6.64920	12.460	4109.743123
159	21	13	7.65720	12.480	4109.728660
159	21	13	8.66520	12.420	4109.730542
159	21	13	9.67320	12.480	4109.735789
159	21	13	10.68120	12.410	4109.724801
159	21	13	11.68920	12.455	4109.733029
159	21	13	12.69720	12.445	4109.722434
159	21	13	13.70520	12.460	4109.716768
159	21	13	14.71320	12.450	4109.712614
159	21	13	15.72120	12.375	4109.717812
159	21	13	16.72919	12.325	4109.702448
159	21	13	17.73720	12.420	4109.745096
159	21	13	18.74519	12.430	4109.715173
159	21	13	19.75319	12.415	4109.704729
159	21	13	20.76120	12.555	4109.726027
159	21	13	21.76920	12.360	4109.697701
159	21	13	22.77719	12.385	4109.697500
159	21	13	23.78519	12.430	4109.687898
159	21	13	24.79320	12.020	4109.675124
159	21	13	25.80119	13.035	4109.690345
159	21	13	26.80919	12.495	4109.672415
159	21	13	27.81720	12.460	4109.676410
159	21	13	28.82520	12.485	4109.698387
159	21	13	29.83319	12.410	4109.658678
159	21	13	30.84119	12.385	4109.664837

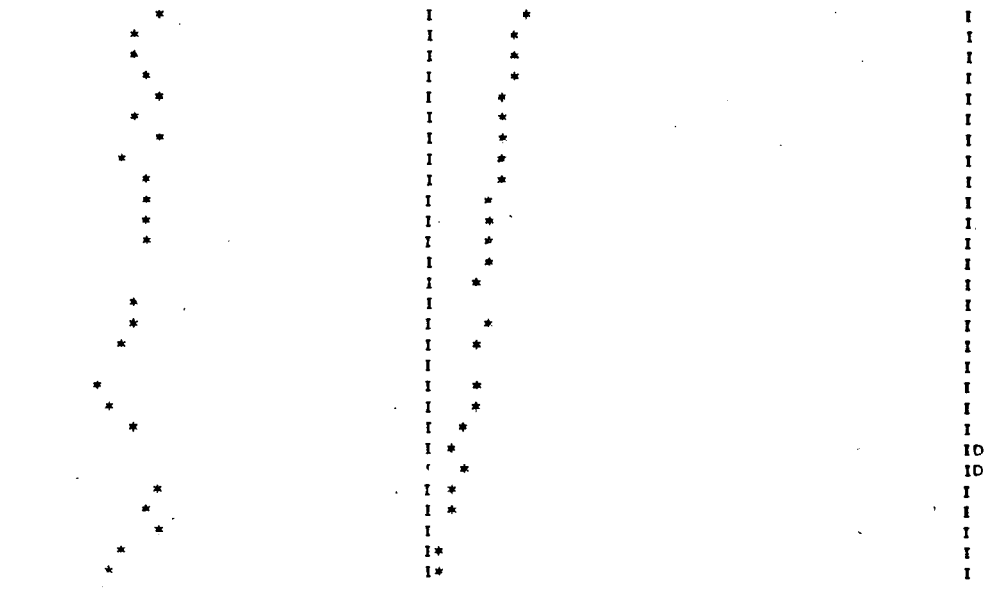

Figure 25. Sheet 4 of 4

RUN 159-18-37 ROSMAN - MOJAVE
SOURCE ATS-3 S-N NREC = 5

DAY	HR	MIN	SECOND	DOPPLER	TAU
159	18	37	0.73320	19.760	4076.495320I
159	18	37	1.74120	19.880	4076.492581I
159	18	37	2.74920	19.785	4076.474389I
159	18	37	3.75720	19.820	4076.465790I
159	18	37	4.76520	19.900	4076.462667I
159	18	37	5.77320	20.100	4076.466990I
159	18	37	6.78120	19.760	4076.444384I
159	18	37	7.78920	19.805	4076.445842I
159	18	37	8.79720	19.780	4076.449248I
159	18	37	9.80520	19.680	4076.433646I
159	18	37	10.81320	19.835	4076.459932I
159	18	37	11.82120	19.725	4076.420547I
159	18	37	12.82920	19.780	4076.421282I
159	18	37	13.83720	19.750	4076.403216I
159	18	37	14.84520	19.760	4076.414455I
159	18	37	15.85320	19.820	4076.420415I
159	18	37	16.86119	19.825	4076.392921I
159	18	37	17.86919	19.815	4076.393219I
159	18	37	18.87720	19.885	4076.411306I
159	18	37	19.88519	19.765	4076.398705I
159	18	37	20.89319	19.810	4076.398620I
159	18	37	21.90120	19.740	4076.390592I
159	18	37	22.90919	19.805	4076.377559I
159	18	37	23.91719	19.775	4076.387034I
159	18	37	24.92519	19.780	4076.372567I
159	18	37	25.93320	19.775	4076.365853I
159	18	37	26.94119	19.770	4076.360962I
159	18	37	27.94919	19.840	4076.348696I
159	18	37	28.95720	19.815	4076.355521I
159	18	37	29.96519	19.800	4076.340315I
159	18	37	30.97319	19.780	4076.330785I
159	18	37	31.98119	19.775	4076.290199I
159	18	37	32.98920	19.810	4076.334969I
159	18	37	33.99719	19.790	4076.321118I
159	18	37	35.00519	19.800	4076.321334I
159	18	37	36.01320	19.830	4076.314838I
159	18	37	37.02119	19.805	4076.304218I
159	18	37	38.02919	19.840	4076.294750I
159	18	37	39.03719	19.795	4076.294691I
159	18	37	40.04520	19.830	4076.292510I
159	18	37	41.05319	19.770	4076.305085I
159	18	37	42.06119	19.815	4076.294219I
159	18	37	43.06920	19.805	4076.306847I
159	18	37	44.07719	19.760	4076.276592I
159	18	37	45.08519	19.820	4076.279743I
159	18	37	46.09319	19.755	4076.258183I
159	18	37	47.10120	19.780	4076.266866I
159	18	37	48.10919	19.820	4076.247400I
159	18	37	49.11719	19.780	4076.259305I
159	18	37	50.12520	19.740	4076.260620I

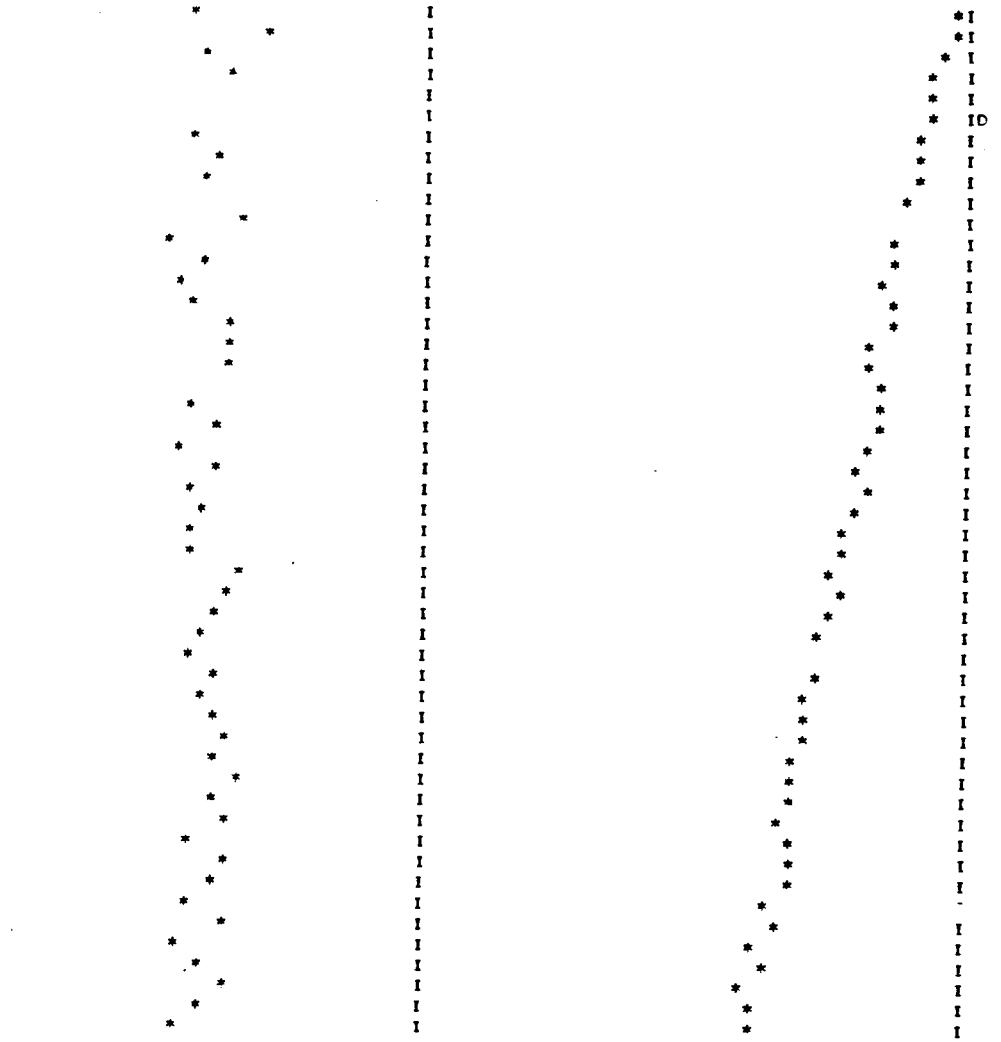

Figure 26. Fringe-Rate and Time-Delay Versus Time for ATS-3 Satellite - Spacecraft Noise - Run No. 159-18-37. Rosman-Mojave Experiment. (Sheet 1 of 3)

PUN 159-18-37 ROSMAN - MOJAVE
SOURCE ATS-3 S-N NREC = 5

DAY	HR	MIN	SECOND	DOPPLER	TAU
159	18	37	51.13319	19.785	4076.240888I
159	18	37	52.14119	19.875	4076.241332I
159	18	37	53.14919	19.775	4076.248627I
159	18	37	54.15720	19.815	4076.222223I
159	18	37	55.16519	19.715	4076.221258I
159	18	37	57.19800	19.790	4076.215639I
159	18	37	58.20599	19.845	4076.216410I
159	18	37	59.21399	19.785	4076.220829I
159	18	38	0.22200	19.695	4076.219278I
159	18	38	1.23000	19.795	4076.212396I
159	18	38	2.23800	19.740	4076.197181I
159	18	38	3.24600	19.775	4076.167543I
159	18	38	4.25400	19.785	4076.196181I
159	18	38	5.26200	19.755	4076.164875I
159	18	38	6.27000	19.780	4076.177711I
159	18	38	7.27800	19.820	4076.179285I
159	18	38	8.28600	19.825	4076.172383I
159	18	38	9.29400	19.670	4076.153120I
159	18	38	10.30200	19.830	4076.161616I
159	18	38	11.31000	19.980	4076.148124I
159	18	38	12.31800	19.820	4076.154932I
159	18	38	13.32600	19.790	4076.167627I
159	18	38	14.33400	19.765	4076.154239I
159	18	38	15.34200	19.810	4076.162859I
159	18	38	16.34999	19.815	4076.134414I
159	18	38	17.35799	19.810	4076.120122I
159	18	38	18.36600	19.785	4076.122444I
159	18	38	19.37399	19.815	4076.129816I
159	18	38	20.38199	19.740	4076.108347I
159	18	38	21.39000	19.315	4076.113492I
159	18	38	22.39799	19.835	4076.130795I
159	18	38	23.40599	20.105	4076.102578I
159	18	38	24.41399	19.780	4076.051160I
159	18	38	25.42200	19.805	4076.097492I
159	18	38	26.42999	19.860	4076.068977I
159	18	38	27.43799	19.775	4076.072930I
159	18	38	28.44600	19.835	4076.069994I
159	18	38	29.45399	19.810	4076.072134I
159	18	38	30.46199	19.795	4076.098775I
159	18	38	31.46999	19.785	4076.072925I
159	18	38	32.47800	19.770	4076.066999I
159	18	38	33.48599	19.785	4076.067563I
159	18	38	34.49399	19.795	4076.033354I
159	18	38	35.50200	19.820	4076.055518I
159	18	38	36.50999	19.735	4076.033979I
159	18	38	37.51799	19.755	4076.028757I
159	18	38	38.52599	19.790	4076.009754I
159	18	38	39.53400	19.805	4076.041907I
159	18	38	40.54199	19.790	4076.009929I
159	18	38	41.54999	19.805	4076.009202I

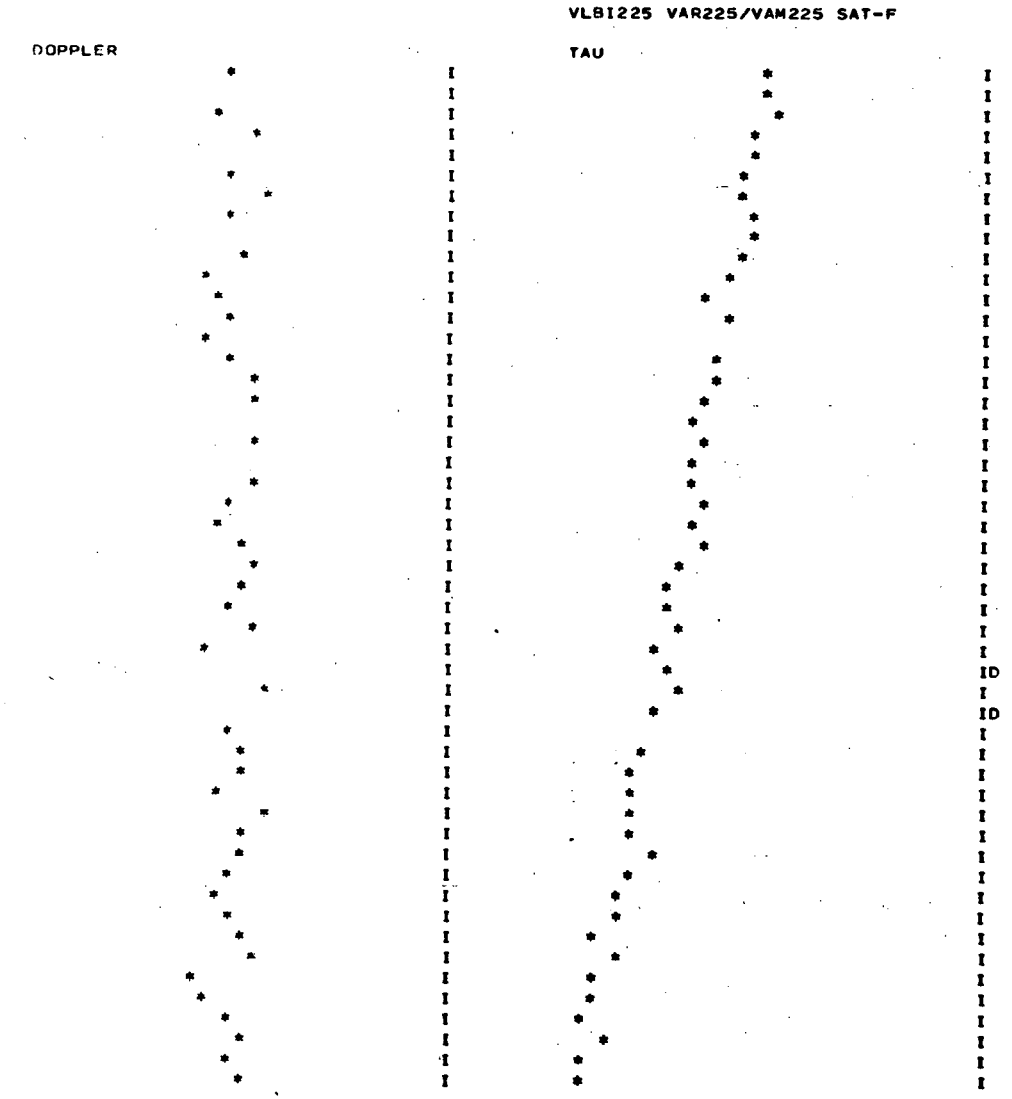

Figure 26. Sheet 2 of 3

RUN 159-18-37 ROSMAN - MOJAVE
SOURCE ATS-3 S-N NREC = 5

VLBI225 VAR225/VAM225 SAT-F

DAY	HR	MIN	SECOND	DOPPLER	TAU
159	18	38	42.55800	19.825	4075.995733
159	18	38	43.56599	19.850	4075.992726
159	18	38	44.57399	19.795	4075.995511
159	18	38	45.58199	19.765	4075.990596
159	18	38	46.59000	19.760	4076.001118
159	18	38	47.59799	19.825	4075.980343
159	18	38	48.60599	19.735	4075.991561
159	18	38	49.61400	19.790	4075.980829
159	18	38	50.62199	19.800	4075.980794
159	18	38	51.62999	19.760	4075.951665
159	18	38	52.63799	19.735	4075.949254
159	18	38	53.64600	19.790	4075.938803
159	18	38	54.65399	19.730	4075.956174
159	18	38	55.66199	19.795	4075.964767
159	18	38	56.67000	19.800	4075.933744
159	18	38	57.67799	19.805	4075.939202
159	18	38	58.68599	19.785	4075.908559
159	18	38	59.69398	19.780	4075.922925
159	18	39	0.70200	19.725	4075.901165
159	18	39	1.71000	19.785	4075.924602
159	18	39	2.71800	19.765	4075.934807
159	18	39	3.72600	19.855	4075.894811
159	18	39	4.73400	19.770	4075.905144
159	18	39	5.74200	19.745	4075.869973
159	18	39	6.75000	19.725	4075.883607
159	18	39	7.75800	19.835	4075.889925
159	18	39	8.76600	19.755	4075.878121
159	18	39	9.77400	19.795	4075.892609
159	18	39	10.78200	19.760	4075.870715
159	18	39	11.79000	19.785	4075.883897
159	18	39	12.79800	19.820	4075.865428
159	18	39	13.80600	19.760	4075.884576

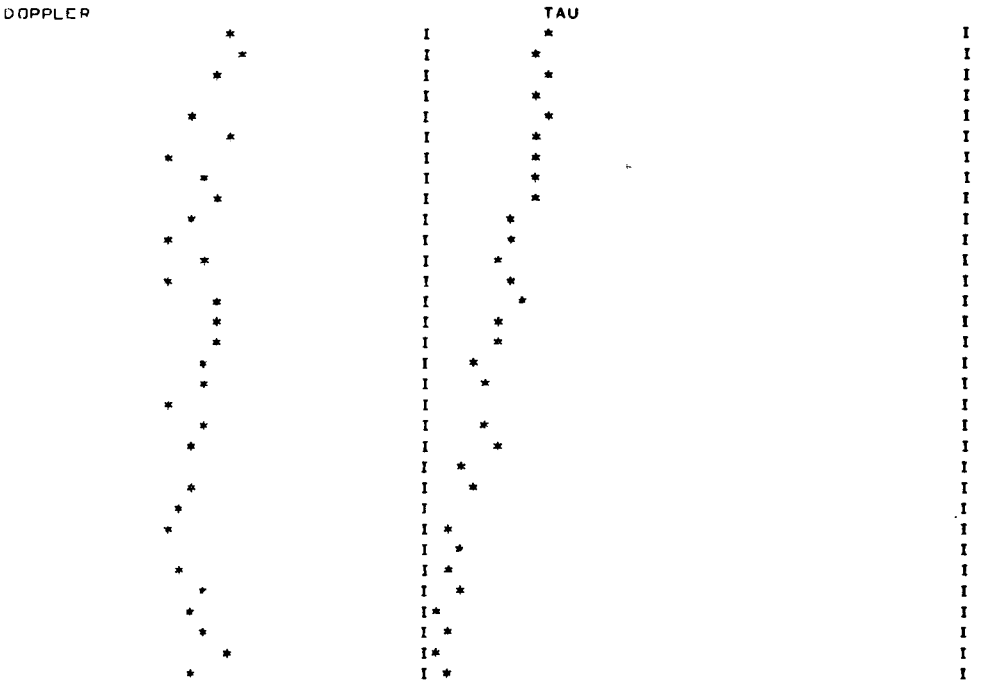

Figure 26. Sheet 3 of 3

TABLE 9

ATS-3 VLBI Runs Processed*

Run#	Signal-Modulation	Delay (Sec)	Doppler (HZ)
152-19-38-31	Noise Translation	4076.454	18.460
152-19-39-11	Noise Translation	4076.242	18.270
152-19-39-58	Noise Translation	4076.075	18.310
152-21-49-00	Noise Translation	4102.998	11.910
152-21-50-30	Noise Translation	4102.745	11.390
152-21-51-59	Noise Translation	4102.495	11.450
153-21-37-01	Spacecraft Noise	4118.150	12.235
153-21-38-30	Spacecraft Noise	4117.898	12.210
153-21-40-00	Spacecraft Noise	4117.623	12.010
153-22-39-31	Noise Translation	4113.592	7.655
153-22-41-00	Noise Translation	4113.420	7.565
153-22-42-30	Noise Translation	4113.259	7.425
153-22-52-01	Pseudo-Random Sequence (500 KB)	4110.170	6.665
153-22-53-30	Pseudo-Random Sequence (500 KB)	4110.144	6.215
153-22-55-00	Pseudo-Random Sequence (500 KB)	4110.058	6.460
154.22-33-00	Spacecraft Noise	4112.925	7.925
154-22-33-45	Spacecraft Noise	4112.847	7.950
154-22-34-28	Spacecraft Noise	4112.812	7.735
154-23-37-01	Noise Translation	4114.256	2.440
154-23-38-20	Noise Translation	4114.197	2.330
154-23-39-40	Noise Translation	4114.140	2.130
158-21-55-01	Spacecraft Noise	4115.624	9.600
158-22-06-31	Noise Translation	4116.889	8.710

*Each run is of 9 minutes duration

TABLE 9 (cont.)

Run #	Signal - Modulation	Delay (sec)	Doppler (Hz)
158-22-29-31	Pseudo-Random Sequence (1MB)	4119.491	6.940
158-23-15-49	Noise Translation	4121.046	2.990
159-12-40-31	Spacecraft Noise	3985.508	12.710
159-13-35-01	Noise Translation	3999.886	12.345
159-15-29-31	Noise Translation	4020.230	18.990
159-15-41-31	Spacecraft Noise	4023.417	19.380
159-16-33-00	Noise Translation	4042.300	20.600
159-18-37-00	Spacecraft Noise	4076.495	19.760
159-19-32-31	Noise Translation	4092.300	17.590
159-21-11-22	Noise Translation	4110.034	12.630
159-21-22-01	Pseudo-Random Sequence (500 KB)	4112.733	11.830
159-21-33-31	Pseudo-Random Sequence (1MB)	4114.183	11.045
159-21-45-01	Spacecraft Noise	4115.940	10.170
159-21-56-31	Sidetone Ensemble	4118.090	9.195
159-22-11-31	Noise Translation	4119.702	7.720
159-22-27-01	Spacecraft Noise	4121.421	6.760
159-22-39-31	Pseudo-Random Sequence (500 KB)	4122.419	5.650

6. DETERMINATION OF THE ATS-3 SATELLITE ORBIT PARAMETERS

Two approaches have been followed to determine the orbital elements of the ATS-3 spacecraft using the VLBI data. The first one is an analysis based on the first order orbit theory that is developed exclusively to fit the VLBI data. The second approach is the utilization of a highly sophisticated orbit determination program - the "GEODYN" program. Both the approaches and the corresponding results are presented in detail.

6.1 ORBIT ANALYSIS

6.1.1 Formulation of the Geometrical Delay

The geometrical relationships involved in the problem are shown in Figure 27. The satellite is located at $\vec{S}$ relative to the Earth's center, and at $\vec{R}_1$ and $\vec{R}_2$ from ground stations A and B, respectively. Stations A and B in turn are located at $\vec{P}_1$ and $\vec{P}_2$ relative to the Earth's center. The baseline $\vec{D}$ is simply $\vec{D} = \vec{P}_1 - \vec{P}_2$. The geometrical delay, $\Delta\tau$, is given by the equation

$$\begin{aligned} c\Delta\tau &= + \frac{\vec{D}\cdot\vec{R}_2}{R_2} + \frac{\vec{R}_1\cdot\vec{R}_2}{R_2} - R_1 \\ &= + \frac{\vec{D}\cdot\vec{S}}{R_2} - \frac{\vec{D}\cdot\vec{P}_2}{R_2} + \left[\frac{\vec{R}_1\cdot\vec{R}_2}{R_2} - R_1\right] \end{aligned} \qquad (43)$$

For $|\vec{S}| \to \infty$, i.e. an infinitely distant source, Equation 43 reduces to $c\Delta\tau = \vec{D}\cdot\hat{S}$. This is the familiar form of the delay equation used in stellar VLBI. For $|\vec{S}|$ large in comparison with the Earth's radius the term $\frac{\vec{D}\cdot\vec{S}}{R_2}$ is still strongly dominant in Equation 43, and the remaining terms can be viewed as "corrections," the factor $\frac{\vec{D}\cdot\vec{P}_2}{R_2}$ representing the contribution of an eccentric baseline vector and the expression within brackets accounting for the finite height of the satellite source.

If L_i denotes the longitude of station i from the satellite's ascending node (Ω) and λ_i its latitude, then

$$\vec{D} \equiv (\cos\lambda_1 \cos L_1 - \cos\lambda_2 \cos L_2, \cos\lambda_1 \sin L_1 - \cos\lambda_2 \sin L_2, \sin\lambda_1 - \sin\lambda_2) \qquad (44)$$

In the following analysis, we assume the Earth's radius to be unity, and all distances are normalized to it.

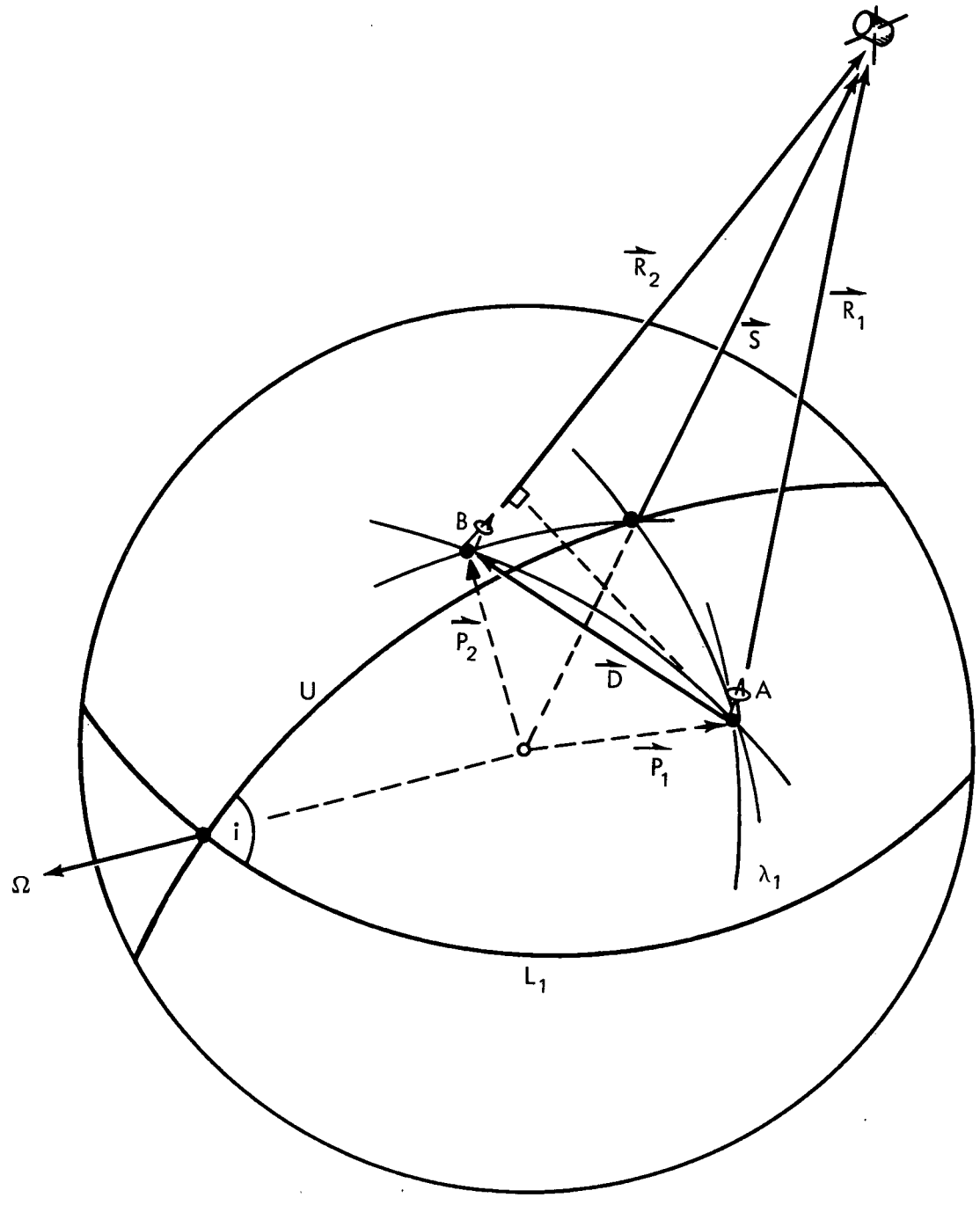

Figure 27. Geometrical Relationships for Satellite VLBI

Let ω_e represent the Earth's angular rotation rate, and a_i the longitude of station i measured from the ascending node at the time of perigee passage, which is taken to be the epoch in the present analysis. Thus $L_i = \omega_c t + a_i$; i = 1, 2. Substituting these expressions in Equation 44, and expanding and collecting terms, one obtains

$$\vec{D} \equiv (A \cos [\omega_e t + a], A \sin [\omega_e t + a], \sin \lambda_1 - \sin \lambda_2) \tag{45}$$

where

$$A = [(\cos \lambda_1 - \cos \lambda_2)^2 + 4 \sin^2 \left(\frac{a_1 - a_2}{2}\right) \cos \lambda_1 \cdot \cos \lambda_2]^{1/2} \tag{46}$$

and

$$\tan a = \frac{\cos \lambda_1 \sin a_1 - \cos \lambda_2 \sin a_2}{\cos \lambda_1 \cos a_1 - \cos \lambda_2 \cos a_2} \tag{47}$$

From Figure 28 it can be seen that (sin λ_1 - sin λ_2) is the length of the projection of $\vec{D}$ onto the polar axis; A represents the length of its equatorial projection; and a is the direction of this equatorial projection relative to the line of nodes at t = 0. One can describe $\vec{S}$, the satellite's position, in terms of u, the argument of the latitude and i orbital inclination as follows:

$$\vec{S} \equiv (S \cos u, S \sin u \cos i, S \sin u \sin i) \tag{48}$$

From Equations 45 and 48, the first term on the right side of Equation 43 becomes

$$\frac{\vec{D} \cdot \vec{S}}{R_2} = \frac{AS}{R_2} [\cos u \cos (\omega_e t + a) + \sin u \sin (\omega_e t + a) \cos i] + \frac{S}{R_2} \sin u \sin i (\sin \lambda_1 - \sin \lambda_2) \tag{49}$$

This is the explicit form of the first term on the right side of Equation 43.

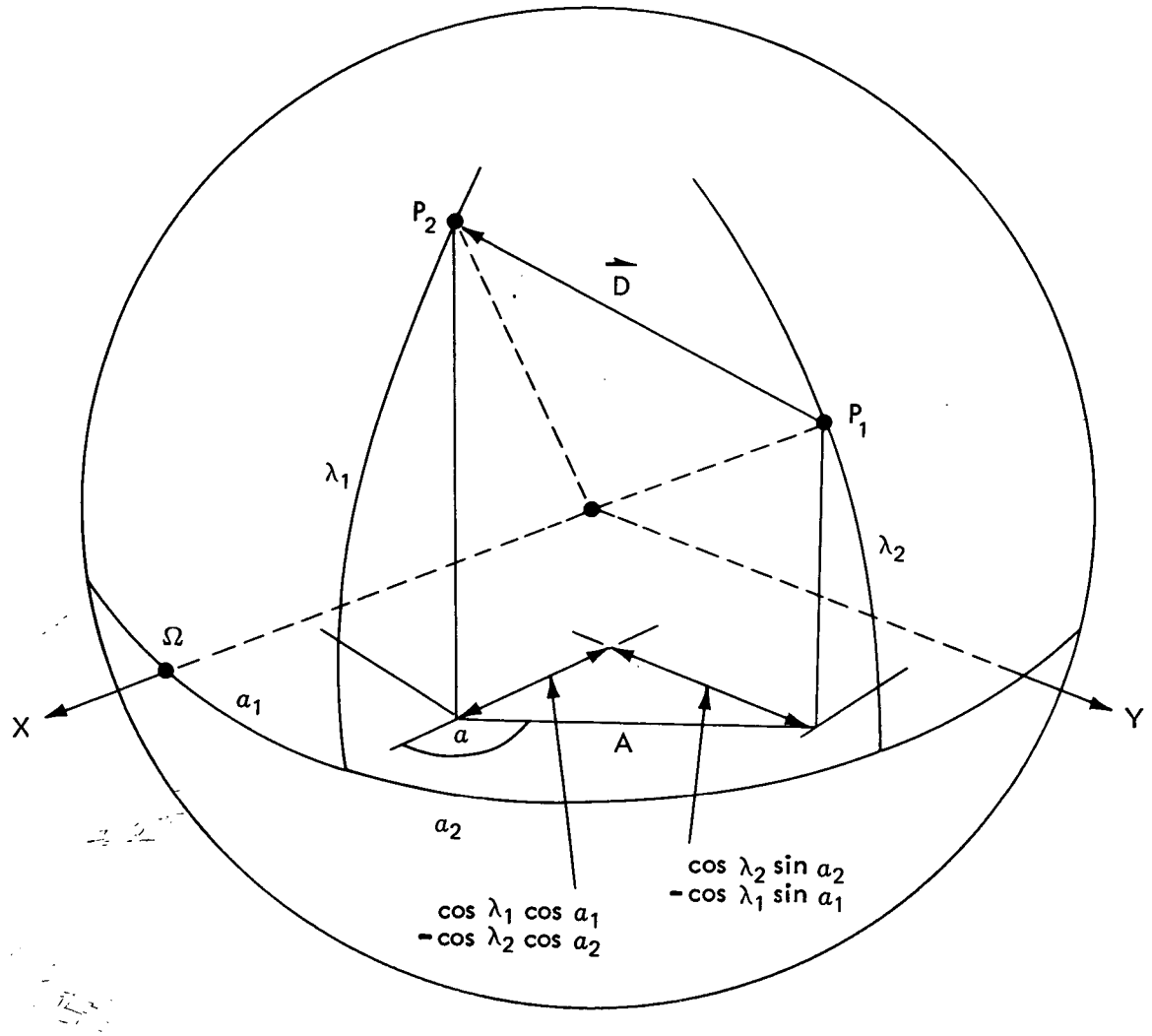

Figure 28. Projections of the VLBI Baseline

The first term on the right side of Equation 49 represents the contribution of the equatorial component of the baseline $\vec{D}$; when $a_1 = a_2$, A = 0 and this term vanishes. Similarly, the second term on the right represents the contribution of the polar component of $\vec{D}$; when $\lambda_1 = \lambda_2$, it vanishes.

The second term on the right side of Equation 43 is $-\frac{\vec{D} \cdot \vec{P}_2}{R_2}$, and its numerator is a constant that depends only on the locations of the two stations.

The third term can be written as (Reference Figure 27)

$$\frac{\vec{R}_1 \cdot \vec{R}_2}{R_2} - R_1 = \sqrt{R_1^2 - D^2 \sin^2 \theta} - R_1$$

$$= R_1 \left[\sqrt{1 - \left(\frac{D}{R_1} \sin \theta \right)^2} - 1 \right] \qquad (50)$$

where $\cos \theta = \frac{\vec{D} \cdot \vec{R}_2}{DR_2}$. This term will be treated later.

6.1.2 The Synchronous Satellite Orbit

For the synchronous satellite orbit we assume $i^2 << 1$ and $e^2 << 1$, from which it follows that $\sin i \sim i$ and $\cos i \sim 1$. For small eccentricity, we can approximate u, the argument of the latitude, in Equation 48 by the well-known form:

$$u = \omega = \Omega' t + 2e \sin \Omega' t \qquad (51)$$

where ω is the argument of the perigee (measured from the node), Ω' is the satellite's mean motion, and t is the time measured from perigee passage. Expression 49 becomes

$$\frac{\vec{D} \cdot \vec{S}}{R_2} = \frac{AS}{R_2} [\cos (\omega_e t + a)] + \frac{S}{R_2} i \sin u \, (\sin \lambda_1 - \sin \lambda_2)$$

Applying Equation 51 and expanding the cosine, we get

$$\frac{\vec{D} \cdot \vec{S}}{R_2} = \frac{AS}{R_2} [\cos (a - \omega) + \eta t \sin (a - \omega) + 2e \sin (a - \omega) \sin \omega_e t]$$

$$+ \frac{S}{R_2} i \sin u \, (\sin \lambda_1 - \sin \lambda_2) \qquad (52)$$

This is for the case of a nearly synchronous satellite orbit. The symbol η represents $\Omega' - \omega_e$.

6.1.3 The Rosman - Mojave Baseline

The coordinates of the stations are:

	Longitude		Latitude
Rosman:	277°.124 E	;	35°.199 N
Mojave:	243°.112 E	;	35°.332 N

Latitude difference is 0.132°, i.e. the baseline lies in a plane essentially parallel to the equator. We shall, accordingly, ignore the term $(\lambda_1-\lambda_2)$, as well as $(\sin\lambda_1 - \sin\lambda_2)$ and $(\cos\lambda_1 - \cos\lambda_2)$. Then the last term in Equation 52 vanishes, as does the first term in brackets within Equation 46. This latter expression becomes

$$A = 2\sin\left(\frac{a_1 - a_2}{2}\right)\cos\lambda_1 = D,$$

while Equation 47 reduces to

$$\tan a = \frac{\sin a_1 - \sin a_2}{\cos a_1 - \cos a_2} = \tan\frac{1}{2}(\pi + a_1 + a_2)$$

Equation 52 reduces to

$$\frac{\vec{D}\cdot\vec{S}}{R_2} = A\frac{S}{R_2}\left[\cos P + \eta t \sin P + 2e \sin P \sin\omega_e t\right] \qquad (53)$$

where P denotes the difference $(a-\omega)$. However, the nodal regression and apsidal rotation of the satellite's orbit are both first order effects in J_2, and P should, therefore, be viewed as $P = P_0 + \dot{P}_0 t$, where P_0 represents the sum of nodal and apsidal rates. Equation 53 becomes:

$$\frac{\vec{D}\cdot\vec{S}}{R_2} = A\frac{S}{R_2}\left[\cos P_o + (\eta - \dot{P}_o)t \sin P_o + 2e \sin P_o \sin\omega_e t\right] \qquad (54)$$

The first term on the right side of Equation 43, therefore, takes a simple form. The third term can also be simplified accordingly. Equation 50 can be expanded in powers of the small parameter $\frac{D}{R_1} < 1$, and the series truncated after the first two terms:

$$\frac{\vec{R}_1\cdot\vec{R}_2}{R_2} - R_1 = -\frac{D^2}{2R_1}\sin^2\theta \qquad (55)$$

Since

$$\cos\theta = \frac{\vec{D}\cdot\vec{R}_2}{DR_2} = \frac{\vec{D}\cdot(\vec{S}-\vec{P}_2)}{DR_2}$$

$$= \frac{\vec{D}\cdot\vec{S}}{DR_2} + (\text{higher order terms})$$

one can write

$$\frac{\vec{R}_1 \cdot \vec{R}_2}{R_2} - R_1 = -\frac{D^2}{2R_1}\left[1 - \left(\frac{AS}{DR_2}\right)^2 \cos^2 P_o\right] + \text{higher order terms}$$

$$\simeq - \frac{D^2}{2R_1} \sin^2 P_o \qquad (56)$$

to first order in small quantities.

The following expression for the geometrical delay is obtained when equations 54 and 56 are inserted into equation 43:

$$T = \left[\cos P_o - \frac{D}{2S}\left(\frac{R_2}{R_1}\right) \sin^2 P_o - \frac{\vec{D} \cdot \vec{P}_2}{DS}\right]$$

$$+ (\eta - \dot{P}_o)t \sin P_o + 2e \sin P_o \sin \omega_e t \qquad (57)$$

where T denotes the expression $\frac{cR_2}{AS} \simeq \frac{c}{D} \cdot \frac{R_2}{S} \cdot \Delta\tau.$

6.1.4 Extracting the Orbital Elements

A best-fit diurnal curve is obtained to fit the observational values of time-delay and fringe-rate using the least squares technique. In accordance with Equation 57, the form of this curve is chosen to be

$$T = T_o + T_1 \omega_e t + T_2 \sin (\omega_e t' + T_3) \qquad (58)$$

where T_0, T_1, T_2, and T_3 are determined by the curve-fitting procedure. The variable t' represents time as measured from some convenient reference, such as 0^h UT on a specific day. When $\omega_e t' = -T_3$, the satellite is passing through perigee, and this value of t' (viz. $t' = -T_3/\omega_e$) is the epoch adopted above.

Equating the expressions 57 and 58 and evaluating them at t = 0, as well as their derivatives at $t = \pi/2$ and t = 0, one gets

$$T_o = \cos P_o - K \sin^2 P_o - M \qquad (59)$$

$$T_1 = \frac{(\eta - \dot{P}_o)}{\omega_e} \sin P_o \qquad (60)$$

$$T_2 = 2e \sin P_o \qquad (61)$$

where $K = \frac{D}{2S} \frac{R_2}{R_1}$ and $M = \frac{\vec{D} \cdot \vec{P}_2}{DS}$

Equation 59 is a quadratic form in cos P_0 whose solution is

$$P_o = \cos^{-1} \left\{ \frac{1}{2K} \left[-1 + \sqrt{1 + 4K(T_o + K + M)} \right] \right\} \qquad (62)$$

With P_0 known, both $\eta - \dot{P}_o$ and e can be found from Equations 60 and 61, viz:

$$\eta - \dot{P}_o = \frac{\omega_e T_1}{\sin P_o} \qquad (63)$$

$$e = \frac{T_2}{2 \sin P_o} \qquad (64)$$

and, as discussed above,

$$t' = -\frac{T_3}{\omega_e} \qquad (65)$$

Equations 62-65 constitute the first-order solution for the elements of the satellite's motion.

6.1.5 Determination of ATS-3 Orbit Parameters

From each tape pair of VLBI data, a representative set of time-delay and fringe-rate parameters are tabulated. A curve of the form of Equation 58 was fit to the time-delay values obtained, using least squares. The curve is shown in Figure 29. If we denote by $\Delta\tau_i$, the quantity $\frac{D}{c} \cdot \frac{S}{R_2} \cdot T_i$ for i = 0, 1, 2, and $\Delta\tau_3 = T_3$, then from the curve as shown:

$\Delta\tau_0$ = 4039.7 μsec

$\Delta\tau_1$ = .005 μsec/deg

$\Delta\tau_2$ = 71.32 μsec

$\Delta\tau_3$ = 91.308 deg

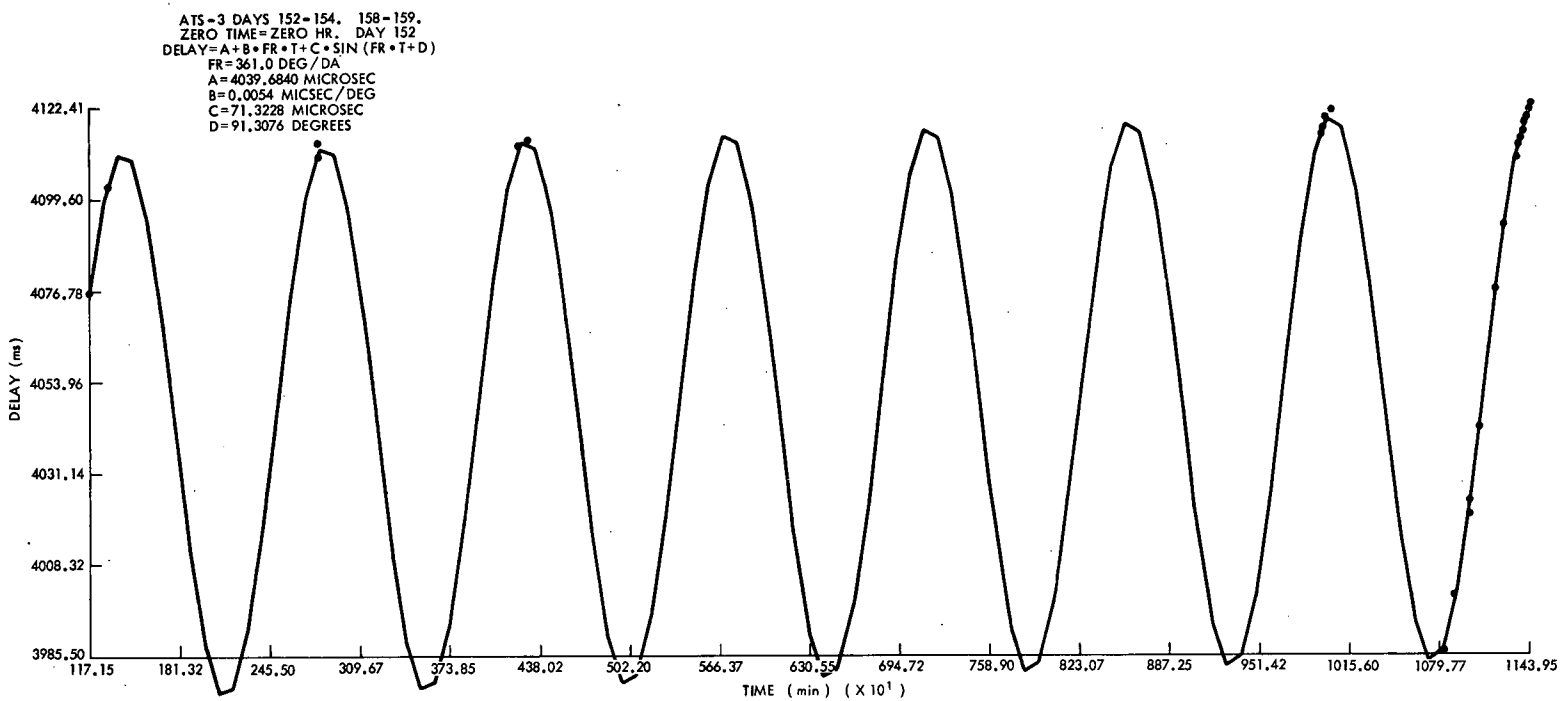

Figure 29. Time-Delay Curve for ATS-3. Days 152-159, 1971

The calculated value for $\frac{c}{D} \cdot \frac{R_2}{S}$ is

$T_0 = .3595$

$T_1 = .487X10^{-6}$ (deg)$^{-1}$

$T_2 = .0063$

$T_3 = 91.308$ deg

For the Rosman-Mojave baseline, $\frac{\vec{D} \cdot \vec{P}_2}{DS} = -0.036$. Inserting the above values into Equations 62 through 65 we find:

$P_0 = 66°20'$

$\eta - P_0 = .011$

$e = .0034$

$t' = 18^h00^m$

The term $\eta = \Omega' - \omega_e$ has a periodic variation that reflects the variation in Ω' (the satellite's mean motion) induced by dynamical resonances at the synchronous altitude. The official ATS-3 Project orbital parameters, for instance, cite values of 1435.98 and 1436.125 min. for the anomalistic period on 8 May 1971 and 31 May 1971, respectively. Thus, the least squares fit will "average out" this variation in η and the above equation for $\eta - \dot{P}_0$ must be interpreted as an equation for $-\dot{P}_0$, i.e. the sum of nodal plus apsidal rates only, rather than for $\eta - \dot{P}_0$. In the limit, as $i \to 0$, $\dot{\omega} = -2\dot{\Omega} = +2\dot{a}$, and that $(\dot{\omega} - \dot{a}) = \dot{P}_0 = -\dot{\Omega}$.

Thus

$\dot{\Omega} = -.001$

If we restrict the delay values to those obtained during a 24-hour period only, then η will not be averaged by the least squares fit, but rather will assume its "instantaneous" value for that day. Accordingly, we fit a curve to the data for days 158 and 159 only. This yields a value of $\Delta\tau = .3767X10^{-3}$, which is appropriate to about noon on day 159. Then

$$\frac{\eta - \dot{P}_o}{-\dot{P}_o} = \frac{.3767X10^{-3}}{5.5X10^{-3}} = .0685$$

from which $\eta = -.0102$ deg/day. If T and T' denote the sidereal day and the instantaneous anomalistic period of the satellite (both in minutes of UT), then $T' - T = -15\eta = .153$. Thus $T' = T + .153$ min., where $T = 1436^m.068$. Finally:

$$T' = 1436^m.22$$

In conclusion, table 10 compares values for the ATS-3 orbit elements supplied by the Project Office, against the first-order values obtained herein:

TABLE 10

Comparison of ATS-3 Orbital Elements

Orbit Element	VLBI Value	ATS Project Value
Period (day 151)	$1436^m.22$	$1436^m.125$
Semi-major axis	42168 km	42165 km
Eccentricity	0.0034	0.0029
Time of perigee	18^h00^m	18^h05^m
Position of perigee	0.5 deg	359.288 deg
Nodal regression rate	-0.011 deg/day	-0.0134 deg/day

6.1.6 Error Analysis

Errors in the measured values of relative delay and delay rate arise chiefly from two sources, tropospheric perturbations and equipment misalignments. These effects manifest themselves as errors in the $\Delta\tau_i$ (i = 0, 1, 2, 3) that are determined from the least-squares fit of Equation 58 to the delay rate.

Equations 62 - 65 can be used to express errors in the orbital elements in terms of errors in the $\Delta\tau_i$. For simplicity of exposition, we shall temporarily replace Equation 62 by

$$T_0 = \cos P_o \qquad (62')$$

Then, as is readily apparent by taking derivatives of Equations 62' and 63-65 with respect to the $\Delta\tau_i$:

$$\frac{\partial P_o}{\partial \Delta\tau_o} = -\frac{\cot P_o}{\Delta\tau_o}$$

$$\frac{\partial \dot{P}_o}{\partial \Delta\tau_o} = \frac{\dot{P}_o \cot^2 P_o}{\Delta\tau_o} \quad ; \frac{\partial \dot{P}_o}{\partial \Delta\tau_1} = \frac{\dot{P}_o}{\Delta\tau_1}$$

$$\frac{\partial e}{\partial \Delta\tau_o} = \frac{e \cot^2 P_o}{\Delta\tau_o} \quad ; \frac{\partial e}{\partial \Delta\tau_2} = \frac{e}{\Delta\tau_2}$$

$$; \frac{\partial t'}{\partial \Delta\tau_3} = \frac{t'}{\Delta\tau_3}$$

Clock-epoch misalignments produce a constant offset in $\Delta\tau_0$, and their effects on P_0, $\dot{P}_0$ and e are analytically described by the expressions for $\frac{\partial(P_0, \dot{P}_0, e)}{\partial \Delta\tau_o}$ cited above. Differential atmospheric path lengths may also produce constant-bias errors in $\Delta\tau_0$ and these will contribute additional errors to $\Delta\tau_0$. Small local oscillator (L.O.) offsets between pairs of terminals will lead to an error in $\Delta\tau$, and this will have an effect on the derived value of $\dot{P}_0$, as described above.

Consider now any errors in the adopted baseline $\vec{D}$. These arise because the positions of the antennas are not precisely known. The constraint that $\lambda_2 = \lambda_1$ limits the consideration of positioned errors to those lying in the plane parallel to the equator at latitude λ_1. Thus, only the difference in longitude between the two stations enters into the analysis. The baseline error, being one-dimensional, can be equivalently expressed as an error in its length, D. From the definition of T_i, we have $\frac{\partial T_i}{\partial D} = -\frac{T_i}{D}$. Again employing Equations 62, 63 and 64:

$$\frac{\partial P_o}{\partial D} = \frac{\cot P_o}{D}$$

$$\frac{\partial \dot{P}_o}{\partial D} = -\frac{\dot{P}_o}{D \sin^2 P_o}$$

$$\frac{\partial e}{\partial D} = \frac{e}{D \sin^2 P_o}$$

6.1.7 Second Order Effects in the Orbit-Analysis

The orbit analysis is extended to include second-order terms in the small quantities $\frac{P_2}{a}$ and $\frac{D}{a}$, where D is the baseline length, and a is the satellite's semi-major axis (= 6.61 earth radii), and P_2 is the distance from the Earth's center to station 2 (= one earth radius). As before, e^2 and i^2 are neglected.

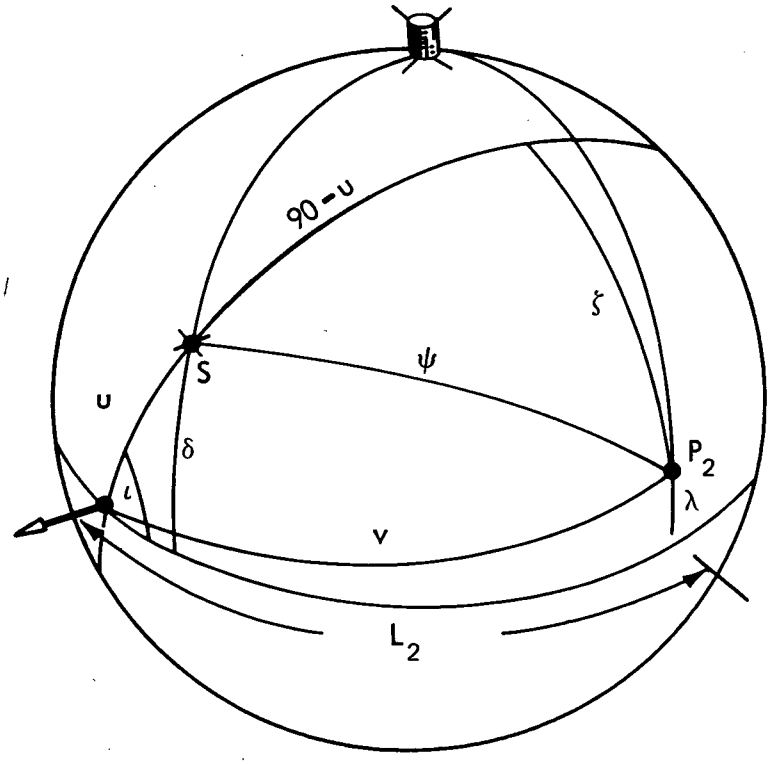

Figure 30. Geometrical Relationships - Second Order Effects

For the general non-equatorial baseline, equations 43, 50 and 52 may be combined to yield:

$$c\Delta\tau = \frac{S}{R_2}\Big\{A[\cos P_o + (\eta - \dot{P}_o)\, t \sin P_o + 2e \sin P_o \sin \omega_e t] + i(\sin \lambda_1 - \sin \lambda_2) \sin u + \frac{\vec{D}\cdot\vec{P}_2}{a}(1 + e\cos[u - \omega])\Big\} + \frac{D}{2R_1}\sin^2\theta \quad (66)$$

If ψ the angle between $\vec{P}_2$ and $\vec{S}$,

$$\left(\frac{R_2}{S}\right)^2 = 1 - 2\left(\frac{P_2}{S}\right)\cos\psi + \left(\frac{P_2}{S}\right)^2$$

from which

$$\frac{S}{R_2} = 1 + \left(\frac{P_2}{S}\right)\cos\psi - \frac{1}{2}\left(\frac{P_2}{S}\right)^2 - \frac{3}{2}\left(\frac{P_2}{S}\right)^2 \cos\psi + \ldots \qquad (67)$$

where (Ref. Figure 30),

$$\begin{aligned} \cos\psi &= \cos v \cos u + \sin u \cos\zeta \\ &\cong \cos\lambda \cos(L_2 - u) + i \sin\lambda \sin u \end{aligned} \qquad (68)$$

and

$$\frac{P_2}{S} \cong \frac{P_2}{a}\,(1 + e\cos[u - \omega]) \qquad (69)$$

Inserting equations 68 and 69 into equation 67, and reducing the terms that result:

$$\begin{aligned} \frac{S}{R_2} = 1 &+ \left(\frac{P_2}{a}\right)\left[\cos\lambda\cos(L_2 - u) + e\cos(u-\omega)\cos(L_2 - u)\cos\lambda + i\sin\lambda\sin u\right] \\ &+ \frac{1}{2}\left(\frac{P_2}{a}\right)^2 - \frac{3}{2}\left(\frac{P_2}{a}\right)^2 \cos\lambda\cos(L_2 - u) \end{aligned} \qquad (70)$$

Equation 70 can be inserted into Equation 66.

Returning to the last term in Equation 66, and using Equation 55:

$$\cos^2\theta = \left(\frac{\vec{D}\cdot\vec{S}}{DR_2}\right)^2 - 2\left(\frac{\vec{D}\cdot\vec{S}}{DR_2}\right)\left(\frac{\vec{D}\cdot\vec{P}_2}{DR_2}\right)$$

Employing equation 54 and simplifying:

$$\begin{aligned} \sin^2\theta = 1 - \left(\frac{A}{D}\right)^2 &\left[\cos^2 P_o + 2\left(\frac{P_2}{S}\right)\cos^2 P_o \cos\lambda\cos(L_2 - u) + (\eta - \dot{P}_o)\,t\sin 2P_o\right. \\ &\left. + 2e\sin 2P_o \sin\omega_e t\right] + 2\left(\frac{A}{D}\right)\left(\frac{\vec{D}\cdot\vec{P}_2}{Da}\right)\cos P_o \end{aligned}$$

Finally, the term $\frac{D}{2R_1}$ can be written as

$$\frac{D}{2R_1} = \frac{D}{2S}\left(\frac{S}{R_1}\right) = \frac{D}{2a}\left[1 + e\cos(u-\omega) + 2\frac{P_1}{a}\cos\nu\right] \tag{71}$$

where ν is the angle between P_1 and S, in Figure 27.

Equations 67-71 can be inserted into Equation 66 to obtain an explicit expression for $c\Delta\tau$ which is accurate to second order in the quantities cited above. Equation 66 supersedes Equation 57. To first order, it is:

$$\begin{aligned} c\Delta\tau = {} & \left\{A\cos P_o - \frac{\vec{D}\cdot\vec{P}_2}{a} - \frac{D^2}{2a}\left[1 - \left(\frac{A}{D}\right)^2\cos^2 P_o\right] + A\left(\frac{P_2}{a}\right)\cos P_o \cos P_2 \cos\lambda\right\} \\ & + A(\eta - \dot{P}_o)t\sin P_o + \left[2Ae\sin P_o + i(\sin\lambda_1 - \sin\lambda_2)\cos\omega\right]\sin\omega_e t \\ & + \left[2Ae\cos P_o + i(\sin\lambda_1 - \sin\lambda_2)\sin\omega\right]\cos\omega_e t \end{aligned} \tag{72}$$

The second order expression contains constant terms, as well as first and second harmonics in $\omega_e t$. The constant and linear terms are ignored here because they add little of qualitative interest to the solution. The terms involving $\sin\omega_e t$ and $\cos\omega_e t$ contribute an important correction to e. They are

$$\begin{aligned} & -e\left[\left(\frac{\vec{D}\cdot\vec{P}_2}{a}\right) + \frac{D^2}{2a}\right]\cos\omega_e t + e\left[2A\left(\frac{P_2}{a}\right)\cos\lambda\sin(P_o + P_2) + \frac{D^2}{a}\left(\frac{A}{D}\right)^2\sin 2P_o\right]\cdot \\ & \sin\omega_e t + i(\sin\lambda_1 - \sin\lambda_2)\left[\cos\omega\sin\omega_e t + \sin\omega\cos\omega_e t\right] \end{aligned} \tag{73}$$

For the Mojave-Rosman baseline, the last term of expression 73 is negligible and the remainder is of order

$$-.1\,De\cos\omega_e t + .2\,De\sin\omega_e t$$

To second order, then, Equation 61 should read:

$$\frac{c}{D}\Delta\tau = \left[2.2\sin\omega_e t + 0.1\cos\omega_e t\right]e = 2.2\sin(\omega_e t + 2.5^\circ)$$

from which the corrected value for e would be

$$e = .0031$$

which compares more favorably with the value of .0029 given by the ATS Project than the value of .0034 as determined by first-order theory.

Also, the value for T_3 obtained by the least-squares fit is 91.2 deg. At the time of perigee then, $2.5° = \Omega t'_\omega + 91.2°$, where t' is time measured from O UT. Thus, the value of UT at perigee passage is $t'_\omega = -5^h55^m$. In other words, the time of perigee passage is $18^h\ 05^m$ which agrees exactly with the figure supplied by the ATS Project Office.

The second-order terms involving the second harmonics are

$$ei(\sin \lambda_1 - \sin \lambda_2) \sin (2\omega_e t + \omega) + \frac{A}{2}\left(\frac{P_2}{a}\right) e \cos P_o \cos (2\omega_e t + \omega - L_2) \quad (74)$$

For the Rosman-Mojave baseline the first term in expression 74 is negligible in comparison with the second. The second term is of order

$$10^{-4} D \sin (2\omega_e t + 35°)$$

By extending the least-squares fit to the data for days 152-158 to include a second-harmonic term of the form b sin $(2\omega_e t + B)$, this term takes the form

$$2 \times 10^{-4} \sin (2\omega_e t + 4°)$$

which indicates reasonably good agreement in the magnitude, but rather poor comparison in phase due to lack of sufficient observations at different phases of the satellite orbit.

6.2 ORBIT DETERMINATION USING THE "GEODYN" PROGRAM

This program is a sophisticated orbit determination program which has been modified to accept the satellite VLBI parameters (time-delay and fringe-rate) from an arbitrary number of baselines as inputs to the program.

The GEODYN program has the capability of estimating that set of

- Orbital elements/determination of definitive orbits
- Station positions/geodetic parameter estimation
- Measured biases/tracking instrument calibration
- Force model parameters

which give the best fit for orbital tracking data. The program is operational on the GSFC IBM 360-95 computer. The total number of adjustable parameters

affecting any one arc may be as large as 70. The total number of adjustable force parameters affecting any one arc may be as large as 20.

The Inputs to the program are:

- VLBI Parameters (time-delay, τ_g and fringe-rate $\dot{\nu}_f$)
- Measurement biases
- Station coordinates
- a priori satellite cartesian elements and epoch time
- Geopotential coefficients through degree 22 and order 22
- Solar-flux and geomagnetic data
- Satellite drag-coefficient, satellite emissivity and mass

The outputs from the program are:

- Double precision adjusted cartesian elements; correlation coefficients between elements; standard deviation of fit
- Kepler elements
- Adjusted geopotential coefficients
- Adjusted Earth-fixed cartesian and geodetic station coordinates; correlation between determined coordinate values; standard deviation of fit for coordinate values
- Instrumental biases - timing and constant biases
- Summary of residual statistics

Other features of the program are:

- The motion of the polar axis is described by a mean pole position averaged over six-year periods since 1900; and by libration and periodic terms
- Luni-solar perturbations on satellite motion

C3

- Orbital perturbations due to earth tides
- Precession and nutation effects of Luni-solar and planetary perturbations
- Planetary perturbations on the plane of the ecliptic
- Tropospheric and ionospheric refraction corrections
- Solar radiation pressure

The numerical integration technique that is used in the program is the "Cowell Predictor" technique. More details about this program can be found in the document titled "GEODYN SYSTEM, Vol I, II and III" by Wolf Research and Development Corporation, NASA, GSFC Contractor Report, 1971.

The station coordinates used in the program are the following:

Station	Latitude	Longitude	Altitude
Mojave ATS (MOJATS)	35° 19' 53".78	243° 06' 43".95	887 (m)
Rosman ATS (ROSATS)	35° 11' 56".05	277° 07' 27".30	828 (m)

The following table (Table 11) gives the orbital elements computed from the GEODYN program for various cases. It is understood that the orbital elements computed from the GEODYN program are more accurate. The orbital elements computed by using first order orbit-theory and a data-fitting procedures is crude and is presented here only to illustrate the VLBI orbit analysis. The last two columns show the orbital elements determined from two independent subsets of data and one can see a remarkable consistency in the results.

TABLE 11

ATS-3 Orbital Elements from GEODYN Program

Epoch $71^{y}\ 149^{d}\ 00^{h}\ 00^{m}\ 00^{s}$

Total Points 843 for Time Delay
843 for Fringe-Rate

ELEMENT \ DATA-SOURCE		Orbital Parameter from SHF R & RR Data	Time-Delay (ν_g) & Fringe-Rate (ν_F) Data from All Days	Data from Days 158 & 159 Only	τ_g AND ν_F Data from All Days with Large Residuals Rejected - Group 1 -	τ_g AND ν_F Data from All Days - Group 2 -
Semi-major axis (km)	a	42,165.43	42,165.28	42,165.17	42,165.270	42,165.280
Eccentricity	e	2.91×10^{-3}	2.879×10^{-3}	2.903×10^{-3}	2.905×10^{-3}	2.905×10^{-3}
Inclination	i	1.706°	1.818°	1.712°	1.712°	1.712°
Position of Perigee	ω	359.288°	2.620°	0.223°	0.277°	0.277°
Right of Ascension of the Ascending Node	Ω	82.214°	78.563°	81.223°	81.195°	81.196°
Mean-Anomaly	M_0	87.150°	87.443°	87.172°	87.159°	87.159°
Mean Orbital Longitude	$\omega + \Omega + M_0$	168.652°	168.628°	168.618°	168.632°	168.633°
Bias Correction done by GEODYN			No	Yes	Yes	Yes
Number of Data Points Used			801	578	700	650
Number of Points Rejected			—	—	72	110
Number of Iterations			4	5	5	5
Period (mts)		1436.125	1436.124	1436.118	1436.123	1436.123
Nodal Regression Rate (deg/day)		-0.01340	-0.01341	-0.01342	-0.01342	-0.01342

7. DISCUSSION

In order to determine the precision of time-delay measurements, each pair of data tapes was broken up into several subsets of data each ~ 1 sec long (5 records) and the delay was computed for each subset separately. The distribution curve of time-delay from each pair of tapes was studied to determine the RMS Scatter. A total of one hundred and twenty pairs of tapes were processed in this manner. The delay-curve exhibited an average RMS Scatter of 5 nsec and the standard deviation of the mean is about 0.1 nsec. The precision of delay-rate measurement, dictated by the phase stability of the VLBI system, is estimated to be about 0.1 psec/sec in most cases. Since there was sufficient time-delay and fringe-rate data covering various portions of the orbit, the overall time-delay resolution can be estimated much more accurately.

As described in an earlier section, the orbit of the ATS-3 spacecraft was computed using the GEODYN program. The GEODYN program insures a high degree of precision in orbit computation since it takes into account most of the conventional and non-conventional forces that influence the spacecraft motion. The orbital elements of the ATS-3 spacecraft were computed using various subsets of VLBI data. The semi-major axis is determined consistently to within 100 meters and the best value differs from that determined by using conventional SHF range and range-rate data by 160 meters. As shown in Table 11, Group "A" and Group "B" (the last two columns) are the different subsets of data used in orbit computation using the GEODYN program. The agreement is remarkable.

The arc-resolution ($R\Delta\theta$) may also be computed. By applying the usual interferometric equations, one can obtain

$$R\Delta\theta \simeq \frac{R}{D} \quad \frac{c\Delta\tau_g}{\sin\theta} \tag{75}$$

where R is the range to the satellite, D is the baseline length, C is the velocity of light, $\Delta\tau_g$ is the time-delay resolution obtained in the interferometric measurements and θ is the source-baseline angle. Using the following values:

$$\frac{R}{D} \simeq 12,\ \Delta\tau_g = 5 \times 10^{-9} \text{ seconds and } \sin\theta = 0.5$$

$$R\Delta\theta \simeq 35 \text{ meters}$$

For a time-delay resolution of 10 nanoseconds, the arc resolution is 70 meters.

Similarly, the arc-rate resolution ($R\Delta\theta$) is obtained from the fringe rate measurements.

$$= R\Delta\dot{\theta} \sim \frac{c\Delta\nu_f}{f \sin\theta} \frac{R}{D} \qquad (76)$$

Where C is the velocity of light, $\Delta\nu_f$ is the fringe rate resolution $\sim$ 100 μ Hz and f is the signal frequency $\sim$ 4 GHz

$$R\Delta\dot{\theta} \sim 0.1 \text{ mm/sec}$$

It can be summarized that the time-delay and the fringe rate measurement precision yield the ATS-3 projected spacecraft position within 100 meters. Higher precision can be accomplished if we use large recording bandwidths. We have the hardware/software needed to synthesize larger bandwidths and plan to utilize them in future experiments. With such a system, a time-delay resolution of the order of 0.1 nsec can be accomplished. An experiment in this direction has been proposed by us to the ATS C-2 project.

The VLBI measurement of one way differential group-delay corresponds to the difference in the direct two way range delay measurements made simultaneously from Rosman and Mojave with SHF ranging transponders on board the satellite. In many ways, for equal accuracy of individual measurements, the direct-delays are more useful than the differential delays. However, the VLBI measurements yield very high angular precision. At present, VLBI differential group-delay data is about two orders of magnitude better than the conventional radio range data. When combined with conventional SHF range measurement, the VLBI parameters yield spacecraft position with very high precision. This leads to the discussion of the vector tracking concept in which three stations (two independent baselines) obtain two independent sets of time delay and fringe-rate by satellite observations. The two sets of VLBI parameters are combined with a single range measurement from the master station (or the common station) to yield the spacecraft position vector with a resolution of the order of ten meters.

VLBI measurement of fringe-rate or differential phase-delay rate is analogous to the difference in the direct doppler measured directly at the two sites with the use of coherent transponders on the spacecraft. In the doppler tracking technique, the phase change of the signal is continuously monitored over a full pass. The slope of the phase versus time plot yields the doppler at any particular time. The differential doppler reading is identical to the VLBI fringe-rate. The use of stable frequency standards in VLBI measurements

enables one to measure the differential doppler with improved resolution. However, it can not be ignored that the same information is obtainable from doppler tracking measurements made at the two terminals. The VLBI technique has certain advantages; (1) it is a passive technique, (2) an inexpensive wide-band noise source and a free running oscillator onboard the spacecraft are all that are needed, (3) ground station equipment is inexpensive and simple. With simplified data processing techniques to perform the cross-correlation, the VLBI measurements will become an operational tool for precision tracking and geodetic applications.

One area of application we have in mind is to use the installations with large antennas to observe both satellites and natural radio sources. The quasar observations are used to calibrate the baseline and the station coordinates. The satellite VLBI observations of time-delay and fringe-rate are then combined with the calibrated baseline coordinates to obtain the spacecraft position very accurately. Then, small, portable terminals at remote sites are used to observe the much stronger signals from the spacecraft(s) [the satellite signals, in general, are six to seven orders of magnitude stronger than those from the celestial sources and permit high resolution time-delay interferometry] whose orbit(s) has been determined precisely relative to the intertial frame by VLBI observations from larger installations. The VLBI observations of satellite signals by the portable terminals are used to establish the geodetic ties directly.

The philosophy outlined above was tried in the Rosman-Mojave experiment and later in the Rosman-Owens Valley-Agassiz experiment. The Rosman-Mojave baseline was determined with a precision of ±2.0 meters from VLBI observations of quasars. The calibrated baseline coordinates were then used in the ATS-3 satellite position determination. The Owens Valley-Agassiz baseline was determined with a precision of ±0.40 meters from quasar observations. (The quasar observations have been reported separately.) But no VLBI observations have been conducted from remote sites using portable terminals. We will do so in our future experiments. The specific role of satellite VLBI measurements in the Earth and Ocean Dynamics studies will become clear in the very near future.

8. ACKNOWLEDGEMENTS

The authors wish to thank the ATS Project Office for their enthusiastic cooperation during the experiments. Dr. F. O. Vonbun, Chief of the Trajectory Analysis of Geodynamics Division has been a driving force behind the GSFC/ VLBI Program.

9. REFERENCES

1. Michelini, R. D., A one-bit VLBI recording and playback system using Video tape-recorders, Radio Science, Vol. 5, p. 1263, October 1970.

2. Mather, N. C., Grossi, M. D., and Pearlman, M. R., Atmospheric Effects in VLBI, Radio Science, Vol. 5, p. 1253, October 1970.

3. Ramasastry, J., Schmid, P. E., and Rosenbaum, B., Very Long Baseline Interferometer Experiments Using ATS-3 and ATS-5 Satellites, NASA/GSFC X-551-70-432, November 1970.

4. Ramasastry, J., Michelini, R. D. and Rosembaum, B., VLBI Experiments Using the ATS Satellites, NASA/GSFC X-550-71-134, 1971.

5. Ramasastry, J., et al., VLBI Clock Synchronization Tests Performed via the ATS-1 and ATS-3 Satellites, NASA/GSFC X-553-71-514, December 1971.

6. S. Ross and Company, Documentation of Computer Programs Used in the VLBI Experiments, NASA/GSFC Contractor Report, NAS-5-20247, November 1971.

7. Preston, R. A., et al, Interferometric Observations of an Artificial Satellite (TACSAT), (unpublished report - MIT), November 1971.

8. Wolf Research and Development Corporation, (Author, Thomas V. Martin); GEODYN SYSTEM, Volume III, Operations Description, Prepared for NASA/GSFC, Contract NAS-5-11736, December 1971.

9. Fanselow, J. L., et al, The Goldstone Interferometer for Earth Physics, JPL Technical Report 32-1526, Vol. V, 1971.

10. Knight, C. A., Shapiro, I. I., Geophysical Applications of Long Baseline Interferometry, "Earthquake Displacement Fields and Rotation of the Earth" (ed. L. Mansinka, D. E. Smyhe and A. E. Beck), Springer Verlag, New York, 1970.

11. Ramasastry, J., SAVE - "SATELLITE VLBI EXPERIMENT" - Experiment Proposal submitted to the ATS C-2 Project Office, NASA/GSFC, X-553-72-252, June 1972.